A STUDY OF WIND LOADING ON TALL STRUCTURES

ATLANTIC-RICHFIELD PLAZA BUILDINGS

by

W. Z. Sadeh

J. E. Cermak

and

G. Hsi

Fluid Mechanics Program
Fluid Dynamics and Diffusion Laboratory
College of Engineering
Colorado State University
Fort Collins, Colorado

August 1969

CER68-69WZS-JEC-GH-36

A STUDY OF WIND LOADING ON TALL STRUCTURES--
ATLANTIC-RICHFIELD PLAZA BUILDINGS

by
W. Z. Sadeh*, J. E. Cermak** and G. Hsi†

for

Metronics Associates, Inc.
3201 Porter Drive
Stanford Industrial Park
Palo Alto, California

Fluid Mechanics Program
Fluid Dynamics and Diffusion Laboratory
College of Engineering
Colorado State University
Fort Collins, Colorado

August 1969 CER68-69WZS-JEC-GH-36

---

* Assistant Professor
** Professor-in-charge, Fluid Mechanics Program
† Research Associate

ABSTRACT

Wind loading on a 1:384 scale model of Atlantic-Richfield Plaza Buildings 666 ft high was investigated in a thick turbulent boundary-layer wind tunnel. Measurements of mean velocity, turbulence intensity and boundary-layer thickness upstream of the model structure verified that the wind-tunnel flow was an adequate simulation of the atmospheric-surface-layer conditions over the full-scale urban area.

Mean pressure and pressure fluctuations were measured for three different wind directions (NE, N and NW). Generally, the mean pressure was found to be the largest near the top and smallest close to the base. An opposite variation was observed for the fluctuating and instantaneous peak pressures. The largest pressure fluctuations were obtained in the case of the N wind.

The turbulence-energy spectra of the upstream flow and surface pressure-fluctuations spectra exhibited consistently a similar qualitative behavior. This is suggestive that the upstream turbulence has a predominant role, together with the wake, in producing the pressure fluctuations.

Direct measurement of mean and fluctuating overturning moment by means of a strain-gage dynamometer revealed that the latter ranged up to about ± 34% of the former. Root-mean-square values of the fluctuating moment were also determined in an effort to relate it to the pressure fluctuations and upstream turbulence.

ACKNOWLEDGEMENTS

The support of Metronics Associates, Inc., in carrying out this study is gratefully acknowledged. The assistance of Mr. J. A. Garrison in constructing the experimental apparatus is highly appreciated. Furthermore, the assistance of Messrs R. D. Sutton and R. P. Johanson in constructing the moment balance and carrying out various calculations is appreciated.

TABLE OF CONTENTS

TABLE OF CONTENTS - Continued

LIST OF TABLES

LIST OF FIGURES

LIST OF FIGURES - Continued

LIST OF FIGURES - Continued

LIST OF SYMBOLS

Symbol

a	- width of wide tower face
b	- width of narrow tower face
B_w	- filter bandwidth
c_p	- mean pressure coefficient
c_{p_f}	- fluctuating pressure coefficient
$c_{p_{max}}$	- instantaneous peak pressure coefficient
d	- nominal diameter of the hot wire
E	- total voltage
E_o	- total voltage in still air
e	- fluctuating voltage
$F(n)$	- frequency-density function
$F_{u'}$	- fluctuating velocity frequency-density function
$F_{p'}$	- pressure fluctuations frequency-density function
h	- tower height
l	- hot-wire length
M	- total overturning moment
n	- frequency
p	- total local pressure
Tu_x	- longitudinal turbulence intensity
U	- wind velocity
u	- fluctuating velocity parallel to the mean flow velocity
x,y,z	- coordinates

LIST OF SYMBOLS - Continued

Symbol

α	- exponent Eq. (2); wind incidence angle
γ	- normalized pressure coefficient difference
δ	- boundary-layer thickness
ρ	-density air

Superscripts

*	- means 'having dimensions'
'	- means fluctuating values
$\bar{}$	- means time-averaged

Subscript

h	- values at z* = h
rms	- root-mean-square
β'	- fluctuating value
∞	-free-stream

1. INTRODUCTION

The study of aerodynamic forces on tall buildings produced by strong turbulent winds can now be accomplished through the use of scaled models placed in a suitable wind tunnel capable of simulating the atmospheric surface layer. The air never flows smoothly but always is accompanied by a certain level of turbulence. When an obstacle, i.e., a structure, is in the path of the wind the flow is deflected. The resultant change in momentum results in a pressure acting on the structure. This dynamic action of wind on tall buildings is of utmost importance for their efficient design.

Knowledge of the mean pressure distribution permits computation of the mean forces and moments. Furthermore, the fluctuating (rms) and instantaneous peak pressure are of particular importance for adequate design of the outer skin panelling and the choice of window glass.

The primary purpose of this investigation was to find the pressure distribution, i.e., mean, fluctuating (rms) and instantaneous peak pressure, on a scaled model of the buildings planned for the Atlantic-Richfield Plaza in Los Angeles. The study has sought mainly to obtain the pressure distribution for various flow directions and under real flow conditions. An adequate model of the buildings and of the upstream urban configuration had to be constructed. Furthermore, a relatively thick turbulent boundary layer was necessary in order to simulate the field flow conditions in the wind tunnel.

Flow visualization by means of tufts was used to give an over-all picture of the flow pattern. Surveys of mean velocity and turbulence intensity of the flow upstream of the structure were performed. Detailed measurements of the pressure distribution on the building model for three wind directions (NE, N and NW) were conducted. Moreover, surveys of the turbulence-energy spectra and pressure-fluctuations spectra on the surface were also made at several locations.

An exploratory effort to measure directly the fluctuating overturning moment produced by a turbulent wind was carried out. The mean pressure enables one to compute the mean overturning moment but the local pressure fluctuation does not yield the fluctuations in the overturning moment since the instantaneous pressure-fluctuations space correlations on the surface are not known. For measuring the instantaneous fluctuating overturning moment a suitable aerodynamic balance was constructed.

2. EXPERIMENTAL APPARATUS

The aim of this work was to obtain the overall and local wind loading on a model of the buildings planned for the Atlantic-Richfield Plaza in Los Angeles. This was achieved by a thorough exploration of mean, fluctuating (rms) and instantaneous peak pressures acting on a suitable model placed in a wind tunnel. The latter is of interest for certain structural considerations. In addition, a direct measurement of the total overturning moment, i.e., mean and fluctuating moment, acting on the building was made.

The experimental objective could not be accomplished by simply placing an appropriate model in a regular aerodynamic wind tunnel [1,2]. A rather detailed discussion of this problem is reported in References 3, 4 and 5. It was desired to obtain a suitable thick boundary layer and a mean velocity profile similar to the real flow conditions prevailing throughout the atmospheric-surface-layer over an urban area. Consequently, the experiments were carried out in an appropriate wind tunnel which is described later.

The flow around buildings can be considered similar to flow around bluff bodies at relatively large Reynolds numbers. When the flow is simulated in a wind tunnel, dynamic similarity needs to be satisfied. However, for sharp edged structures at relatively large Reynolds number, i.e., of the order of 10^5, the drag coefficient and, thus,

the pressure distribution and the resulting forces, are independent of the Reynolds number [3,6]. The Reynolds number based on the largest dimension of the building model cross-section and/or the equivalent (hydraulic) diameter of the model is about 150,000. Hence, it follows that the flow may be assumed Reynolds number independent.

For these reasons, it was decided to use a simple model placed in a relatively thick turbulent boundary layer formed over a rough surface. The latter simulated the urban configuration upstream of the model. A schematic diagram of the experimental arrangement and of the low-speed wind tunnel used is displayed in Fig. 2.1, which also shows all important dimensions.

2.1 The model building

A scaled model of two towers planned for the Atlantic-Richfield Plaza was made of "Lucite" 0.375 in. thick. Both buildings are of similar rectangular shape and 666 ft high. A geometrical length scale of 1:384 was employed. This scale was chosen for obtaining a meaningful simulation of the natural wind over a build-up area and to restrict wind-tunnel blockage. Generally, the atmospheric boundary layer is about 1600 ft thick, thus, about 2.4 times the building height. Consequently, a boundary layer about 50 in. thick was desired.

A schematic diagram of the model arrangement in the wind tunnel is shown in Fig. 2.1. The model towers employed are portrayed in Fig. 2.2 which also shows the system of coordinates used and all important dimensions. Since both towers are similar, the static pressure taps were drilled only on two walls and the roof of a single tower. The 1/16-in. diameter taps were located as follows: 32 on the wide wall, 22 on the narrow wall and 13 on the roof. For measuring the pressure distribution along the other two walls it was necessary to rotate the model by 180°. Hence, it was possible to monitor the pressure at 121 locations for each tower. Next, interchanging of towers permitted measurement of the pressure distribution on the second tower under the same upstream conditions. The static pressure tap stations are shown in Fig. 2.3.

The surrounding buildings in the immediate vicinity were also modeled employing a similar scale. They were constructed of styrofoam. Both towers and these buildings were mounted on a rotatable plywood sheet base (see Figs. 2.1 and 2.2). For investigating the dependence of pressure distribution on the approaching wind direction it was possible to rotate the table 360°. Furthermore, the rotating base permitted visualization of the flow pattern for various wind azimuths. Photographs showing this arrangement for the NE and N wind directions are provided by Figs. 2.4 and 2.5, repectively.

2.2 Wind tunnel

The experimental investigation reported herein was conducted in the low-speed wind tunnel of the Fluid Dynamics and Diffusion Laboratory, Colorado State University. This tunnel is of closed circuit type and has a working section 36.5 ft long (see Fig. 2.1). Its axial-flow blower is driven by a 75 hp constant speed motor. The blower is capable of generating air speed up to 65 fps in a 6 x 6 ft test section. The air speed can be changed continuously by varying the fan-blade pitch. The center of the model base was placed 29.15 ft downstream of the entrance section. Therefore, the model buildings were located in a thick boundary-layer region.

The removable side panels of the working section are made of glass in order to allow flow visualization. Along the center line of the top panel a Pitot-static tube was inserted above the upstream building for continuous monitoring of the free-stream velocity, i.e., outside the boundary layer. Its location is shown in Fig. 2.1.

An electrically operated traversing and positioning mechanism was used for continuous movement of the Pitot-static tube and/or hot-wire probe. This mechanism permitted fine control of position within 0.05 in. along lines parallel to the x, y and z-axes, respectively.

2.3 Upstream conditions

A complete simulation of the natural wind characteristics includes the generation of a suitably thick and turbulent boundary layer [3,4]. Furthermore, the modeling of the upstream urban configuration is necessary for simulating the real flow conditions. As a result, the upstream urban topography was appropriately modeled by using the same scale as for the buildings. The upstream model extended over a distance of more than one mile (see Fig. 2.1). This was achieved by covering the tunnel floor with an adequate configuration of modular bricks (2-1/4 x 3-5/8 x 7-5/8 in). For every particular wind azimuth, i.e., free-stream velocity direction, an appropriate upstream roughness configuration was employed.

For generating a flow with a relatively high turbulence level a vortex generator [7] was installed at the entrance of the working section (see Fig. 2.1). This generator also caused an initial thickening of the boundary layer. For this purpose an asymmetric arrangement of two rows of modular bricks 1.3 ft total height was used. A photograph of the vortex generator is shown in Fig. 2.6. Both the upstream roughness, i.e., the upstream modeled city, and the vortex generator produced the necessary thickening of the boundary layer and the desired turbulence intensity level.

3. EXPERIMENTAL TECHNIQUE AND INSTRUMENTATION

3.1 Flow visualization

Two visualization methods were employed, paper tufts and thread tufts. The former, attached to wire grids and placed upstream and/or downstream of the model buildings, was used to obtain a qualitative picture of the flow pattern for various wind directions.

On the other hand, the thread tufts were glued directly on the model faces. They permitted an acceptable qualitative indication of the flow pattern along the building faces to be obtained. As will be seen later both visualization methods established clearly the overall flow pattern and the existence of vortices downstream of the buildings. Moreover, the influence of the surrounding buildings on the flow was also observed.

3.2 Pressure and velocity measurement

Average static pressures on the model faces were measured by means of an electronic pressure meter (Trans-Sonic, Type 120 A) with a resolution of 0.0001 mm Hg. The overall range of this manometer is 30 mm Hg divided in eight ranges.

A Pitot-static tube located 2.43 ft above the model, as shown in Fig. 2.1, was employed to measure the static pressure and the mean velocity of the uniform flow. A Prandtl standard Pitot-static tube with a hemispherical impact head was employed [8]. Its impact orifice is

1/32-in. in diameter. This probe was also used to measure the velocity profile upstream of the building. The velocity change along the z-axis was measured 1 ft upstream of the model. In performing these measurements the Trans-Sonic pressure meter was utilized. Furthermore, the velocity variation along the vertical direction was also recorded by means of a x-y plotter (F. L. Moseley Co., Model 135). This was carried out by moving the Pitot-static probe continuously using the traversing mechanism.

The fluctuating pressure, rms and instantaneous peak pressure, on the model faces were measured at the pressure taps by means of low-pressure differential pressure transducers (Statham, Model PM 283). The pressure difference was measured with respect to the static pressure of the uniform free stream at 2.43 ft above the top of the buildings. Six similar transducers were utilized. These transducers were installed inside the model and connected closely to the pressure taps. The transducers with the associated tubing (3/8-in. I.D. vinyl tubing, about 3 in. long) had a frequency response larger than about 200 Hz. The transducers exhibited a reasonable linear calibration curve. The latter was carried out by using a precise micromanometer (The Meriam Instrumentation Co., Model 34 FB 2). A sample of the kind of calibration curves obtained is shown in Fig. 3.1. The reproducibility of the calibration curves was within 3%.

In connection with these measurements the following auxiliary equipment was used:

(1) A variable range amplifier (Dana, Model 3500). Generally, an amplification of 200 was utilized;

(2) A seven-channel tape recorder (Mincom, Type 100) for recording and storing the amplified signal for further analysis;

(3) An electronic voltmeter (Bruel and Kjaer, Type 2416) for measurement of rms and peak values;

(4) A recording wave analyzer (General Radio, Recording Sound and Vibration Analyzer, Type 1911-A) for frequency spectra measurement;

(5) A dual-beam oscilloscope (Tektronix Storage Oscilloscope, Type 564) for quick assessment of the output signal pattern;

(6) A Polaroid camera (Type C-12) for taking oscillograms of the output signal;

(7) A digital DC voltmeter (Hewlett-Packard, Model 3440 A) for monitoring various output signals.

The bridge used in relation with the pressure transducer was conceived and built at the Fluid Dynamics and Diffusion Laboratory. A simplified block diagram of this system is shown in Fig. 3.2, and a general view of the auxiliary equipment is provided by Fig. 3.3.

3.3 Turbulence-intensity measurement

The longitudinal turbulence intensity was measured upstream of the model by means of a single hot-wire anemometer. The measurements were carried out at the same distance

from the model as for the mean velocity, i.e., at 1 ft upstream of the model along the z-axis. When performing these measurements the hot-wire probe was positioned by means of the traversing mechanism. The hot-wire anemometer unit used in the present experiment is a constant-temperature fully transistorized system conceived, designed and built at the Fluid Dynamics and Diffusion Laboratory. Its output noise level is less than 200 μV over its entire range and its frequency response is beyond 100 KHz. A tungsten wire of 0.00025 is nominal diameter and aspect ratio, l/d, of 240 (l being the wire length and d its diameter) was employed.

The hot-wire calibration was effected by placing it in the free stream above the model. It was carried out by employing a Pitot-static tube. The calibration curves revealed that the so-called King's law [9], i.e., the 1/2 power linear relation ($E^2 \propto \sqrt{U}$) was satisfied for the velocity range of interest--from about 10 to 60 fps. A sample of the kind of calibration curve obtained is provided by Fig. 3.4. It was reproducible within 3%.

The turbulence intensity, which is commonly defined as $u_{rms}/\bar{U}$, is given by [10]

$$\frac{u_{rms}}{\bar{U}} = \frac{4\bar{E}^2}{\bar{E}^2 - E_o^2} \frac{e_{rms}}{\bar{E}}, \qquad (1)$$

where the subscript rms denotes square-root of mean (time-averaged) square value, i.e., $\sqrt{\overline{u^2}}$ and $\sqrt{\overline{e^2}}$, and, the overbar denotes time-averaged (or mean) values. In the above relationship the mean velocity is designated by $\bar{U}$ and $\bar{E}$ stands for the time-averaged voltage drop across the wire, i.e., the DC voltage necessary to balance the bridge under steady conditions. The fluctuating velocity is denoted by u and the corresponding instantaneous voltage drop by e, i.e., the instantaneous AC voltage. The voltage drop across the wire in still air (zero velocity or shielded hot-wire) is denoted by E_o. It is constant for a particular wire and a chosen resistance ratio (overheating ratio). In connection with the hot-wire unit a true RMS meter, a digital DC voltmeter and a dual-beam oscilloscope were used.

3.4 Moment measurement

As mentioned earlier, a direct measurement of the total overturning moment, i.e., mean and fluctuating, was also made. In order to eliminate all the other force components a suitable strain-gage dynamometer system was conceived and built at the Fluid Dynamics and Diffusion Laboratory. The model was mounted in the wind tunnel by attaching it rigidly to an aluminum beam (2 x 1 x 5 in) by means of four rods 90° apart. In turn, the beam was stiffly anchored to a massive base located underneath the wind-tunnel floor. Thus, the dynamometer-building model system constituted a cantilever beam with an end-load.

Aerodynamic forces acting on the model building were transmitted to the beam by two adjustable pins 180° apart. These pins were positioned close to the free-end of the beam and were tightened manually to the former. At the lower end of the beam four foil strain-gages (Micro-Measurement, Type ED-DY-250B6-350) were cemented. They constituted the four arms of a Wheatstone bridge. Thus, the overall sensitivity of the strain-gage system was increased four times. This balance was sensitive only to the overturning moment about the weak axis of the building. The response of the strain-gage for any lateral load was about 20 times smaller than for the frontal force producing the overturning moment. In order to stiffen the model and to increase its natural frequency an aluminum rib and stiffening rods were mounted rigidly between its two wider faces. A sketch of the balance system is portrayed in Fig. 3.5. Figure 3.6 is a photograph which shows the beam with the cemented strain-gages.

For obtaining reliable and dependable measurements of the moment due only to aerodynamic forces in a stationary structure the natural frequency of the entire aeroelastic system, i.e., the beam and the building model, should be larger than any forcing frequencies. The pressure survey revealed that the maximum frequency of interest was smaller than about 200 Hz. Consequently, the balance system was conceived such that its natural frequency was 200 Hz. The strain of the beam for a moment of about 25 lb-in was of order of 6μin/in.

As a result, a relatively stiff model was obtained. For a free-stream velocity of 50 fps the reduced velocity [4] U_∞/an was about 0.43, where a is the largest dimension of the model cross section and n the natural frequency of the dynamometer system. Thus, the tip deflections of the model were negligible. The reduced velocity is equivalent to the reciprocal of the Strouhal number.

A simplified block diagram of the moment measuring system is provided by Fig. 3.7. Essentially, the same auxiliary equipment as employed for the pressure measuring system was utilized. The excitation and balance network of the strain-gage are also shown in Fig. 3.7.

The balance was calibrated by applying various forces at different heights along the building under static air conditions. A sample of calibration curve obtained is shown in Fig. 3.8. A satisfactory linear variation was obtained. The reproducibility of the calibration curves was within 2 to 5%.

4. RESULTS

The experimental investigation of the flow about the building has the following main purposes:

(1) To obtain the pressure distribution (mean, fluctuating and instantaneous peak pressure) on the buildings. It was measured for three wind directions, NE, N and NW, as portrayed in Fig. 2.2. This was achieved by suitable rotation of the turnable base and adequate arrangement of upstream roughness.

(2) To measure directly the total overturning moment (mean and fluctuating). It was carried out only for NE wind direction. The direction was found to be the most suited one for this study due to the problems related to the aerodynamic balance design.

The system of coordinates used in the presentation of the results is portrayed in Figs. 2.1 and 2.2. A similar system was employed for each tower. For generality, the results are presented in dimensionless form. Dimensional variables, wherever employed, are denoted by an asterisk. As the experimental results are presented below, some pertinent discussion is interspersed wherever it is deemed helpful for the proper interpretation of the results.

4.1 Establishment of the flow

An extensive series of flow visualization trials were carried out for the purpose of obtaining a picture of the flow pattern upstream and, mainly, downstream of the building.

Visualization of the flow by means of paper tufts gave a clear picture of the flow pattern within the wake. Its strongly turbulent features and its vortex structure were clearly discerned. Typical photographs of the paper tufts for all three wind directions are shown in Fig. 4.1. In all cases the wake extended vertically above the model up to about 10% of its height. The disturbed state of the approaching flow in the case of N wind is clearly observed (see Fig. 4.1). It is caused by a building 17.5 in. tall located immediately upstream of the towers.

The thread tufts glued to the model walls gave a relatively good indication of the flow pattern along them. By using the same tower as L - and/or R - tower the flow along both buildings was visualized. Generally, a down draft was discerned along the upwind wall. Near its bottom a rotational trend was observed. On the other hand, along the leewind wall an upward draft and a rather turbulent rotational pattern was indicated by the tufts. A similar flow pattern is reported in References 6 and 11. Along the faces parallel to the flow a rather disturbed and rotating flow pattern was observed. Samples of the photographs of the thread tufts for the three wind directions, i.e., NE, N and NW, along faces 4-1 and 1-2 of both towers are displayed in Figs. 4.2, 4.3 and 4.4, respectively. A motion picture of the flow visualization was also taken.

4.2 Mean velocity survey

The wind velocity gradient upstream of the building is of utmost importance in determining the flow characteristics. Its variation with height depends upon the particular configuration of the upstream roughness structure [12]. Generally, the mean velocity profile over terrains of differing roughness configuration is given either by a logarithmic or a power law [12]. The latter may be described by

$$U^* \propto z^{*\alpha} , \qquad (2)$$

where z^* denotes the height. The value of the exponent α depends on the particular roughness structure. This representation was employed in the present work.

The mean velocity variation along the z direction was measured upstream of the model, i.e., at 1 ft upstream of the building model, at more than 15 stations over a distance of about 55 in. All the measurements were performed at an uniform free-stream velocity of 50 fps. At this velocity, denoted by U_∞^* a sufficiently thick boundary layer (approximately 50 in.) at the building location could be obtained. The Reynolds number based on the largest dimension of the cross-section is about 182,000 whereas based on the equivalent diameter it is 130,000.

The mean velocity was measured for various upstream conditions. This experiment was performed for verifying the adequacy of the atmospheric-surface-layer flow simulation

in the wind tunnel. The measurements were carried out for the following cases: (1) clear wind tunnel; (2) vortex generator installed; (3) vortex generator and upstream roughness, i.e., the scaled model of the upstream city configuration, installed (real flow conditions). In all these three cases the scaled model of the building and of the immediate surrounding buildings were located in the wind tunnel (see Fig. 2.1). It was found that the velocity change is strongly affected by the upstream conditions. The power law was satisfied in all the cases, but the value of the exponent α differed for each case.

Hereafter, all the results are presented in dimensionless form. The dimensionless coordinates are defined by

$$x, y, z = x^*/h, y^*/h, z^*/h, \tag{3}$$

where h is the building height (20.75 in), and the dimensionless velocity by

$$U = U^*/U_h^* , \tag{4}$$

where U_h^* is the measured upstream mean velocity at $z^* = h$. Hence, the dimensionless mean velocity is given by

$$U = z^{\alpha} . \tag{5}$$

The mean velocity variation along the vertical direction for the aforementioned three cases and NE wind direction are displayed in Fig. 4.5. The results

were reproducible within 3 to 5%. The field wind profile (case (4)) is also shown in this figure. The latter is based on 100-year wind data at 250 ft height above the ground. The wind variation was obtained by using 1/3-power law for selected heights between 250 ft and 1000 ft. On the other hand, a 1/3-power law was employed for heights below 250 ft [13]. The velocity profiles for the N and NW wind directions and for case (3) are displayed in Fig. 4.6. No measurements for the cases (1) and (2) were carried out for these two flow directions.

For the sake of comparison the results are summarized below:

Wind Direction	NE		N		NW		Field	
Case	U_h^* (fps)	α	U_h^* (fps)	α	U_h^* (fps)	α	U_h^* (fps)	α
1	46.9	0.107	----	-----	----	-----	---	-----
2	45.1	0.206	----	-----	----	-----	---	-----
3	45.6	0.446	45.6	0.410	45.0	0.520	---	-----
4	----	-----	----	-----	----	-----	100	0.157

Note that $h = 20.75$ in. for the wind tunnel result whereas $h = 666$ ft for the field results (case (4)).

The small value of α based on the field data reported in Ref. 13 is probably caused by the assumptions used for computing the wind profile from data at a single height.

The values of the exponent are in general agreement with its representative values reported in References 12 and 14. For instance, a value of 0.40 for flow over cities is suggested in Reference 12 whereas in Reference 14 the suggested value of α varies between 0.25 to 0.45 depending upon the particular urban conditions. The influence of the upstream conditions, i.e., vortex generator and/or upstream modeled city, is clearly observed. Thus, the simulation of the atmospheric surface layer was acceptable.

As mentioned earlier, a suitable thick boundary layer was desired for meaningful simulation of atmospheric surface layer conditions. Consequently, it was important to find out the vertical extent of the boundary layer immediately upstream of the model. The boundary-layer thickness was defined, as is commonly done, as the distance from the wind tunnel floor where $U^*/U^*_\infty = 0.995$. The recorded dynamic head profiles, which are proportional to the velocity, upstream of the model for all three flow directions in case (3) are displayed in Fig. 4.7. During the experiments the ambient pressure was 24.75 in. Hg and air temperature 75° F. The corresponding air density is 0.00187 slugs/ft^3. Note that the wind tunnel is situated at an elevation of about 5000 ft. The records were obtained by continuously moving the Pitot-static tube using the traversing mechanism. Based on these measurements the boundary-layer thicknesses were approximated. For the sake of comparison the results for all three flow directions are summarized below:

Wind Direction	δ^* (in)	δ
NE	49.7	2.40
N	48.5	2.34
NW	47.6	2.30

Thus, the boundary-layer thickness varies slightly depending on the flow direction. This corresponds to a real boundary layer of about 1530 to 1600 ft thick. Hence, a sufficiently thick boundary layer was achieved and the simulation conditions were fulfilled.

4.3 Turbulence intensity measurement

Simultaneously with mean velocity measurements the turbulence intensity based on local mean velocity,

$$Tu_x = \frac{u_{rms}(z)}{\overline{U(z)}} , \qquad (6)$$

was monitored. In this relationship u is the fluctuating velocity parallel to the mean flow velocity $\overline{U}$, and the subscript rms denotes square root of mean (time averaged) square value, i.e., $(\overline{u^2})^{\frac{1}{2}}$.

The results for NE wind in case (3) are displayed in Fig. 4.8. They were reproducible within 2 to 3%. Both the turbulence intensity based on local and on free-stream mean velocity, i.e., based on $\overline{U}(z)$ and $\overline{U}_\infty$, are shown. Based on the local mean velocity a maximum turbulence intensity of about 29% was measured at $z = 0.05$, whereas based on $\overline{U}_\infty$ a maximum of about 12.5% was monitored at $z = 0.4$. The different location of the maximum is caused by the

variation of the local mean velocity. As the free-stream region is approached the difference between them diminishes. It practically vanishes at about 0.2 h above the building. The turbulence intensity at the outer edge of the boundary layer, i.e., at $z = 2.4$, was about 0.2%. This is practically the free-stream turbulence intensity. The relative high turbulence level throughout the boundary layer was caused by the upstream conditions, i.e., vortex generator and upstream roughness. Similar turbulence intensity variations were measured for the other two flow directions, N and NW.

Unfortunately, no satisfactory field data is available for comparing the turbulence intensity distribution. However, it is important to notice that the results exhibit a reasonable agreement with the measurements in the lowest atmosphere reported by Singer [15].

4.4 Pressure survey

The aerodynamic forces and moments acting on a structure are determined by the approaching wind characteristics. Due to the velocity gradient and turbulence within the atmospheric surface layer (the boundary layer) both mean and fluctuating forces are of importance in finding the structural response to wind loading. Furthermore, the local instantaneous peak force together with the fluctuating force are of main concern in designing outer skin panelling and window glass. Knowledge of the pressure distribution,

i.e., mean, fluctuating and peak pressure, permits computation of these forces.

A detailed survey of the pressure distribution along the building model was carried out for all three flow directions in case (3), i.e., vortex generator and upstream roughness installed, at a constant upstream velocity, U_∞^*, of 50 fps. The local pressure was measured with respect to the static pressure of the free stream above the model, i.e., the static pressure outside the boundary layer. The latter was monitered by means of a Pitot-static tube located as shown in Fig. 2.1.

The total local pressure at any point on the wall is

$$p - p_\infty = (\overline{p} + p') - p_\infty \quad , \tag{7}$$

where p is the total local pressure, $\overline{p}$ the local mean pressure, p' the local fluctuating pressure and p_∞ the free-stream static pressure. The overbar denotes time-averaged (or mean) values. Next, Eq. (7) can be written

$$\Delta p = \overline{\Delta p} + p' \quad , \tag{8}$$

where

$$\overline{\Delta p} = \overline{p} - p_\infty \quad . \tag{9}$$

The free-stream pressure fluctuations are completely negligible with respect to the pressure fluctuations on the structure. It should be recalled that the turbulence intensity of the free stream flow is about 0.2%. Then, by taking the mean-square of the total local pressure we obtain

$$\overline{\Delta p^2} = \overline{\Delta p}^2 + \overline{p'^2} \quad . \tag{10}$$

For incompressible flow at low velocities the local mean pressure coefficient is defined by

$$c_p = \frac{\overline{\Delta p}}{1/2\rho U_\infty^{*2}} \quad . \tag{11}$$

Similarly, the local fluctuating pressure coefficient can be defined by

$$c_{p_f} = \frac{p_{rms}}{1/2\rho U_\infty^{*2}}, \tag{12}$$

where p_{rms} denotes square-root of mean (time-averaged) square values, i.e., $\sqrt{\overline{p'^2}}$. In the above two relationships U_∞^* represents the free-stream velocity above the model and ρ is the air density ($\rho = 0.00187$ slug/ft^3, see Section 4.2). In a similar fashion the local instantaneous peak pressure coefficient is defined by

$$c_{p_{max}} = \frac{p'_{max}}{1/2\rho U_\infty^{*2}}, \tag{13}$$

where p'_{max} is half of instantaneous peak-to-peak pressure fluctuation. In terms of the mean pressure coefficient, the local fluctuating and peak pressure coefficient are

$$\frac{c_{p_f}}{c_p} = \frac{p_{rms}}{\overline{\Delta p}} , \tag{14}$$

and

$$\frac{c_{p_{max}}}{c_p} = \frac{p'_{max}}{\overline{\Delta p}} . \tag{15}$$

Generally, along the upwind faces of a tall building relatively large positive pressure occurs since the flow is brought to rest. Due to the upstream velocity gradient the pressure is usually larger along the building upper part than along its lower portion. As a result a downward flow carrying energy to ground level exists along these faces. Simultaneously, high pressure fluctuations develop along the lower part. Furthermore, local changes can occur due to various particular upstream conditions, i.e., surrounding buildings and/or local upstream topographic conditions. These local distributions may affect strongly the pressure fluctuations.

A peculiar property of any building shape, which is classified as a bluff body, is the wake of separated flow surrounding its rear part. The flow is deflected by the

upwind faces but separates completely from the surface at a sharp edge. This is because the fluid inability to undergo a large acceleration necessary to follow the surface at the corners. Throughout the wake the velocity is much smaller than the mean flow and, as a result, almost uniform negative mean pressure with respect to the surrounding exists on the rear surfaces. Moreover, high velocity and pressure fluctuations do prevail in this region due to the entrainment process along it. The negative mean pressure is determined by the pressure at the separation region. Since it depends upon the shape and relative position of the structure with respect to the approaching wind it follows that the pressure distribution does depend on the flow direction. It is, further, important to notice that the wake extends vertically above the structure up to more than 10% of its height. Consequently, negative mean pressure and relatively large fluctuations occur along the roof. The separation location depends upon the particular shape and size of the building and wind velocity and direction. For buildings with sharp edges (as most buildings) the separation line is fixed along the edges. A qualitative sketch of the flow pattern around a tall building is depicted in Fig. 4.9 [11].

The twin-tower configuration of the Atlantic - Richfield Plaza buildings causes a more complicated flow pattern and, hence, pressure distribution. The pressure

varies not only with wind direction but also with the relative position of the two towers and position of surrounding structures. For instance, in the case of NE wind the R tower is located in the wake of the L tower. Consequently, a completely different pressure distribution prevails along the former as on the latter. Negative mean pressure (suction) and high pressure fluctuations characteristic of the wake develop on the R tower.

The effect of the immediate surrounding buildings is most prominent in the case of N wind. A building about 3/4 of tower height is located immediately upstream of both towers. As a result they are situated in the wake of this building and, thus, low mean pressure and high fluctuations exist along most of their front faces.

The simpler flow pattern occurs for the NW wind. In this case the wind is almost normal to the narrow faces of both towers and no surrounding buildings are located upstream of them. A sketch of the wind directions with respect to the buildings is portrayed in Fig. 2.2.

The pressure was measured at 121 stations on each tower for the N wind and only along the R tower in NE wind. On the other hand, along the L tower in NE wind and along both towers in NW wind, it was measured only at three levels and on the roof. These levels are located at $z = 0.268$, 0.750 and 0.966 ($z^* = 5.56$, 15.56 and 20.06 in) corresponding to the 14th, 38th and 51st floor, respectively.

At these stories large windows are planned and, therefore, it is important to know the local pressure distribution.

The system of corrdinates used in the presentation of the results is portrayed in Fig. 2.2. For obtaining a complete picture of the pressure distribution, its value was approximated by linear interpolation and/or extrapolation at any location of interest. The latter was carried out along all three axes (x, y, and z) as required. The detailed results for all flow directions and along the towers at all measurement stations are presented in Appendix I. However, the main features of the pressure distribution for each flow direction are summarized in the following three sections.

4.4.1 *Pressure survey for NE Wind*

The wind incidence angle measured counterclockwise from the x-axis is 6° and, hence, it is practically normal to the wide face of the tower. In order to test the variation in time of the fluctuating pressure at every position on the tower, the pressure transducer signal was monitored on an oscilloscope over a period of several minutes. The observed changes were completely negligible. A typical oscillogram of the output signal along the narrow face is displayed in Fig. 4.10.

Mean pressure coefficient distribution and contours of ratios of the fluctuating and peak pressure coefficient to the former along all faces of L tower are portrayed in

Figs. 4.11a to 4.11c. Since mean pressure coefficient can be either positive or negative, its absolute values was employed in computing the aforementioned ratios.

The results along upwind face 4-1 of L tower are shown in Fig. 4.11a. The highest pressure was measured along the upper part. A sevenfold decrease was monitored as the base is reached. Concurrently, an opposite trend was discerned for the fluctuating and peak pressure. Their largest values were monitored near the base. Note that turbulence level was higher near the base than along the upper part of the tower. In general, the fluctuating pressure coefficient was smaller than or of the same order of magnitude as the mean pressure coefficient whereas the peak pressure coefficient is almost always larger than both mean and fluctuating pressure coefficients at same locations. Near the base, where the smallest mean pressure prevails, peak pressure up to 3 to 4 times larger than the mean pressure was measured. It is caused by the flow turbulence on the the upwind face and by the wake on the leewind surface.

As previously mentioned, the flow separation occurred at the sharp edges 44 and 11 of the L tower. Consequently, negative mean pressures were measured along faces 1-2, 2-3 and 3-4, as shown in Figs. 4.11a and 4.11b, respectively. Along the leewind wide face (face 2-3) a much smaller variation than along the upwind face was found. It decreases only by about 3 times as the base is approached. Furthermore, a more uniform pressure distribution was found along the narrow faces parallel to the flow (faces 1-2 and 3-4).

The fluctuating and peak pressure on faces 1-2, 2-3 and 3-4 exhibited a similar variation as on the upwind face. Their values were higher near the base than close to the top.

The results along the L tower's roof are displayed in Fig. 4.11c. A relatively even mean pressure distribution exist. Its maximum variation is only about 12%. Both fluctuating and peak pressure undergo a gradual augmentation from the upwind edge toward the leewind edge. Roughly, a twofold amplification was measured.

The pressure distribution at the three levels along the R tower is depicted in Fig. 4.11d. In this figure the fluctuating and peak pressure coefficients are presented directly without dividing them by the local mean pressure coefficient. Recall that the R tower is located in the wake of the L tower. Relatively small negative mean pressure and relatively high fluctuating and peak pressure were measured. Particularly, the pressure distribution on the upwind face 4-1 indicates the wake effect. On its leewind face smaller mean, fluctuating and peak pressure coefficient than along the upwind and side faces, respectively, were monitored. It is important to notice that this face is under the influence of the wakes generated by the L tower and of it own. As a result of this situation larger pressure fluctuations (fluctuating and peak pressure) were measured at the higher two levels than along the corresponding heights on the L tower. Along R tower's roof only the mean pressure was measured. The results are

also displayed in Fig. 4.11d. The prevailing pressure is about half of that measured on L tower's roof.

It is possible to define an average pressure for each cross-wise area element, i.e., pressure per unit area normal to the mean velocity. These averages were computed for the upwind and leewind faces of L tower. The variations of the average mean, fluctuating and peak pressure coefficient with height are displayed in Fig. 4.12. The mean and fluctuating pressure exhibit a linear variation along both faces. The slope of the former is positive for both faces whereas of the latter is positive along the upwind side but negative along the leewind face. It can be inferred that the mean force acting on the tower will reveal a similar behavior with height. On the other hand, the average peak pressure reveals roughly a periodical change along both faces. The wavelength is approximately $0.2\ z$ and the oscillations along both faces are in phase along the upper half of the model. This periodical change is probably caused by the flow turbulence. In other words, if most of the turbulence energy is concentrated at some particular frequencies, then, the resulting pressure fluctuations may also exhibit similar predominant frequencies.

It was important to verify the pressure distribution invariance with Reynolds number. This was achieved by measuring the mean pressure coefficient at two different upstream velocities of 30 and 50 fps, respectively, while other conditions were unchanged. The Reynolds numbers,

based on the largest width of the tower, are about 108,000 and 180,000 respectively. A normalized pressure coefficient difference,

$$\gamma = \left| \frac{c_{p(50)} - c_{p(30)}}{c_{p(50)}} \right| , \qquad (16)$$

was computed. In this relationship $c_p(50)$ and $c_p(30)$ are the local mean pressure coefficients at $U^*_\infty = 50$ and 30 fps, respectively. Both pressure coefficients were measured at 97 randomly selected sample points. In Fig. 4.13 the number of points at constant γ are displayed. At 77 sample points $\gamma<0.2$ whereas at 41 points $\gamma = 0.025$. Only at one sample station $\gamma > 0.8$. It is suspected that the latter was caused by some experimental error. Hence, the change in pressure coefficient with wind velocity is completely negligible. Consequently, it is conceivable to assume that the pressure distribution is Reynolds-number independent.

4.4.2 *Pressure survey for N wind*

In this case the flow incidence angle measured counter-clockwise from x-axis is 51°. It is, further, important to remark that a relatively high building (about 3/4 of the tower height) is located immediately upstream of the model towers. As a result relatively low mean pressure and simultaneously high fluctuating and peak pressures were obtained. This particular variation is due to both the

approaching turbulent flow and the wake produced by the upstream high building.

The results along the wide and narrow upwind surfaces, i.e., faces 4-1 and 1-2, of L tower are displayed in Figs. 4.14a and 4.14b. The mean pressure diminishes gradually from maxima at the upper part to a low at the center zone. The latter extends roughly from $z = 0.4$ to 0.6. Its location is due to the wake generated by the upstream surrounding building. This low is followed by an increase as the base is approached. The wake effect is stronger on the narrow face than along the wide face. On the former the low is about ten to fifteen times smaller than on the latter. Moreover, a higher ridge was measured on the face 1-2 than on side 4-1 near the base. A fifteenfold increase was recorded on the narrow face while only a twofold amplification on the wide surface. Concurrently, $^{c}p_{f}/\ |c_{p}|$ and $^{c}p_{max}/\ |c_{p}|$ reached their high values at the center region. Furthermore, they are larger close to the base than near the top. For instance, on the wide face (face 4-1) fluctuating and peak pressures up to 2 and 9 times, respectively, larger than the mean were monitored at the center. On the narrow side (face 1-2) fluctuating and peak pressure as high as 15 and 60 times, respectively, the mean pressure were measured. Thus, the local perturbations produced by the tall upstream building are clearly discerned.

The pressure distribution along the wide and narrow leewind faces, i.e., faces 2-3 and 3-4, of L tower, are shown in Fig. 4.14b. Negative mean pressure (suction) exist along both surfaces. The lowest values were measured near the model base. At the same time, $^{c}p_{f} / |c_{p}|$ and $^{c}p_{max} / |c_{p}|$ reached their high values in the same region.

The results for the R tower are displayed in Figs. 4.14c and 4.14d. On faces 4-1 and 1-2 the mean pressure is largest near the upper part and decreases monotonically toward the base. It is interesting to remark that c_{p} is positive along face 1-2 but negative along the leewind half of the wide face 4-1 (see Fig. 4.14c). This indicates that the separation does occur along the leewind part of face 4-1 and not along the edge 11. Its peculiar location is due to the relatively complicated flow pattern caused by the surrounding building. An opposite behavior was found for both $^{c}p_{f} / |c_{p}|$ and $^{c}p_{max} / |c_{p}|$. Their high values were monitored between the center and base. Along the leewind faces, i.e., faces 2-3 and 3-4, a similar variation was observed. Note that the mean pressure is negative along these faces.

The pressure changes along the roofs of both L and R tower are protrayed in Fig. 4.14e. The suction diminishes as the trailing edge is approached. An opposite gradient was monitored for $^{c}p_{f}/ |c_{p}|$ and $^{c}p_{max}/ |c_{p}|$. They are larger near the leading edge than at the trailing edge.

4.4.3 *Pressure survey for NW wind*

As mentioned earlier, the pressure was measured at three particular stories and along the roof. On the latter only the mean pressure was recorded. The flow incident angle measured with respect to x-axis is 96°. Thus, the mean flow is almost normal to narrow upwind faces of both towers. At the lowest story, i.e., at $z = 0.268$, the pressure was monitored only at one station on each of the narrow faces.

The results are shown in Figs. 4.15a and 4.15b for L and R tower, respectively. On the upwind narrow faces of both towers (face 1-2) the mean pressure was found to be larger at the upper two levels than at the lower level. On the other hand, along the leewind narrow sides (face 3-4) it was approximately constant at all three levels on both towers. The wide faces are parallel to the flow and, consequently, larger pressure was observed along them than on the narrow sides. Since there is no any immediate upstream building the separation occurred along edges 11 and 22.

The fluctuating and peak pressure coefficients are also shown directly in the aforementioned two figures. A similar behavior was monitored along both towers. They are larger at the lower levels than at higher stories. In general, the pressure fluctuations reveal a similar behavior to that observed along the L tower in NE wind.

The mean pressure distribution along roofs is also shown in Figs. 4.15a and 4.15b, respectively. It increases as the trailing edge is approached. For instance, more than a threefold augmentation was monitored.

It is interesting to examine the local pressure variation with change of flow direction. In other words, to find out the wind direction effect on the pressure at a given position on the building. The comparison was carried out for the measurement stations located at the geometric center of the all four faces at three heights, i.e., at $z = 0.966$, 0.750 and 0.268. The results for the L and R tower are displayed in Fig. 4.16. Note that the wind angle changes from 6° to 96°.

Along the wide face (face 4-1) of L tower and at the two higher heights the mean pressure coefficient decreased drastically with incoming incident flow angle. For instance, it diminished from 0.7 at 6° to about -0.4 at 96°. On the other hand, an opposite variation was observed on the upwind narrow surface (face 1-2). Along both wide and narrow leewind faces (faces 3-2 and 4-3) the mean pressure changes slightly with flow direction. Generally, a similar variation was monitored at the lower height for the upwind faces but a relatively larger change was found on the leewind sides.

The mean pressure variation on the R tower seems to depend upon its relative position with respect to the L tower. Recall that in the case of the NE wind, i.e.,

$\alpha = 6°$, it is situated in the wake of the L tower. Similar changes were observed at $z = 0.966$ and 0.750. The mean pressure increases roughly linearly with the flow angle on face 1-2 but exhibits a parabolic variation on side 1-4 with vertex at 51°. This is probably due to its position relative to the L tower. On the leewind faces a smaller variation was measured. Near the tower base, i.e., at $z = 0.268$, a similar change was recorded but the pressure is smaller than at the other two heights.

On the other hand, the fluctuating pressure coefficient exhibits a smaller change. No drastic variations with wind direction and height was observed. Roughly, it changes between 0.1 to 0.3 at all positions. This behavior indicates that it depends mainly on the turbulence of the approaching flow. It should be recalled that the turbulence intensity variation was similar for all three flow directions.

The variation of the peak pressure coefficient with flow angle is also portrayed in Fig. 4.16. A rather drastic variation was observed. Furthermore, its gradient is stronger along the R tower than on the L tower. The highest changes were obtained at the lower height, i.e., near the base. Generally, in this region the smallest mean pressure was measured.

The important aspect of these results is that the fluctuating pressure does not depend strongly on the flow direction but, probably, upon the upstream turbulence and wake characteristics.

4.5 Moment measurement

The local fluctuating and peak pressure do not yield sufficient information for appropriate estimation of the fluctuating overturning moment. The reason for this is that the correlation of pressure fluctuation acting on the structure is not known. Consequently, a direct measurement of the total overturning moment was carried out. As mentioned earlier, for obtaining the moment due to wind action alone a stiff model was used. Its so-called reduced velocity, $\frac{U}{an}$, was found to be 0.43. The natural frequencies of the model-balance unit was about 200 Hz.

The total overturning moment is defined by

$$M = \bar{M} + m' , \qquad (17)$$

where $\bar{M}$ is the mean (time-averaged) moment and m' the fluctuating moment.

The overturning moment was measured for both smooth upstream condition (without upstream roughness) and with upstream roughness installed. All measurements were carried out using the L tower in a NE wind of 50 fps. The latter was chosen because of structural consideration related to the balance design since the flow is roughly normal to the wide surface of the L tower.

An oscillogram of the fluctuating moment taken under real flow condition, i.e., the upstream roughness installed, is shown in Fig. 4.17. It reveals a predominant frequency of about 25 Hz. Note that the predominant frequency moritored during the pressure measurement ranged roughly

from 15 to 30 Hz depending upon the wind direction (see section 4.6). Thus, the existence of a predominant frequency and eddy size is clearly indicated.

Records of total overturning moment variation with time for both cases are displayed in Fig. 4.18. The measurements were reproducible within less than 4%. The mean moment for smooth upstream conditions was about 37 lb-in and on the average the peak value of the fluctuating moment ±8% of the former. The latter was estimated from the record of the total overturning moment.

When the upstream roughness was installed a smaller mean moment was monitored. It was only about 23.6 lb-in, therefore, smaller by 56% than without the upstream roughness. The decrease is due to change in the upstream velocity gradient throughout the boundary layer. The latter is strongly affected by the upstream roughness as shown in Fig. 4.5. In this case the velocity up to about $z = 0.4$ is lower than for upstream smooth conditions. On the other hand, the instantaneous peak value of the fluctuating moment was larger than for smooth upstream condition. It reached up to about ±34% of the mean moment which correspond to a peak moment of 8 lb-in. Concurrently, the rms value of the fluctuating moment was also directly measured. It was found to be 4.8 lb-in, thus 20% of the mean moment. It is important to notice that the turbulence intensity averaged over the tower height was approximately of same order of magnitude. The relatively large increase of the

fluctuating moment is probably due to the turbulence of the approaching flow. Thus, the turbulence energy is presumably the main cause of the fluctuating moment and, hence, they probably exhibit a direct correlation. The latter would depend strongly on the turbulence characteristics of the approaching flow.

The aerodynamic balance yields immediately a direct and rapid measurement of the total overturning moment. Since these results are obtained for a stationary model structure they may be used as a standard reference loading for analyzing dynamic response of structures with specified elastic and mass distribution characteristics.

4.6 Turbulence-energy and surface pressure fluctuations spectrum survey

A survey of the turbulence-energy spectra of the approaching flow along the z-axis and of the surface pressure fluctuations spectra along the model tower were carried out. Following are the results for the NE wind.

The turbulence and pressure fluctuation are random functions of time and space but for stationary flow (on the average), by Taylor's hypothesis [16], the variation in time is essentially the same as in space. Then, the usual spectral analysis is feasible. The one-dimensional total energy for any random fluctuation (per unit mass) is

$$\overline{\beta'^2} = \overline{\beta'^2} \int_0^\infty F_{\beta'}(n)\,dn \quad , \tag{18}$$

where β' denotes the fluctuating value (velocity u' or pressure p') and $F_\beta(n)$ is the fraction of energy within the frequency interval n to $n + dn$, i.e., the frequency-density function. In terms of the mean-square output signal of a wave analyzer, the fraction of energy at each frequency is

$$F(n) = \frac{1}{B_w} \overline{e^2 (n, B_w)}, \qquad (19)$$

where $\overline{e^2(n,B_w)}$ is the square of the rms output at any selected frequency n, B_w the filter bandwidth and n the central frequency within the bandwidth.

The frequency spectra were measured by employing a wave analyzer with a constant-percentage bandwidth of 1/3 octave (23%). For such a bandwidth the bias error caused by its finite size is less then 5% if the changes in the mean-square values are less than 15 db/octave [10]. Furthermore, the side-band effects are negligible if the response time at each frequency is short enough.

The frequency spectra of both fluctuating velocity and pressure were monitored at 8 stations along the z-axis over a distance of about 14 in. They were recorded at same height or within a difference of less than 20%. The former was recorded at 1 ft upstream of the structure simultaneously with the measurement of turbulence intensity whereas the latter along the upwind face of the L tower

concurrently with the pressure measurement. A sample of fluctuating pressure spectrum obtained is displayed in Fig. 4.19. The signal-to-noise ratio (S/N) was about 30 over most of the range of interest. A same S/N was obtained during the turbulence-energy spectrum survey.

The turbulence-energy and pressure-fluctuations spectra are displayed in Figs. 4.20 and 4.21. Generally, both do exhibit a congruent behavior. Most of the turbulence energy and pressure fluctuations are concentrated, at all stations, within the same low frequency range. The latter extends up to about 15 to 20 Hz depending upon the position. Furthermore, within the inertial subrange, i.e., at relatively high frequencies, the -5/3 power is approximately satisfied by both spectra at all stations. It is important to remark that at $z = 0.145$, i.e., near tower base, this similarity breaks down. At this position the pressure-fluctuations spectrum differs drastically from the turbulence energy distribution. Moreover, its slope in the inertial subrange is about -1. It is suspected that this discrepancy is caused by the surrounding buildings located upstream of the tower. Since the natural frequency of the structure is about 200Hz the results within its range, i.e. 200Hz $\pm$ 20%, are discarded.

No drastic shift of energy within the low frequencies was observed. The turbulence energy does decrease slightly with height but a definite trend was not observed. However, most of the energy is concentrated within the same

range. At high frequencies the slope does not change with height. In general a similar variation is observed for the pressure spectrum. At low frequencies, where most of the pressure "energy" is concentrated, the intensity changes randomly with height. On the other hand, in the so-called inertial subrange it is practically the same and the -5/3 power law is approximately satisfied at all heights except near the base.

The important aspect of these results is the general congruence between the turbulence-energy and the surface pressure-fluctuations spectra. It can be inferred that the latter are produced by the boundary-layer turbulence. Furthermore, it is suspected that they do correlate directly since it appears that they do differ by some constant of proportionality. This is clearly indicated by the results presented.

5. CONCLUSIONS

The surveys of mean velocity, turbulence intensity and boundary-layer thickness indicated that the atmospheric-surface-layer can be simulated acceptably in a wind tunnel. The mean velocity variation with height was reasonably described by a power law. The values of the exponent were found to be congruent with representative values in situ. Its value depended slightly upon the flow direction but strongly on the roughness configuration of the upstream urban area. A sufficiently thick turbulent boundary layer about 2.3 to 2.4 times the model height was obtained.

The flow was found to be Reynolds-number independent. No significant changes in the pressure distribution were observed when the Reynolds number was almost doubled.

Generally, the mean pressure was found to be larger near the top than close to the base independently of flow direction. On the other hand, the pressure gradient along the various tower faces did depend on the wind direction. On the upwind faces positive pressure was measured whereas suction was monitored along the leewind surfaces and the roof. The wake generated by the towers and surrounding buildings and the relative positions of the two towers had a strong influence on the resulting pressure distribution. The effect of the immediate surrounding buildings was most important in the case of N wind. The minimum pressure was monitored around the center of the upstream tower and not near its base.

For all flow directions the fluctuating and peak pressure exhibited an opposite variation. They were found to be the largest at the same regions where the mean pressure was the smallest. In general, the fluctuating pressure (rms) was of the same order of magnitude or larger than the mean pressure whereas the instantaneous peak pressure ranged up to maximum 30 times the mean pressure. The largest fluctuating and peak pressure was observed in the case of the N wind which is the most critical flow direction.

Furthermore, it was found that the mean and peak pressure depend more strongly on the flow direction than the fluctuating pressure. It seems that the latter, is mainly determined by the turbulence of the approaching flow.

The pressures when averaged over a horizontal strip extending across the width of the building face revealed that these average mean and fluctuating pressures change linearly with height.

The direct measurement of the overturning moment revealed that it depends strongly on the upstream surface conditions. The fluctuating moment does depend on the upstream turbulence. A decrease in the mean moment and an increase in the fluctuating moment was observed in the case of the rough upstream conditions as compared with smooth upstream conditions. In the former case the instantaneous peak fluctuating moment was found to be about 34% of mean moment whereas in the latter case only about 8%. The mean moment for the rough case was about 56% less than for the

smooth case. Moreover, the turbulence intensity of the upstream flow averaged over the model tower height was found to be of same order of magnitude as the rms value of the fluctuating moment. These results indicate that the direct measurement of the overturning moment provides information of major importance to the structural engineers.

The surveys of turbulence-energy spectra and pressure-fluctuations spectra along the upwind force of the model showed consistently that both exhibit a qualitative congruent local variation. Most of turbulence energy and pressure "energy" were concentrated within the same low frequency range. It can be inferred that the upstream turbulence has a predominant role, together with the wake, in causing the pressure fluctuations on the structure.

REFERENCES

1. Jensen, M., "The model-law for phenomena in natural wind," Ingenioren, Int. Ed. 2 (1958).

2. Jensen, M. and Franck, N., "Model-scale tests in turbulent wind," Part I and II, The Danish Tech. Press, Copenhagen (1965).

3. Cermak, J. E. et al, "Simulation of atmospheric motion by wind tunnel flow," TR-CER66JEC-SI17, FDDL, Colorado State University, Fort Collins, Colorado (1966).

4. Davenport, A. G. and Isynmov, N., "The application of the boundary layer wind tunnel to the prediction of wind loading," Proceedings of the Intern. Res. Seminar on Wind Effects on Buildings and Structures, Vol. 1, N.R.C., Ottawa, Canada (1967).

5. McVehil, G. E., Ludwig, G. R. and Sundaram, T. R., "On the feasibility of modeling small scale atmospheric motions," TR ZB-2328-P-1, Cornell Aeron. Lab., Buffalo, N. Y. (1967).

6. Leutheusser, H. J. and Baines, W. D., "Similitude problems in building aerodynamics," Proceedings ASCE, J. Hyd. Div., HY3, 35-49 (1967).

7. Armitt, J., "The simulation of the atmospheric boundary layer in a wind tunnel," C.E.G.B., Lab. Note No. RD/L/N 83/66 (1966).

8. Parkhurst, R. C. and Holder, D. W., Wind Tunnel Technique (Sir Isaac Pitman & Sons, Ltd., London, 1952).

9. Landenburg; R. W. et al, (editors) Physical Measurements in Gas Dynamics and Combustion, Article F, 2, Kovasznay, L.S.G., "Hot-wire method," 219-285, (High Speed Aerodynamics and Jet Propulsion, Vol. 12, Princeton Univ. Press, Princeton, N. J., 1954).

10. Sadeh, W. Z., Sutera, S. P. and Maeder, P. F., "An investigation of vorticity amplification in stagnation flow," TR AF 1754/4, WT50, Brown Univ., Div. of Eng., Providence, R. I. (1968).

11. Baines, W. D., "Effects of velocity distribution on wind loads and flow patterns on buildings," NPL Symposium on Wind Effects on Buildings and Structures, Vol. 1, (1963).

12. Davenport, A. G., "Gust loading factors," Proceedings ASCE, J. Struc. Div., ST3, 11-34, (1967).

13. Pavelka, B. R., "Wind study, Atlantic-Richfield Plaza, Los Angeles, California," Meteo. Report, TR151, Aerosol Lab., Metronics Associated Inc., Palo Alto, Calif., (1968).

14. Davenport, A. G., "The dependence of wind loads on meteorological parameters," Proceedings of the Intern. Res. Seminar, Wind Effects on Buildings and Structures, University of Toronto Press, Ottawa, Canada, (1967).

15. Singer, I. A., "A study of the wind profile in the lowest 400 ft. of the atmosphere," PR5, Brookhaven Nat. Lab. (1960).

16. Lin, C. C., Statistical theory of turbulence, (Princeton, University Press, Princeton, N. J., 1961).

17. Maskell, E. C., "A theory of the blockage effects on bluff bodies and stalled wing in a closed wind tunnel." Report AERO 2685, R. A. E., (1963).

APPENDIX I

Surface Mean, Fluctuating and Peak Pressure Coefficients

The tower and face notation is shown in Fig. 2.3. The pressure tap stations are designated by two numbers as following: the first number indicates the horizontal position (row); the second number stands for the vertical position (column).

The pressure coefficients were computed for U_∞ = 50 fps and ρ = 0.00187 slug/ft^3. The blockage correction coefficient was estimated using the method presented in Ref. 17. Its value is between 0.03 to 0.1 depending upon the particular pressure station location.

Table 1: Surface mean, fluctuating and peak pressure coefficients, L-Tower, NE wind.

Face 4-1				Face 1-2				Face 2-3				Face 3-4				Roof	
Station No.	C_p	C_{p_f}	$C_{p_{max}}$	Station	C_p	C_{p_f}	$C_{p_{max}}$	Station No.	C_p	C_{p_f}	$C_{p_{max}}$	Station No.	C_p	C_{p_f}	$C_{p_{max}}$	Station No.	C_p
1-1	.43	.19	.54	1-1	-.50	.15	.70	1-1	-.31	.17	.48	1-1	-.39	.17	.80	1-2	-.46
1-3	.58	.21	.49	1-2	-.52	.18	.91	1-3	-.33	.11	.37	1-2	-.38	.17	1.01	1-3	-.47
1-4	.60	.20	.60	1-3	-.41	.17	.75	1-4	-.33	.11	.40	1-3	-.37	.13	.60	1-4	-.44
1-5	.66	.20	.75					1-5	-.32	.12	.44						
1-7	.61	.20	.54	2-2	-.51	.22	.93	1-7	-.33	.13	.41	2-2	-.39	.15	.80	2-1	-.43
																2-5	-.46
2-2	.62	.17	.50	3-1	-.51	.11	.55	2-2	-.30	.12	.35	3-1	-.43	.15	.76		
2-4	.72	.18	.49	3-2	-.53	.24	.95	2-4	-.31	.12	.34	3-2	-.39	.12	.63	3-2	-.46
2-6	.73	.18	.51	3-3	-.51	.23	1.07	2-6	-.31	.08	.37	3-3	-.34	.21	1.00	3-3	-.46
																3-4	-.45
3-1	.36	.16	.44	4-2	-.55	.27	.83	3-1	-.34	.16	.48	4-2	-.40	.18	.97		
3-4	.67	.19	.56					3-4	-.29	.11	.47					4-1	-.44
3-7	.48	.18	.47	5-1	-.54	.16	.50	3-7	-.26	.13	.59	5-1	-.44	.16	.80	4-5	-.47
				5-2	-.59	.25	.97					5-2	-.38	.18	.90		
4-2	.51	.13	.44	5-3	-.46	.36	1.19	4-2	-.33	.11	.43	5-3	-.34	.22	1.05	5-2	-.46
4-4	.58	.13	.43					4-4	-.29	.12	.34					5-3	-.50
4-6	.56	.14	.42	6-2	-.55	.23	1.03	4-6	-.23	.11	.44	6-2	-.37	.18	.98	5-4	-.44
5-1	.27	.17	.49	7-1	-.55	.15	.50	5-1	-.34	.15	.60	7-1	-.36	.17	.70		
5-4	.55	.17	.56	7-2	-.54	.24	.52	5-4	-.25	.12	.46	7-2	-.39	.19	.95		
5-7	.34	.18	.51	7-3	-.43	.14	.54	5-7	-.23	.17	.89	7-3	-.36	.19	.67		
6-2	.38	.16	.48	8-2	-.52	.26	1.03	6-2	-.29	.18	.64	8-2	-.40	.20	1.15		
6-4	.51	.16	.44					6-4	-.26	.19	.56						
6-6	.52	.16	.46	9-1	-.58	.14	.50	6-6	-.24	.16	.59	9-1	-.31	.17	.56		
				9-2	-.43	.26	1.27					9-2	-.39	.20	.87		
7-1	.19	.13	.44	9-3	-.29	.25	.74	7-1	-.31	.22	.80	9-3	-.38	.20	1.15		
7-4	.44	.12	.32					7-4	-.24	.15	.53						
7-7	.31	.13	.44	10-1	-.60	.13	.48	7-7	-.26	.16	.63	10-1	-.23	.17	.73		
				10-2	-.25	.28	1.27					10-2	-.31	.24	.95		
8-2	.29	.13	.50	10-3	-.19	.26	.70	8-2	-.37	.21	.81	10-3	-.40	.22	1.10		
8-4	.39	.12	.46					8-4	-.28	.18	.50						
8-6	.33	.14	.48					8-6	-.26	.20	.55						
9-1	.11	.11	.42					9-1	-.39	.24	1.05						
9-4	.32	.12	.43					9-4	-.20	.16	.75						
9-7	.17	.14	.45					9-7	-.23	.14	.52						
10-1	.08	.12	.44					10-1	-.46	.30	1.05						
10-4	.32	.12	.48					10-4	-.03	.20	.75						
10-7	.44	.48	.50					10-7	-.17	.14	.53						

Table 2: Surface mean, fluctuating and peak pressure coefficients, R-Tower, NE wind.

Face 4-1				Face 1-2				Face 2-3				Face 3-4				Roof	
Station No.	C_p	C_{p_f}	$C_{p_{max}}$	Station No.	C_p	C_{p_f}	$C_{p_{max}}$	Station No.	C_p	C_{p_f}	$C_{p_{max}}$	Station No.	C_p	C_{p_f}	$C_{p_{max}}$	Station No.	C_p
1-1	-.25	.33	1.19	1-1	-.09	.36	1.12	1-1	-.13	.12	.36	1-1	-.15	.19	.86	1-2	-.15
1-3	-.23	.22	1.03	1-2	-.06	.25	.79	1-3	-.13	.10	.45	1-2	-.16	.31	.98	1-3	-.14
1-4	-.22	.26	1.10	1-3	-.09	.20	.78	1-4	-.13	.11	.50	1-3	-.18	.43	1.26	1-4	-.13
1-5	-.17	.32	1.30					1-5	-.15	.13	.54						
1-7	-.02	.52	1.61	2-2	-.06			1-7	-.15	.13	.49	2-2	-.17			2-1	-.19
																2-5	-.12
2-2	-.26			3-1	-.06	.30	.95	2-2	-.13			3-1	-.17	.16	.81		
2-4	-.25			3-2	-.05	.22	.66	2-4	-.14			3-2	-.19	.19	.70	3-2	-.15
2-6	-.24			3-3	-.09	.13	1.50	2-6	-.15			3-3	-.22	.21	.75	3-3	-.12
																3-4	-.10
3-1	-.24	.24	1.01	4-2	-.06			3-1	-.13	.12	.69	4-2	-.21				
3-4	-.26	.15	.83					3-4	-.13	.05	.16					4-1	-.16
3-7	.12	.34	1.14	5-1	0			3-7	-.20	.09	.61	5-1	-.17			4-5	-.10
				5-2	-.02							5-2	-.21				
4-2	-.25			5-3	-.08			4-2	-.14			5-3	-.26			5-2	-.12
4-4	-.30							4-4	-.14							5-3	-.10
4-6	-.26			6-2	-.01			4-6	-.15			6-2	-.22			5-4	-.09
5-1	-.26			7-1	.08			5-1	-.13			7-1	-.13				
5-4	-.25			7-2	0			5-4	-.14			7-2	-.15				
5-7	-.12			7-3	-.07			5-7	-.16			7-3	-.23				
6-2	-.23			8-2	0	.12	.53	6-2	-.14			8-2	-.08	.21	.80		
6-4	-.26							6-4	-.15								
6-6	-.21			9-1	.05			6-6	-.16			9-1	-.07				
				9-2	-.01							9-2	-.01				
7-1	-.19			9-3	-.10			7-1	-.14			9-3	0				
7-4	-.16							7-4	-.15								
7-7	.07			10-1	-.08			7-7	-.17			10-1	-.02				
				10-2	-.08							10-2	0				
8-2	-.01	.20	1.10	10-3	-.09			8-2	-.17	.09	.35	10-3	.07				
8-4	-.03	.24	1.30					8-4	-.19	.10	.37						
8-6	0	.20	1.08					8-6	-.17	.10	.39						
9-1	0							9-1	-.20								
9-4	.06							9-4	-.20								
9-7	.20							9-7	-.20								
10-1	.10							10-1	-.20								
10-4	.01							10-4	-.17								
10-7	-.10							10-7	-.06								

Table 3: Surface mean, fluctuating and peak pressure coefficients, L-Tower, N wind.

Face 4-1				Face 1-2				Face 2-3				Face 3-4				Roof			
Station No.	C_p	C_{p_f}	$C_{p_{max}}$	Station No.	C_p	C_{p_f}	$C_{p_{max}}$	Station No.	C_p	C_{p_f}	$C_{p_{max}}$	Station No.	C_p	C_{p_f}	$C_{p_{max}}$	Station No.	C_p	C_{p_f}	$C_{p_{max}}$
1-1	.10	.11	.39	1-1	.67	.24	.92	1-1	-.36	.11	.39	1-1	-.20	.10	.30	1-2	-.35	.20	.69
1-3	.24	.13	.54	1-2	.48	.23	.73	1-3	-.41	.12	.41	1-2	-.14	.08	.27	1-3	-.08	.14	.51
1-4	.28	-	-	1-3	.24	.12	.44	1-4	-.37	-	-	1-3	-.13	.06	.27	1-4	-.07	.08	.32
1-5	.33	.11	.45					1-5	-.31	.14	.52								
1-7	.48	.15	.93	2-2	.42	.25	.88	1-7	-.29	.14	.53	2-2	-.22	.08	.31	2-1	-.55	.22	.65
																2-5	-.17	.09	.27
2-2	.22	.11	.39	3-1	.26	.29	.96	2-2	-.41	.15	.56	3-1	-.27	.11	.43				
2-4	.34	.10	.36	3-2	.23	.30	.92	2-4	-.41	.11	.40	3-2	-.21	.09	.42	3-2	-.22	.22	.84
2-6	.41	.15	.70	3-3	.09	.33	.98	2-6	-.31	.13	.50	3-3	-.16	.08	.34	3-3	-.10	.14	.46
																3-4	-.15	.06	.25
3-1	.08	.13	.54	4-2	.07	.18	.68	3-1	-.47	.28	1.01	4-2	-.17	.08	.31				
3-4	.28	.16	.61					3-4	-.41	.19	.66					4-1	-.87	.59	1.31
3-7	.27	.27	1.06	5-1	-.05	.16	.82	3-7	-.21	.11	-	5-1	-.22	.15	.56	4-5	-.17	.20	.62
				5-2	.05	.20	.71					5-2	-.16	.10	.46				
4-2	.20	.15	.65	5-3	-.02	.26	.93	4-2	-.53	-.34	-.21	5-3	-.13	.11	.64	5-2	-.17	.11	.47
4-4	.22	.17	.67					4-4	.33	.21	.15					5-3	-.27	.40	.97
4-6	.20	.21	.81	6-2	.01	.17	.79	4-6	1.00	.84	.59	6-2	-.13	.12	.53	5-4	-.63	.29	.90
5-1	.09	.16	.60	7-1	.02	.17	.71	5-1	-.53	.52	1.35	7-1	-.12	.12	.39				
5-4	.19	.16	.61	7-2	.03	.18	.72	5-4	-.21	.16	.66	7-2	-.10	.11	.40				
5-7	.07	.16	.72	7-3	0	.22	.83	5-7	-.13	.11	.41	7-3	-.10	.13	.69				
6-2	.19	.12	.52	8-2	.06	.15	.59	6-2	-.23	.16	1.02	8-2	-.07	.07	.29				
6-4	.20	.12	.63					6-4	-.09	.10	.49								
6-6	.14	.12	.52	9-1	.07	.15	.58	6-6	-.07	.07	.31	9-1	-.05	.07	.30				
				9-2	.10	.19	.69					9-2	-.06	.07	.36				
7-1	.12	.03	.08	9-3	.08	.22	.81	7-1	-.26	.21	.74	9-3	-.05	.07	.32				
7-4	.22	.15	.57					7-4	-.08	.13	.49								
7-7	.12	.10	.58	10-1	.11	.14	.56	7-7	-.06	.07	.24	10-1	-.05	.05	.26				
				10-2	.19	.15	.66					10-2	-.05	.07	.29				
8-2	.20	.12	.50	10-3	.16	.18	.65	8-2	-.19	.19	.73	10-3	-.05	.07	.33				
8-4	.22	.12	.57					8-4	-.08	.13	.51								
8-6	.20	.12	.59					8-6	-.05	.09	.33								
9-1	.14	.07	.40					9-1	-.28	.21	.78								
9-4	.21	.10	.43					9-4	-.07	.13	.40								
9-7	.17	.19	.64					9-7	-.05	.09	.31								
10-1	.10	.07	.30					10-1	-.33	.38	1.30								
10-4	.21	.09	.38					10-4	-.07	.08	.30								
10-7	.16	.17	.69					10-7	-.03	.06	.24								

Table 4: Surface mean, fluctuating and peak pressure coefficients, R-Tower, N wind.

Face 4-1				Face 1-2				Face 2-3				Face 4-1				Roof			
Station No.	C_p	C_{p_f}	$C_{p_{max}}$	Station No.	C_p	C_{p_f}	$C_{p_{max}}$	Station No.	C_p	C_{p_f}	$C_{p_{max}}$	Station No.	C_p	C_{p_f}	$C_{p_{max}}$	Station No.	C_p	C_{p_f}	$C_{p_{max}}$
1-1		.08	.27	1-1	.62	.15	.56	1-1	-.29	.08	.24	1-1	-.22	.08	.30	1-2	-.44	.18	.50
1-3	.08	.08														1-3	-.17	.11	.41
1-4	.10	.09	.30	1-3	.15	.09	.36	1-4	-.30	.09	.36	1-3	-.18	.08	.23	1-4	-.16	.07	.41
1-5	.20	.08	.25					1-5	-.30	.12	.42								
1-7	.35	.15	.76	2-2	.44	.12	.40	1-1	-.34	.11	.75	2-2	-.24	.06	.24	2-1	-.58	.17	.49
																2-5	-.21	.17	.58
2-2	-.03	.05	.19	3-1	.66	.21	.68	2-2	-.29	.07	.16	3-1	-.29	.08	.30				
2-4	.08	.07	.28	3-2	.41	.16	.40	2-4	-.31	.07	.21	3-2	- 26	.07	.25	3-2	-.34	.32	.75
2-6	.24	.10	.51	3-3	.14	.11	.31	2-6	-.33	.09	.41	3-3	-.25	.06	.19	3-3	-.19	.10	.56
																3-4	-.20	.20	.50
3-1	-.15	.06	.19	4-2	.41	.15	.46	3-1	-.29	.08	.21	4-2	-.28	.11	.25	4-1	-1.00	.40	1.40
3-4	.02	.09	.28					3-4	-.31	.08	.27					4-5	-.34	.20	.57
3-7	.27	.26	1.02	5-1	.51	.21	.67	3-7	-.35	.12	.51	5-1	-.33	.12	-				
				5-2	.35	.16	.56					5-2	-.31	.11	.59	5-2	-.37	.27	.65
4-2	-.10	.07	.20	5-3	.09	.12	.35	4-2	-.33	.07	.25	5-3	-.27	.09	.44	5-3	-.62	.23	.64
4-4	-.02	.08	.27					4-4	-.35	.07	.28					5-4	-.49	.18	.64
4-6	.15	.14	.56	6-2	.34	.18	.48	4-6	-.36	.09	.48	6-2	-.31	.13	.55				
5-1	-.17	.06	.23	7-1	.38	.20	.64	5-1	-.36	.09	.23	7-1	-.36	.12	.59				
5-4	-.01	.10	.30	7-2	.26	.15	.49	5-4	-.38	.11	.54	7-2	-.30	.12	.54				
5-7	.06	.35	1.07	7-3	.02	.12	.42	5-7	-.37	.14	.61	7-3	-.28	.13	.67				
6-2	-.09	.09	.30	8-2	.21	.15	.52	6-2	-.38	.11	.43	8-2	-.25	.18	.67				
6-4	-	.10	.31					6-4	-.39	.13	.62								
6-6	.08	.17	.54	9-1	.26	.11	.37	6-6	-.39	.15	.57	9-1	-.31	.12	.47				
				9-2	.15	.13	.42					9-2	-.20	.20	.74				
7-1	-.13	.07	.22	9-3	-.02	.10	.33	7-1	-.42	.11	.36	9-3	-.17	.14	.76				
7-4	-.01	.08	.30					7-4	-.43	.12	.87								
7-7	.07	.29	.92	10-1	.17	.15	.56	7-7	-.38	.18	.47	10-1	-.31	.31	1.28				
				10-2	.09	.07	.21					10-2	-.19	.10	.37				
8-2	-.06	.07	.21	10-3	-.03	.10	.31	8-2	-.44	.13	.50	10-3	-.20	.14	.59				
8-4	.01	.09	.30					8-4	-.44	.16	.77								
8-6	.07	.13	.38					8-6	-.34	.19	.61								
9-1	-.07	.11	.25					9-1	-.43	.19	.64								
9-4	-.01	.09	.31					9-4	-.42	.20	.83								
9-7	.10	.18	.66					9-7	-.17	.18	.59								
10-1	-.12	.09	.28					10-1	-.51	.18	.96								
10-4	-.03	.08	.32					10-4	-.33	-	-								
10-7	.02	.11	.42					10-7	-.06	.18	.67								

Table 5: Surface mean, fluctuating and peak pressure coefficients, L-Tower, NW wind.

Face 4-1				Face 1-2				Face 2-3				Face 3-4				Roof	
Station No.	C_p	C_{p_f}	$C_{p_{max}}$	Station No.	C_p	C_{p_f}	$C_{p_{max}}$	Station No.	C_p	C_{p_f}	$C_{p_{max}}$	Station No.	C_p	C_{p_f}	$C_{p_{max}}$	Station No.	C_p
1-1	-.36	.21	.82	1-1	.38	.17	.47	1-1	-.80	.29	.91	1-1	-.21	.12	.35	1-2	-.27
1-3	-.41	.24	.87	1-2	.58	.20	.51	1-3	-.47	.34	.91	1-2	-.22	.12	.40	1-3	-.21
1-4	-.45	.20	.70	1-3	.58	.21	.54	1-4	-.22	.24	.85	1-3	-.24	.16	.57	1-4	-.24
1-5	-.44	.14	.64					1-5	-.19	.17	.62						
1-7	-.38	.12	.41	2-2	.66			1-7	-.19	.13	.60	2-2	-.24			2-1	-.38
																2-5	-.35
2-2	-.40			3-1	.40	.15	.39	2-2	-.69			3-1	-.23	.07	.26		
2-4	-.40			3-2	.60	.18	.51	2-4	-.22			3-2	-.28	.08	.28	3-2	-.49
2-6	-.35			3-3	.58	.15	.42	2-6	-.19			3-3	-.28	.08	.26	3-3	-.26
																3-4	-.38
3-1	-.43	.22	.80	4-2	.57			3-1	-.77	.24	1.08	4-2	-.22				
3-4	-.38	.14	.54					3-4	-.20	.33	.90					4-1	-.60
3-7	-	.10	.38	5-1	.48			3-7	-	.16	.57	5-1	-.23			4-5	-.60
				5-2	.55							5-2	-.23				
4-2	-.41			5-3	.60			4-2	-.59			5-3	-.28			5-2	-.67
4-4	-.41							4-4	-.19							5-3	-.64
4-6	-.36			6-2	.41			4-6	-.20			6-2	-.24			5-4	-.70
5-1	-.44			7-1	.19			5-1	-.74			7-1	-.23				
5-4	-.38			7-2	.38			5-4	-.17			7-2	-.24				
5-7	-.27			7-3	.35			5-7	-.14			7-3	-.29				
6-2	-.43			8-2	.27	.17	.63	6-2	-.44			8-2	-.27	.15	.55		
6-4	-.44							6-4	-.16								
6-6	-.40			9-1	.06			6-6	-.19			9-1	-.23				
				9-2	.21							9-2	-.27				
7-1	-.43			9-3	.23			7-1	-.62			9-3	-.29				
7-4	-.47							7-4	-.16								
7-7	-.43			10-1	-.06			7-7	-.20			10-1	-.27				
				10-2	.23							10-2	-.27				
8-2	-.44	.17	.52	10-3	.13			8-2	-.23	.40	1.18	10-3	-.29				
8-4	-.48	.17	.55					8-4	-.14	.20	.68						
8-6	-.47	.15	.48					8-6	-.17	.11	.44						
9-1	-.36							9-1	-.36								
9-4	-.47							9-4	-.13								
9-7	-.45							9-7	-.17								
10-1	-.02							10-1	-.08								
10-4	-.41							10-4	-.13								
10-7	-.48							10-7	-.16								

Table 6: Surface mean, fluctuating and peak pressure coefficients, R-Tower, NW wind.

Face 4-1				Face 1-2				Face 2-3				Face 3-4				Roof	
Station No.	C_p	C_{p_f}	$C_{p_{max}}$	Station No.	C_p	C_{p_f}	$C_{p_{max}}$	Station No.	C_p	C_{p_f}	$C_{p_{max}}$	Station No.	C_p	C_{p_f}	$C_{p_{max}}$	Station No.	C_p
1-1	-.28	.29	.95	1-1	.50	.71	.62	1-1	-.74	.16	.80	1-1	-.19	.10	.35	1-2	-.17
1-3	-.44	.28	.96	1-2	.18	.18	.27	1-3	-.79	.27	.94	1-2	-.21	.10	.35	1-3	-.14
1-4	-.66	.26	.90	1-3	.44	.52	.71	1-4	-.41	.29	.90	1-3	-.22	.16	.56	1-4	-.15
1-5	-.64	.24	.80					1-5	-.17	.31	.84						
1-7	-.62	.18	.64	2-2	.84			1-7	-.14	.21	.78	2-2	-.21			2-1	-.35
																2-5	-.27
2-2	-.45			3-1	.58	.17	.43	2-2	-.73			3-1	-.21	.09	.33		
2-4	-.64			3-2	.74	.20	.52	2-4	-.52			3-2	-.20	.08	.33	3-2	-.62
2-6	-.59			3-3	.65	.15	.47	2-6	-.22			3-3	-.22	.11	.40	3-3	-.56
																3-4	-.44
3-1	-.37	.31	.98	4-2	.72			3-1	-.66	.20	.91	4-2	-.20				
3-4	-.60	.24	.81					3-4	-.50	.30	.85					4-1	-.73
3-7	-.01	.20	.69	5-1	.45			3-7	.08	.29	.66	5-1	-.21			4-5	-.76
				5-2	.60							5-2	-.20				
4-2	-.47			5-3	.52			4-2	-.73			5-3	-.24			5-2	-.71
4-4	-.60							4-4	-.44							5-3	-.74
4-6	-.59			6-2	.63			4-6	-.23			6-2	-.23			5-4	-.80
5-1	-.35			7-1	.33			5-1	-.73			7-1	-.19				
5-4	-.60			7-2	.48			5-4	-.35			7-2	-.22				
5-7	-.58			7-3	.42			5-7	-.15			7-3	-.29				
6-2	-.41			8-2	.42	.15	.45	6-2	-.70			8-2	-.20	.12	1.22		
6-4	-.59							6-4	-.23								
6-6	-.69			9-1	.16			6-6	-.09			9-1	-.15				
				9-2	.27							9-2	-.19				
7-1	-.26			9-3	.27			7-1	-.67			9-3	-.27				
7-4	-.57							7-4	-.10								
7-7	-.69			10-1	.10			7-7	-.08			10-1	-.17				
				10-2	.22							10-2	-.20				
8-2	-.21	.19	.72	10-3	.20			8-2	-.37	.37	1.23	10-3	-.15				
8-4	-.38	.35	.99					8-4	0	.15	.62						
8-6	-.76	.39	1.22					8-6	-.01	-	-						
9-1	-.12							9-1	-.47								
9-4	-.14							9-4	-.03								
9-7	-.85							9-7	-.03								
10-1	-.08							10-1	-.01								
10-4	-.16							10-4	-.06								
10-7	-.44							10-7	-.01								

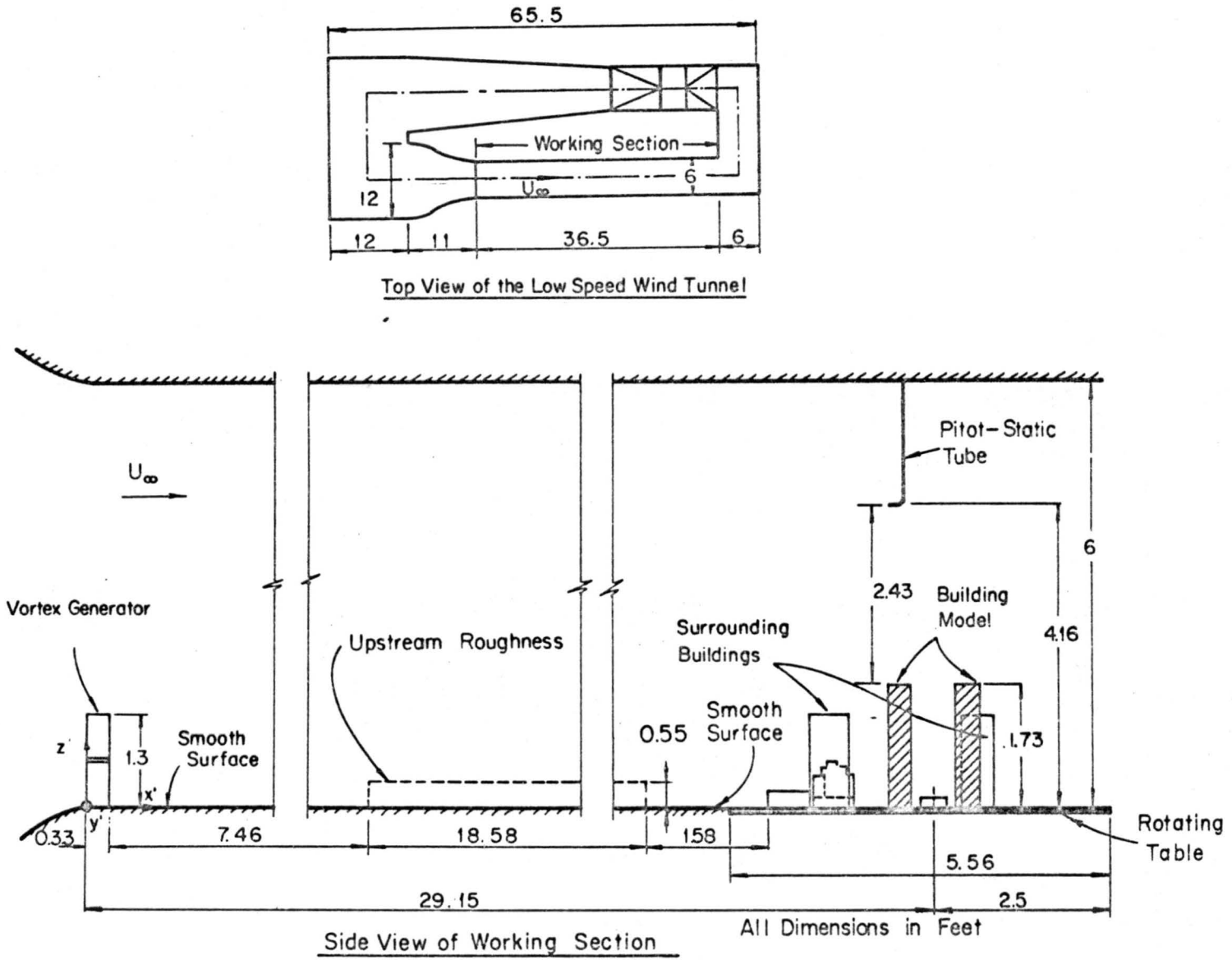

Fig. 2.1 Sketch of the experimental arrangement and the low speed wind tunnel.

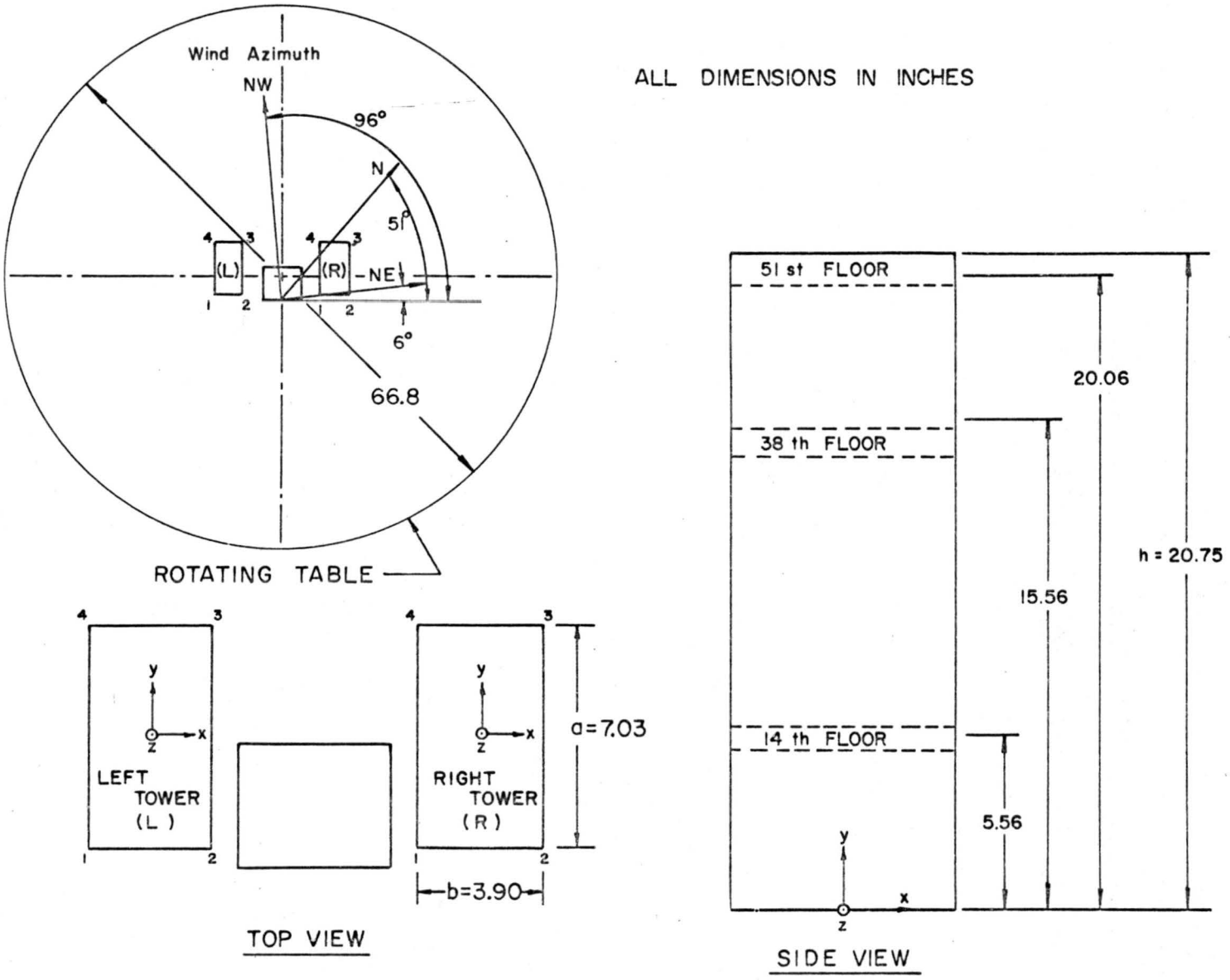

Fig. 2.2 Sketch of the model towers.

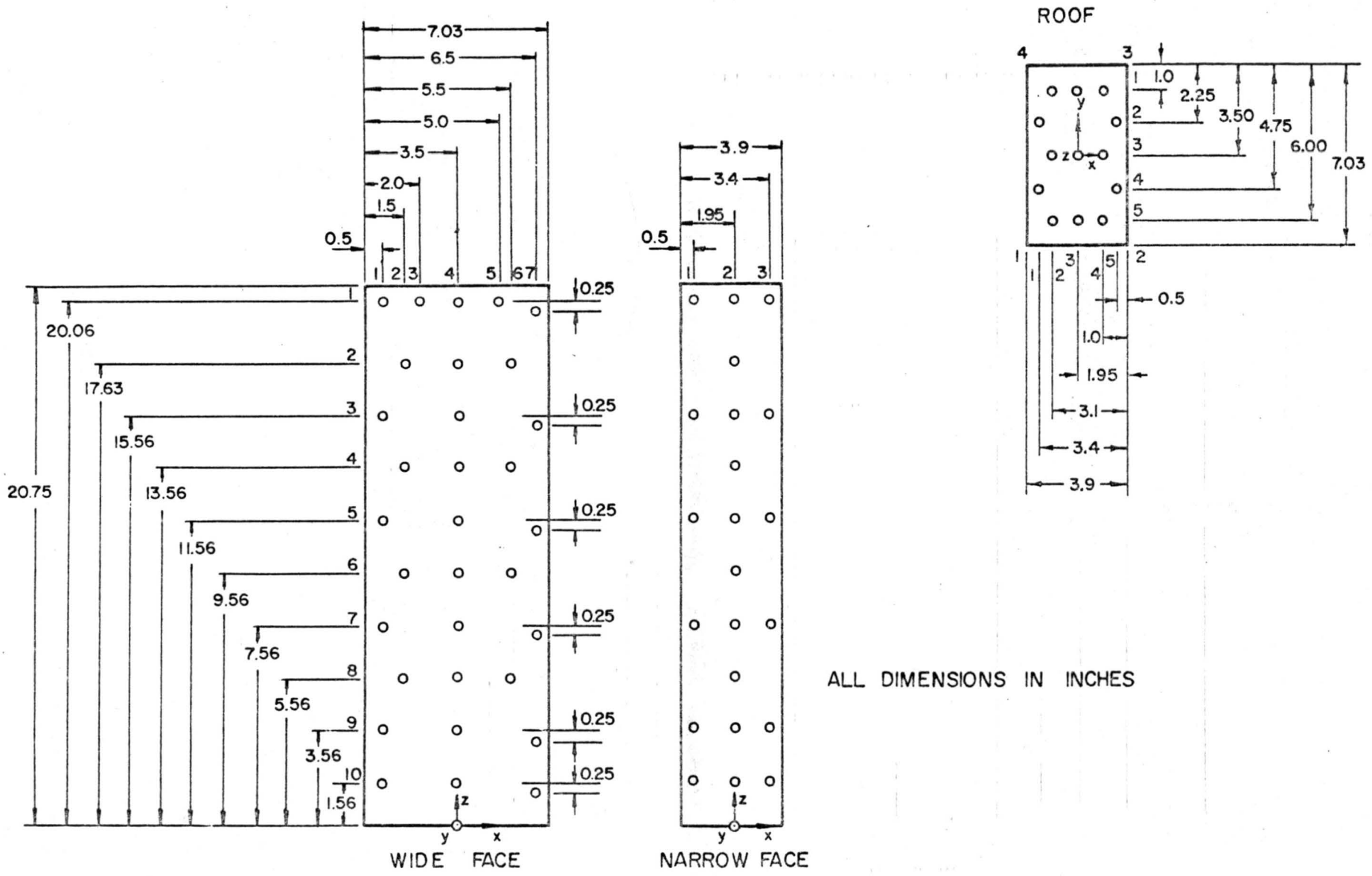

Fig. 2.3 Static-pressure tap stations.

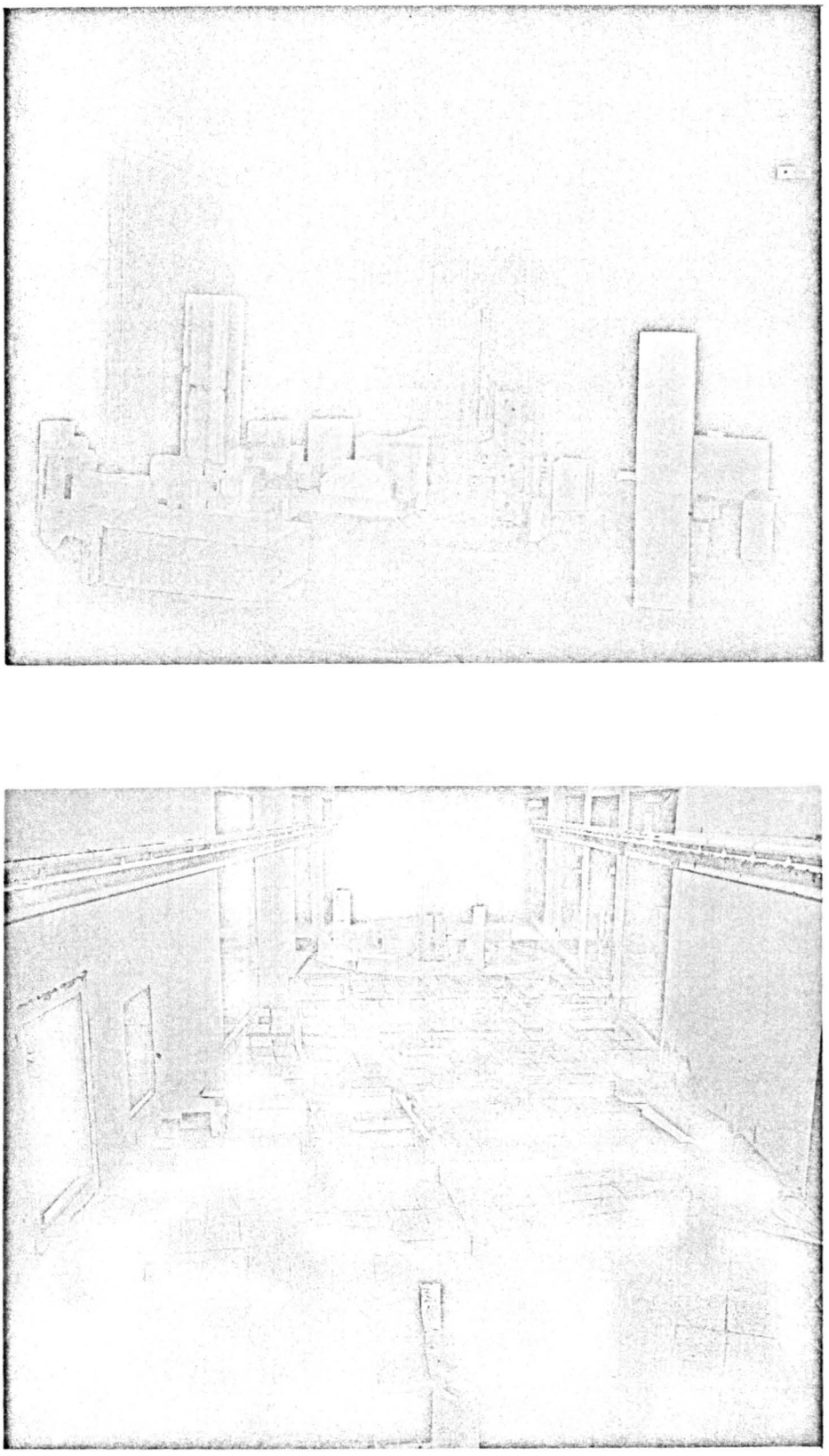

Fig. 2.4 Overall view of the model towers and upstream city; NE wind.

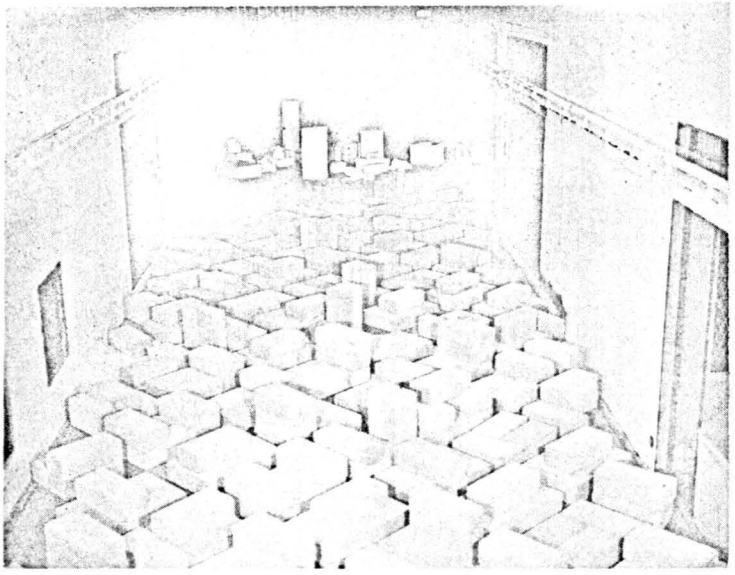

Fig. 2.5 Overall view of model towers and upstream modeled city; N wind.

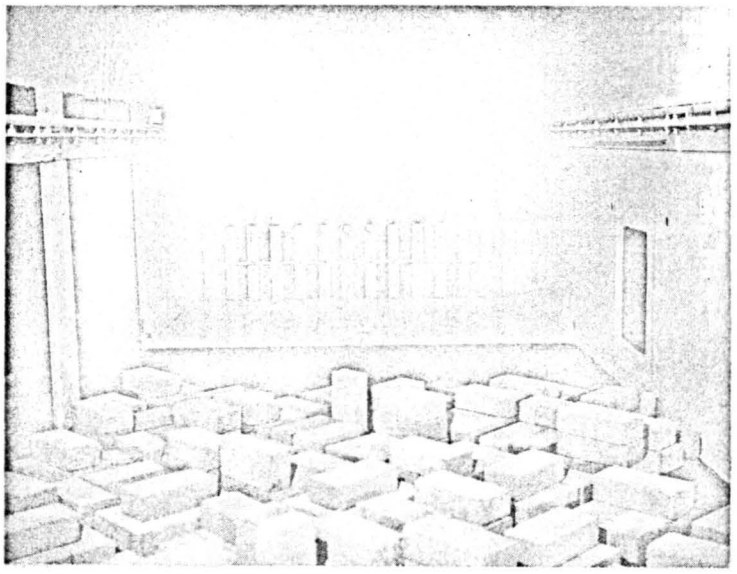

Fig. 2.6 View of vortex generator.

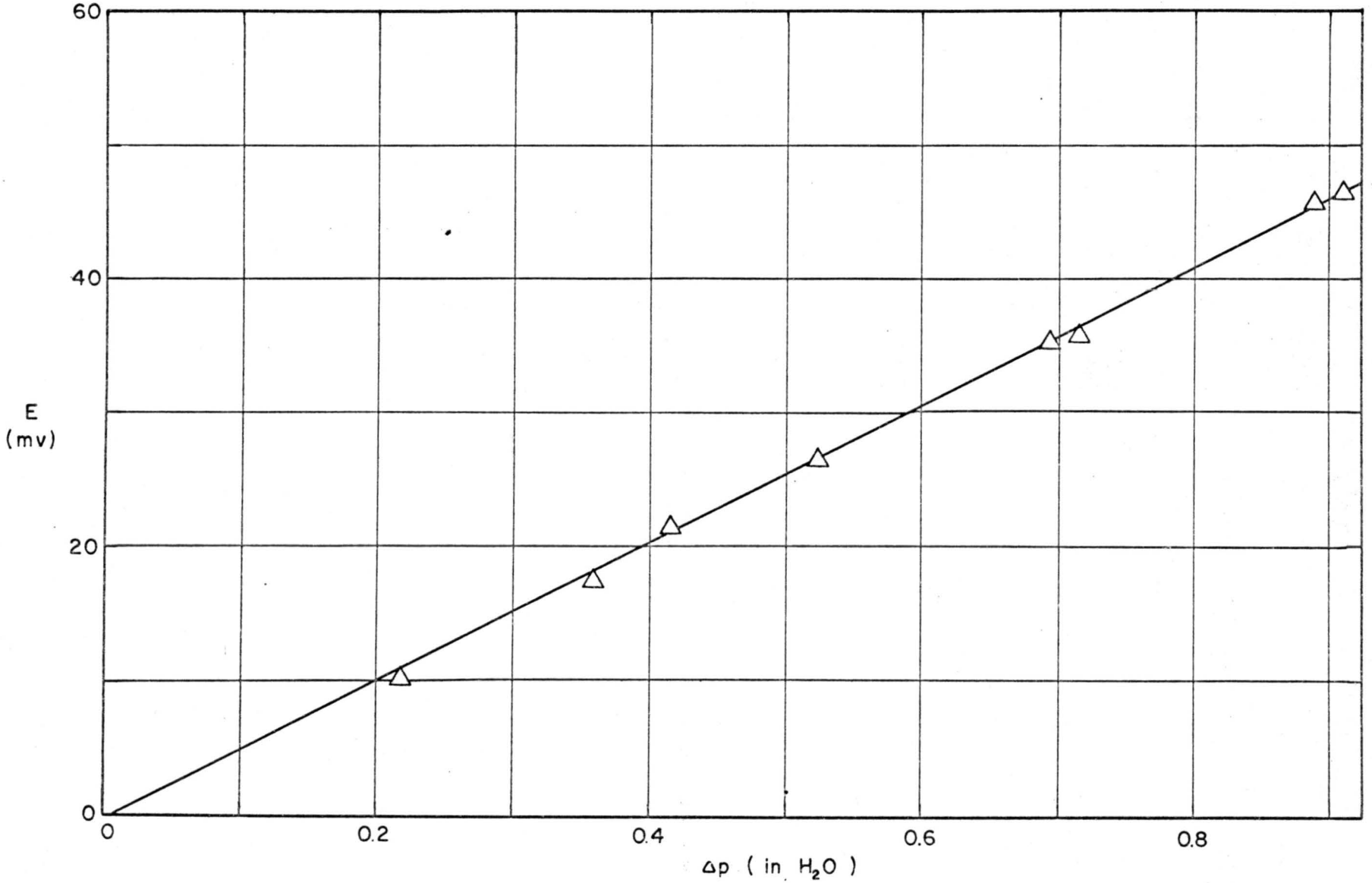

Fig. 3.1 Typical pressure transducer calibration curve.

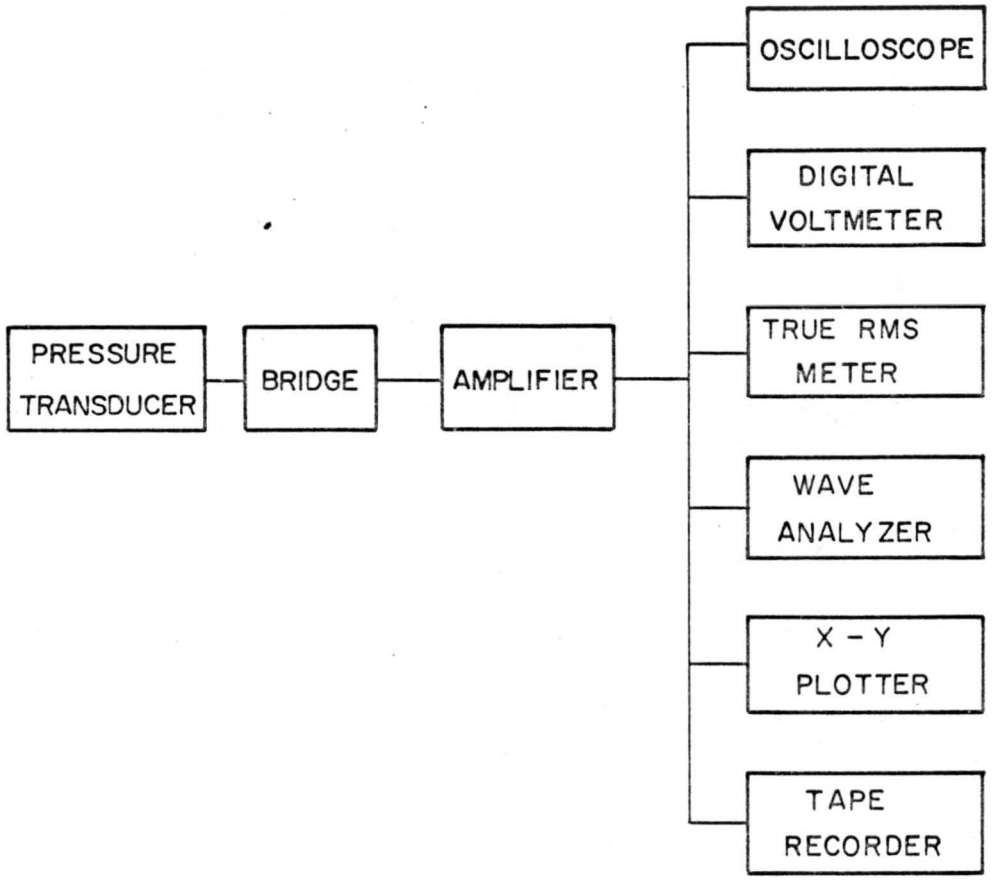

Fig. 3.2 Simplified block diagram of the pressure-transducer measurement system.

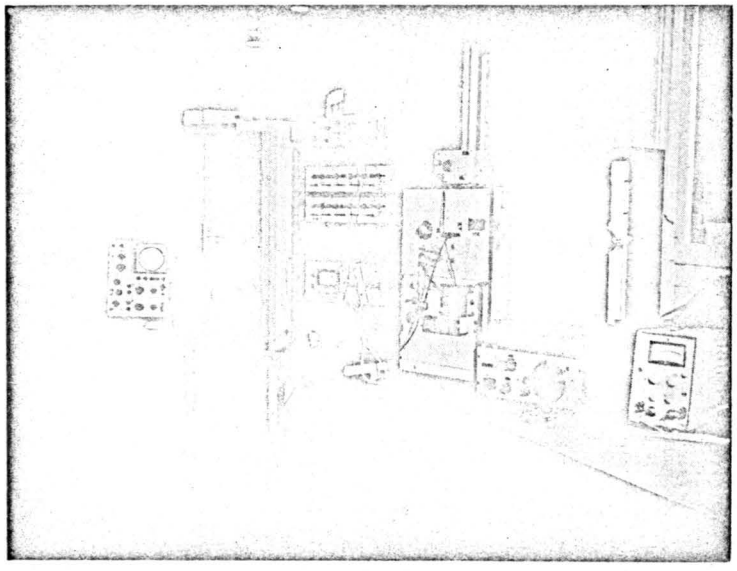

Fig. 3.3 General view of the pressure measurement system.

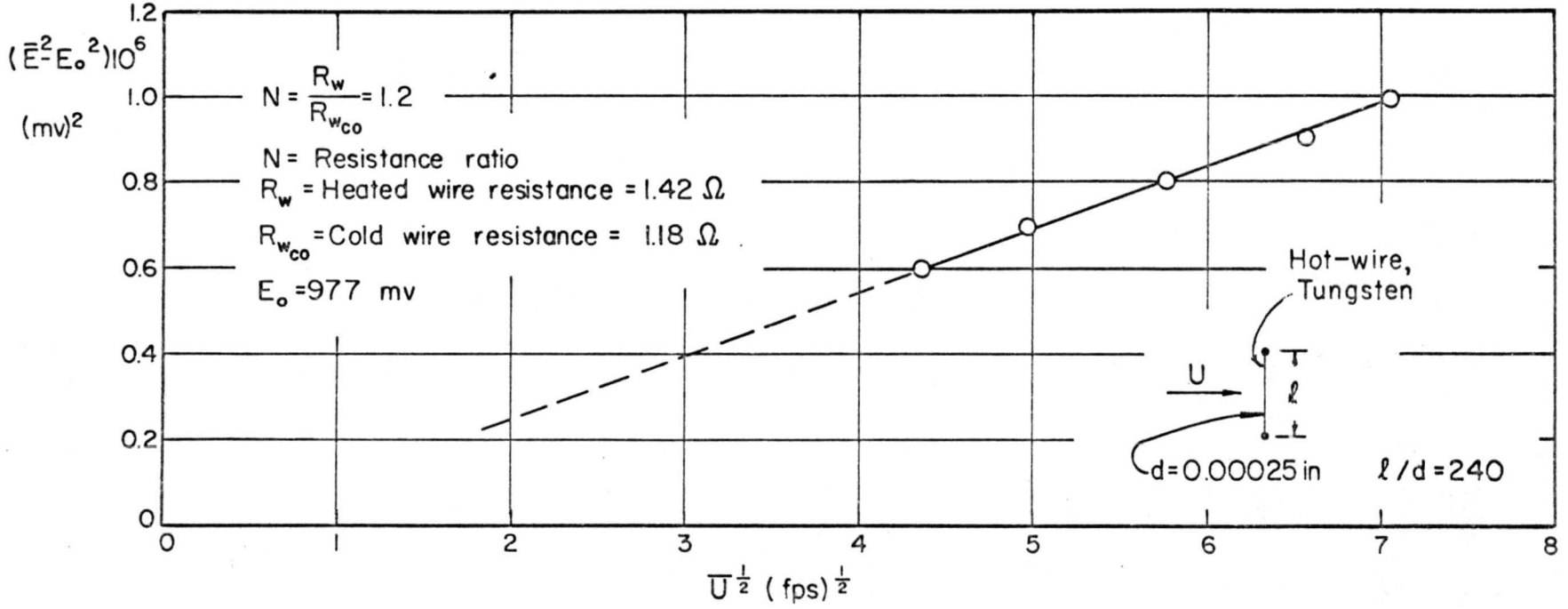

Fig. 3.4 Typical hot-wire calibration curve.

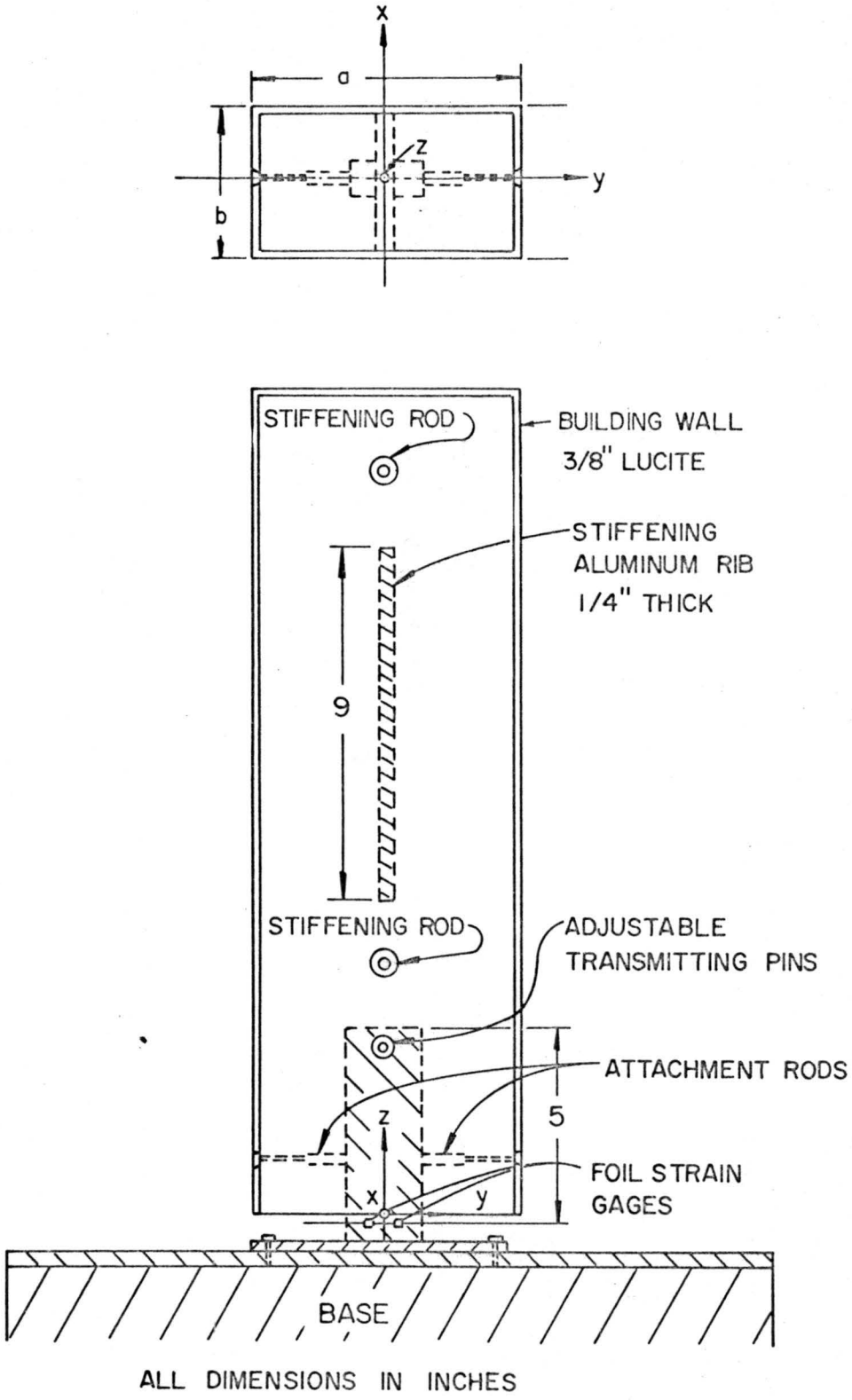

Fig. 3.5 Sketch of the balance.

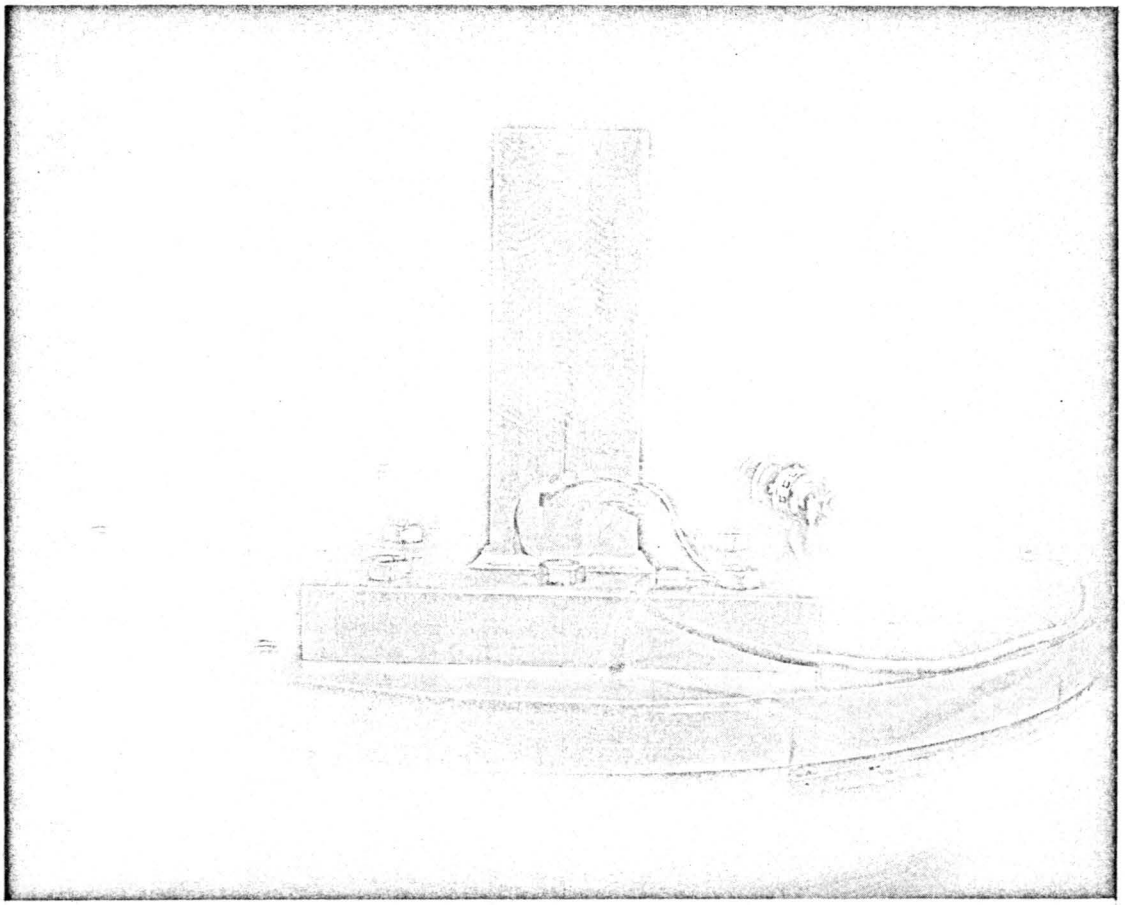

Fig. 3.6 View of the balance.

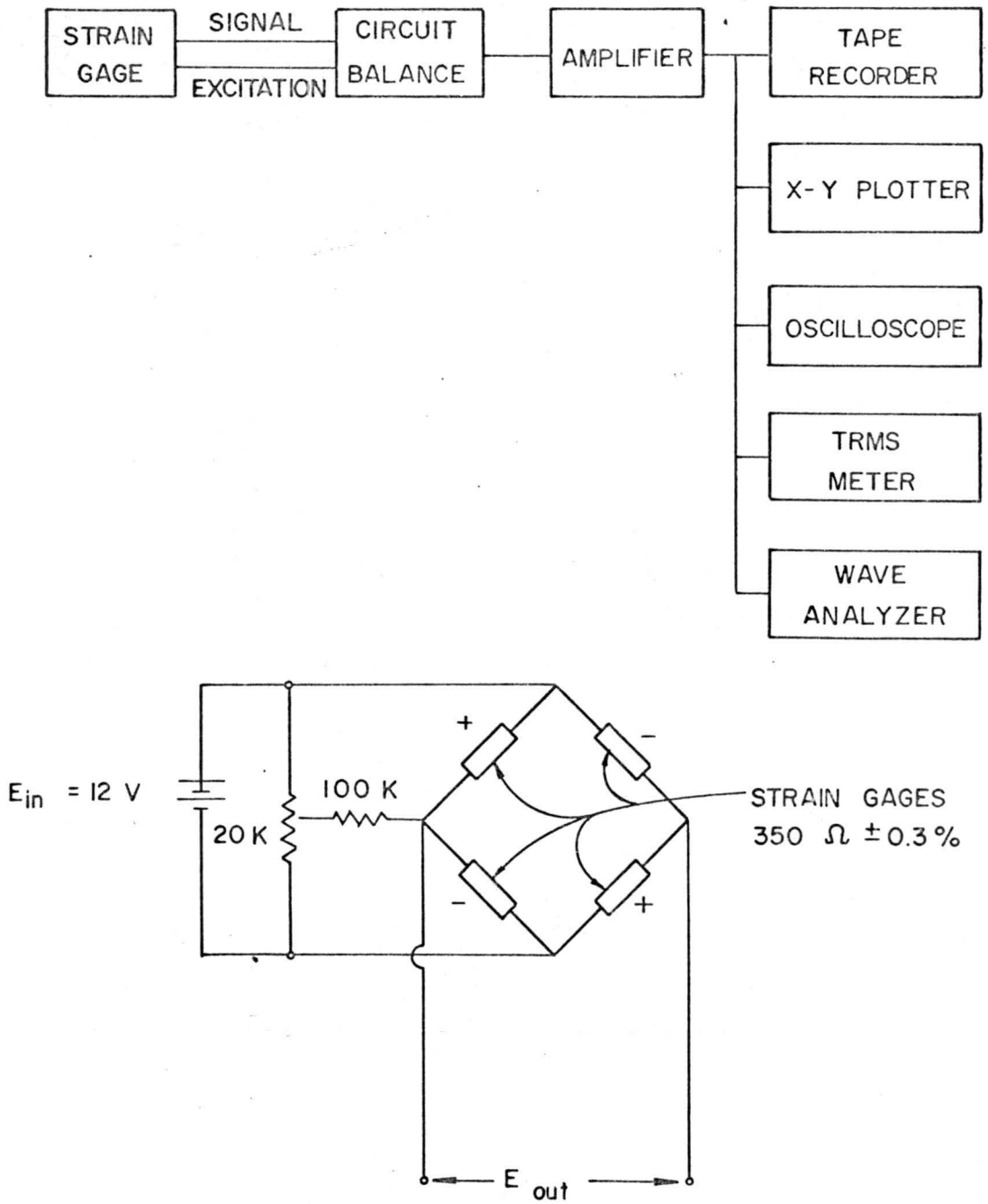

Fig. 3.7 Simplified block diagram of the moment measuring system.

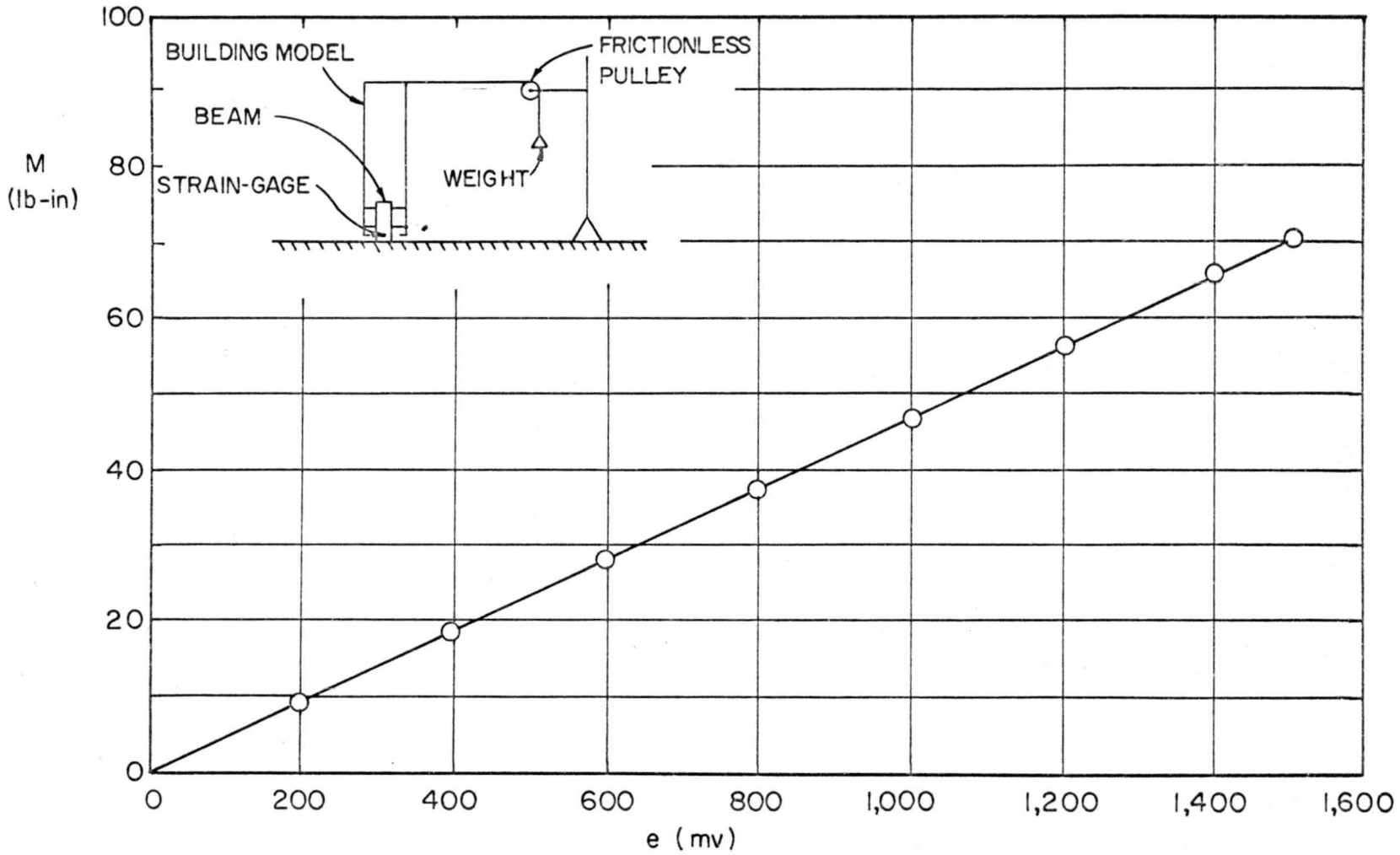

Fig. 3.8 Typical calibration curve of the balance.

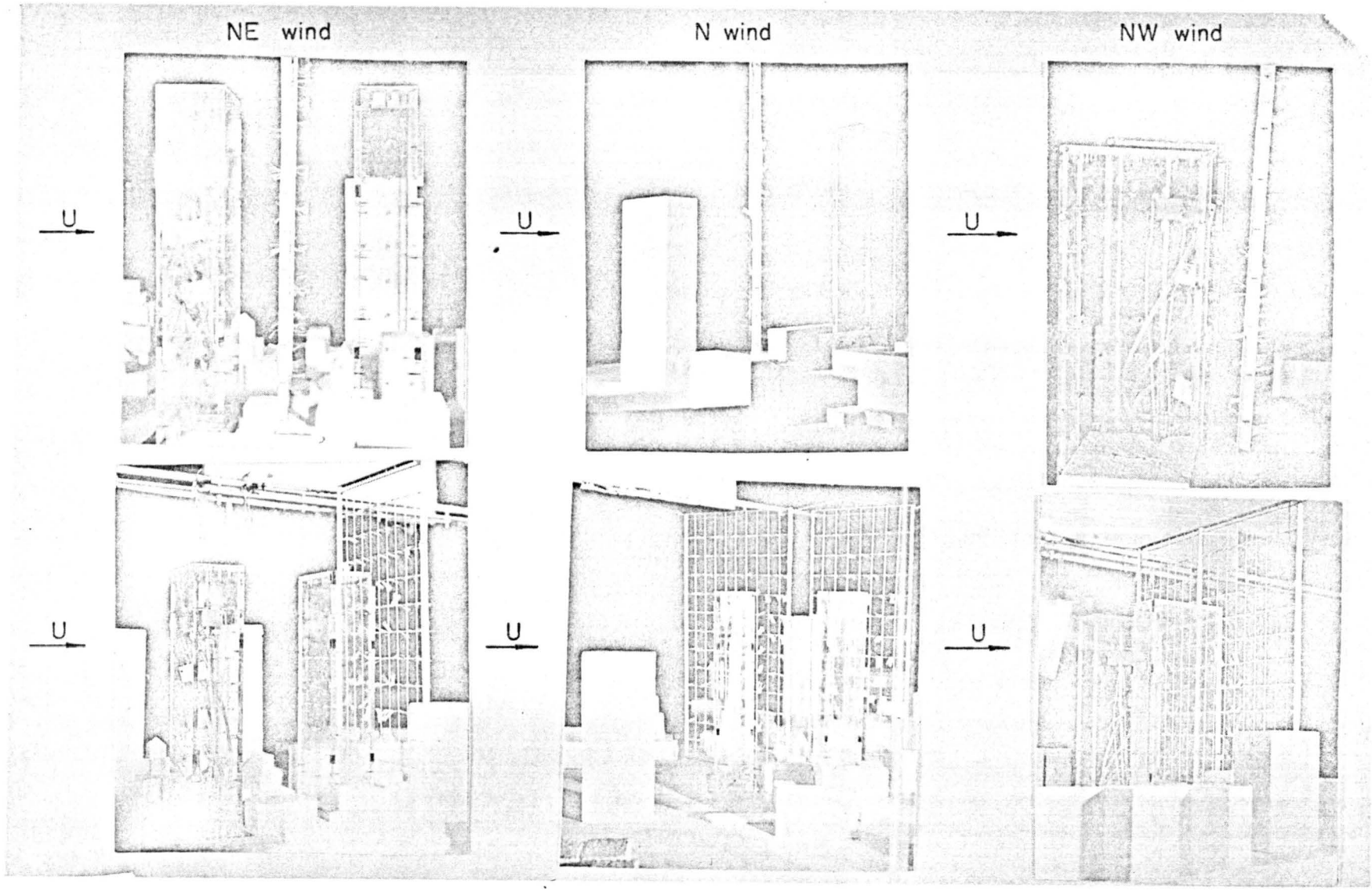

Fig. 4.1 Visualization of the flow by means of paper tufts.

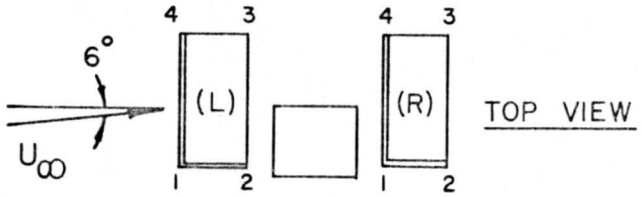

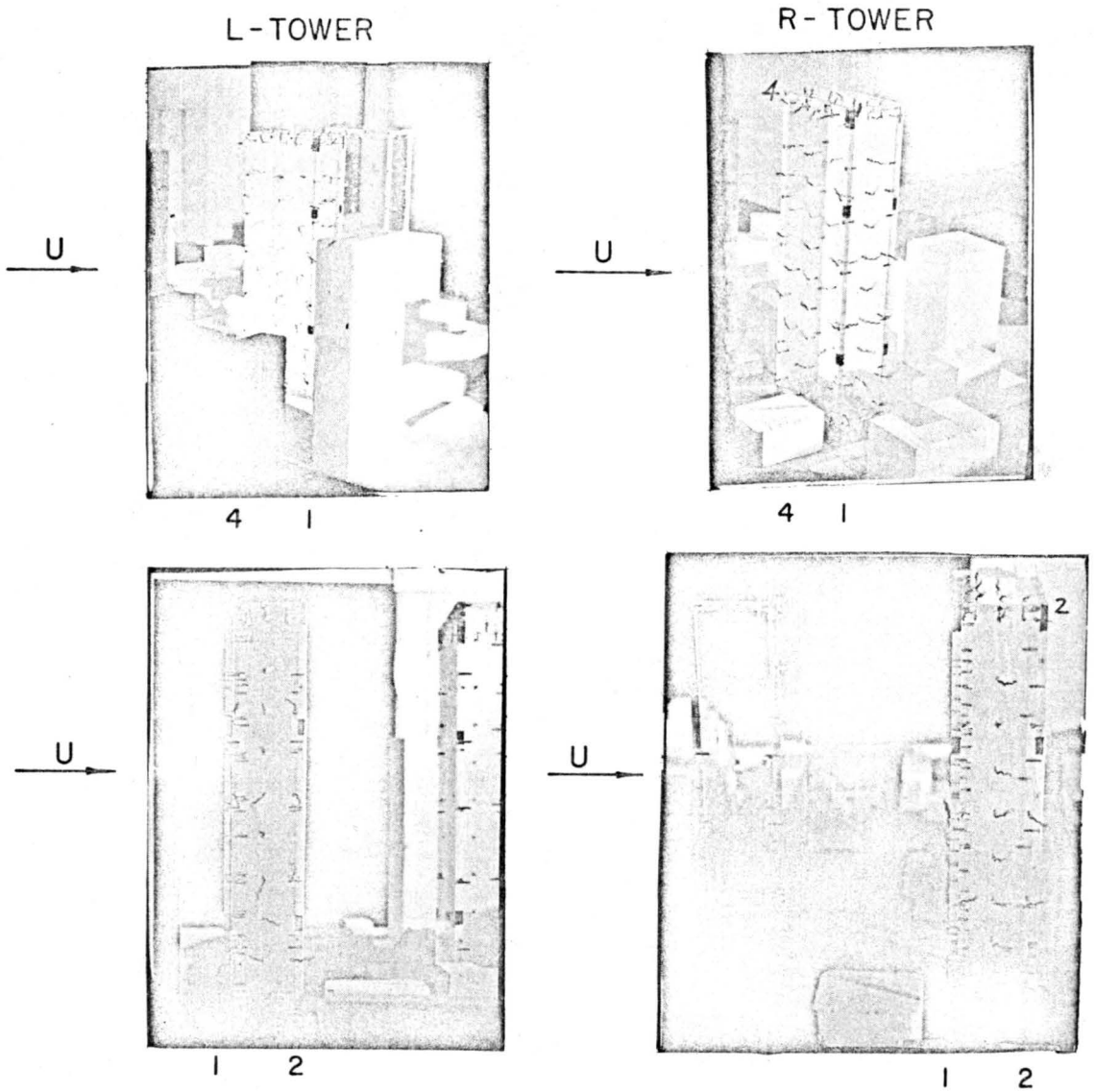

Fig. 4.2 Visualization of the flow pattern by means of thread tufts; L and R tower, faces 4-1 and 1-2, NE wind.

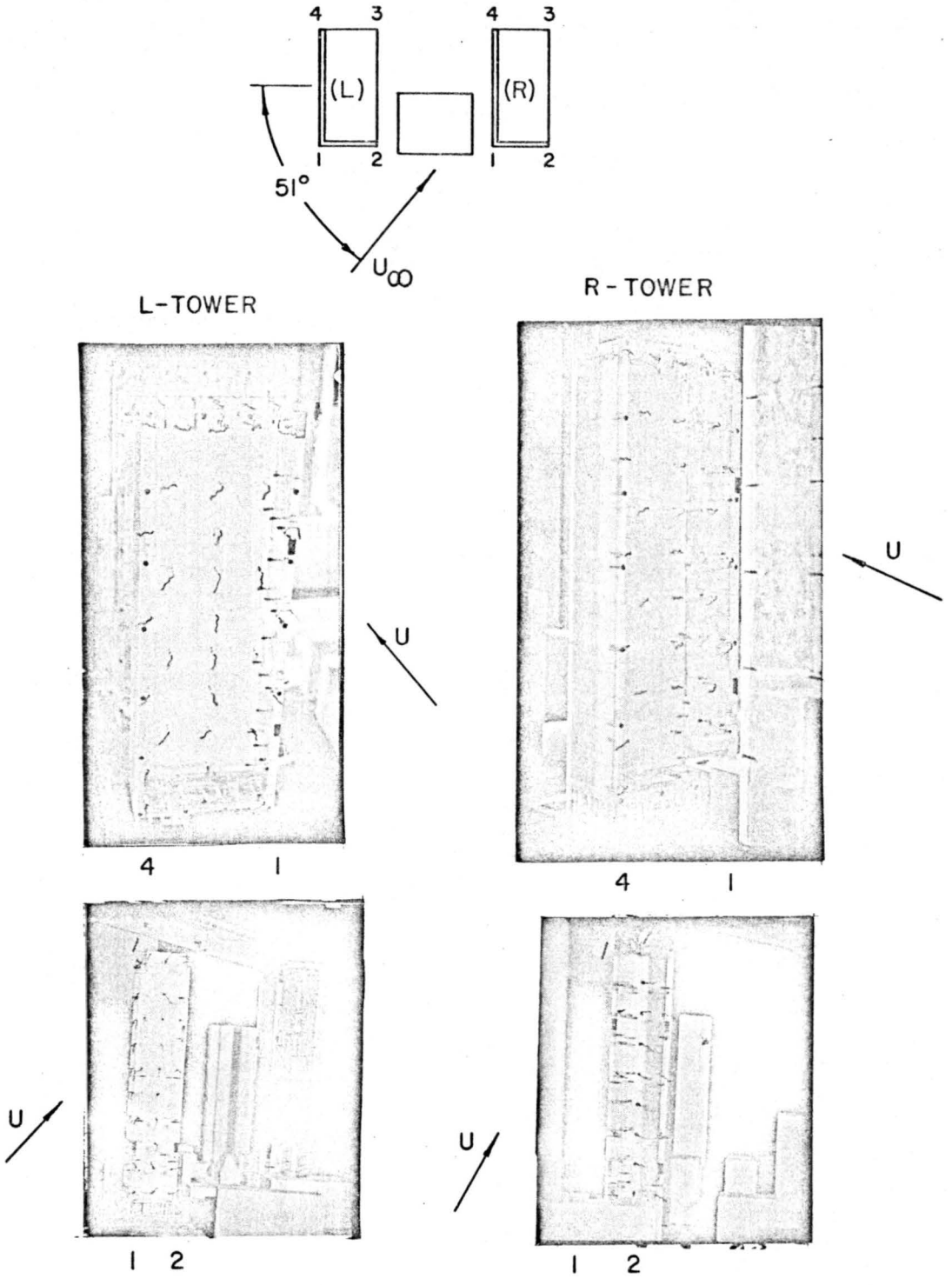

Fig. 4.3 Visualization of the flow pattern by means of thread tufts; L and R tower, faces 4-1 and 1-2, N wind.

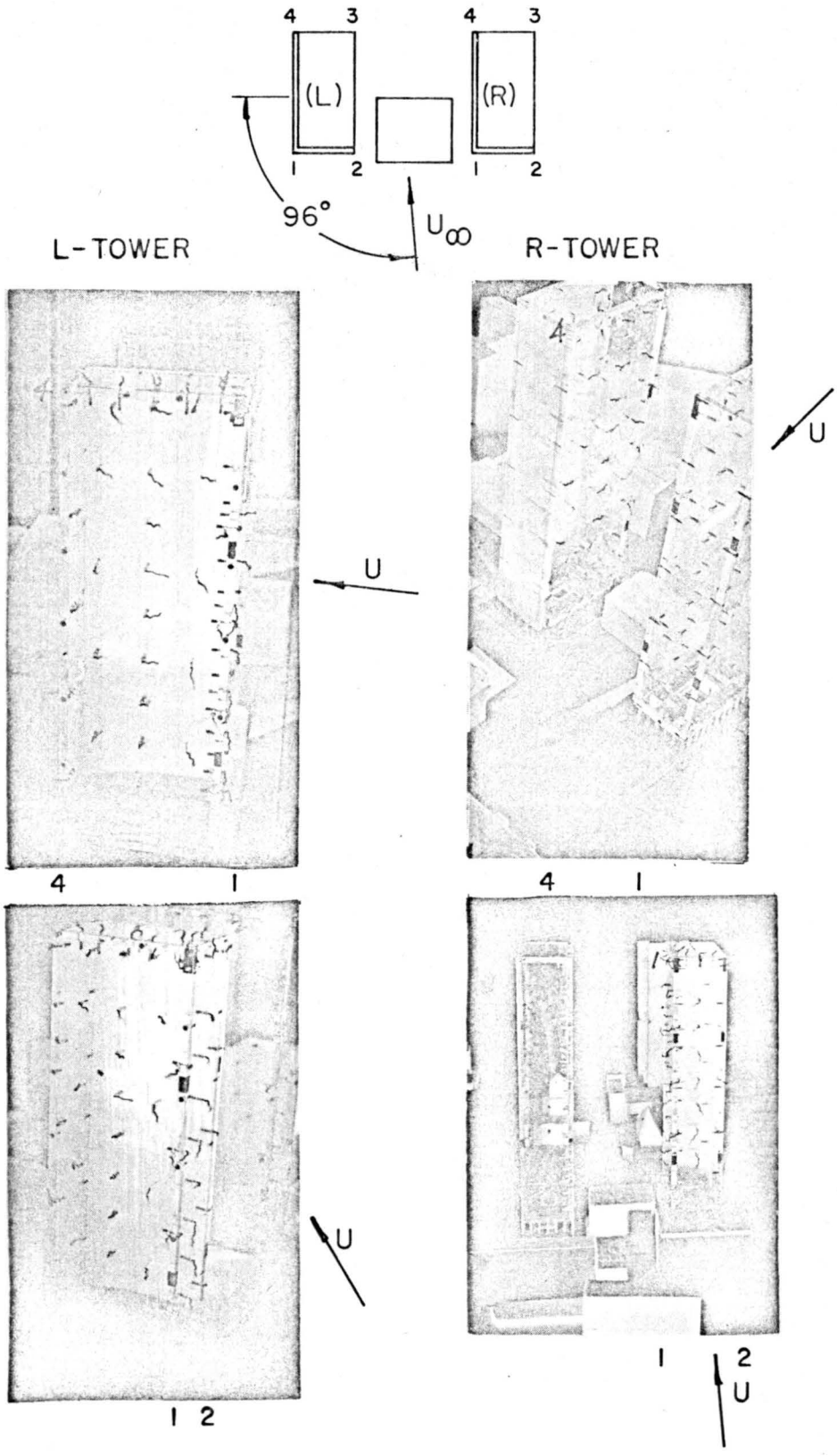

Fig. 4.4 Visualization of the flow pattern by means of thread tufts; L and R tower, face 4-1 and 1-2, NW wind.

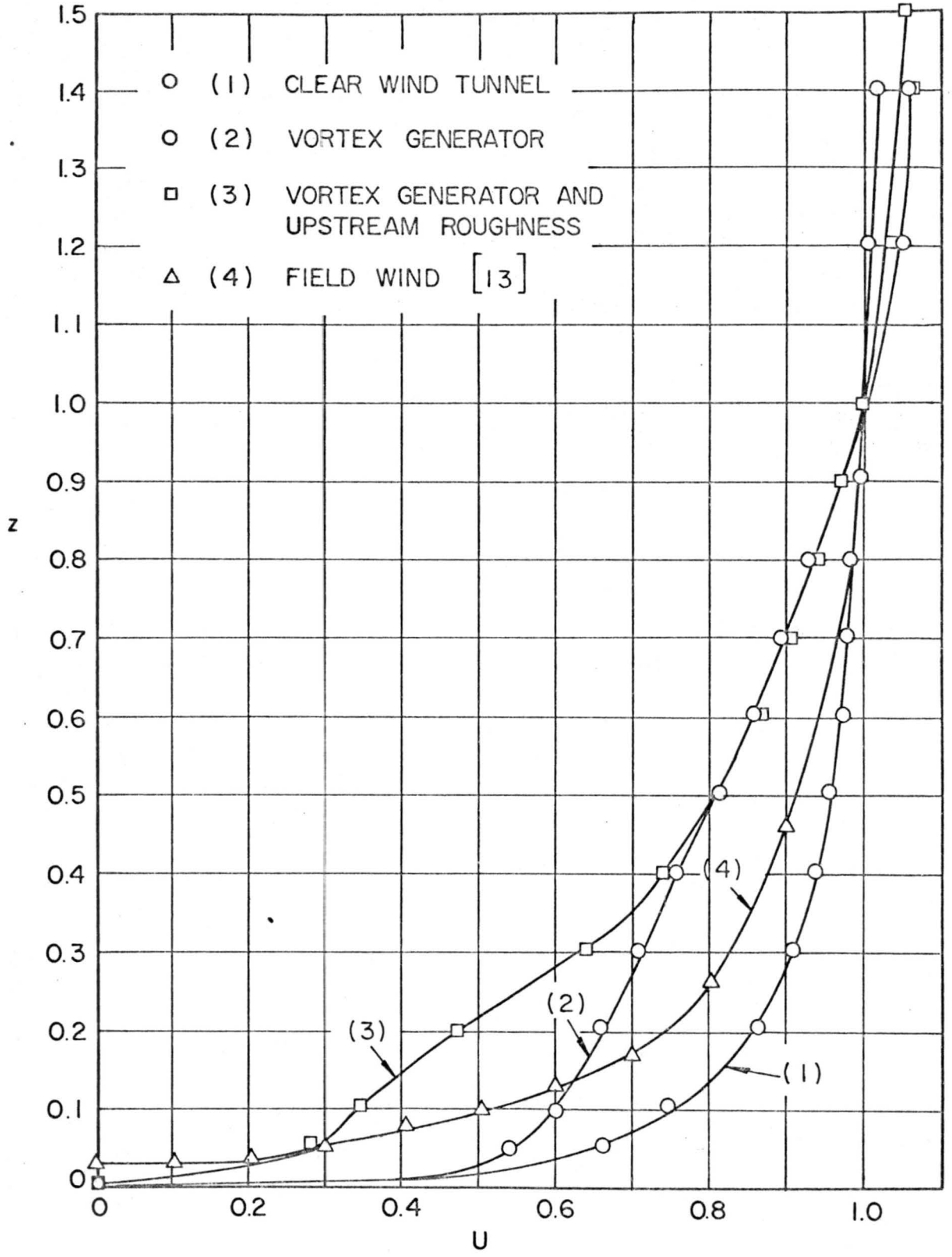

Fig. 4.5 Velocity profiles upstream of the model tower for NE wind and field wind velocity profile.

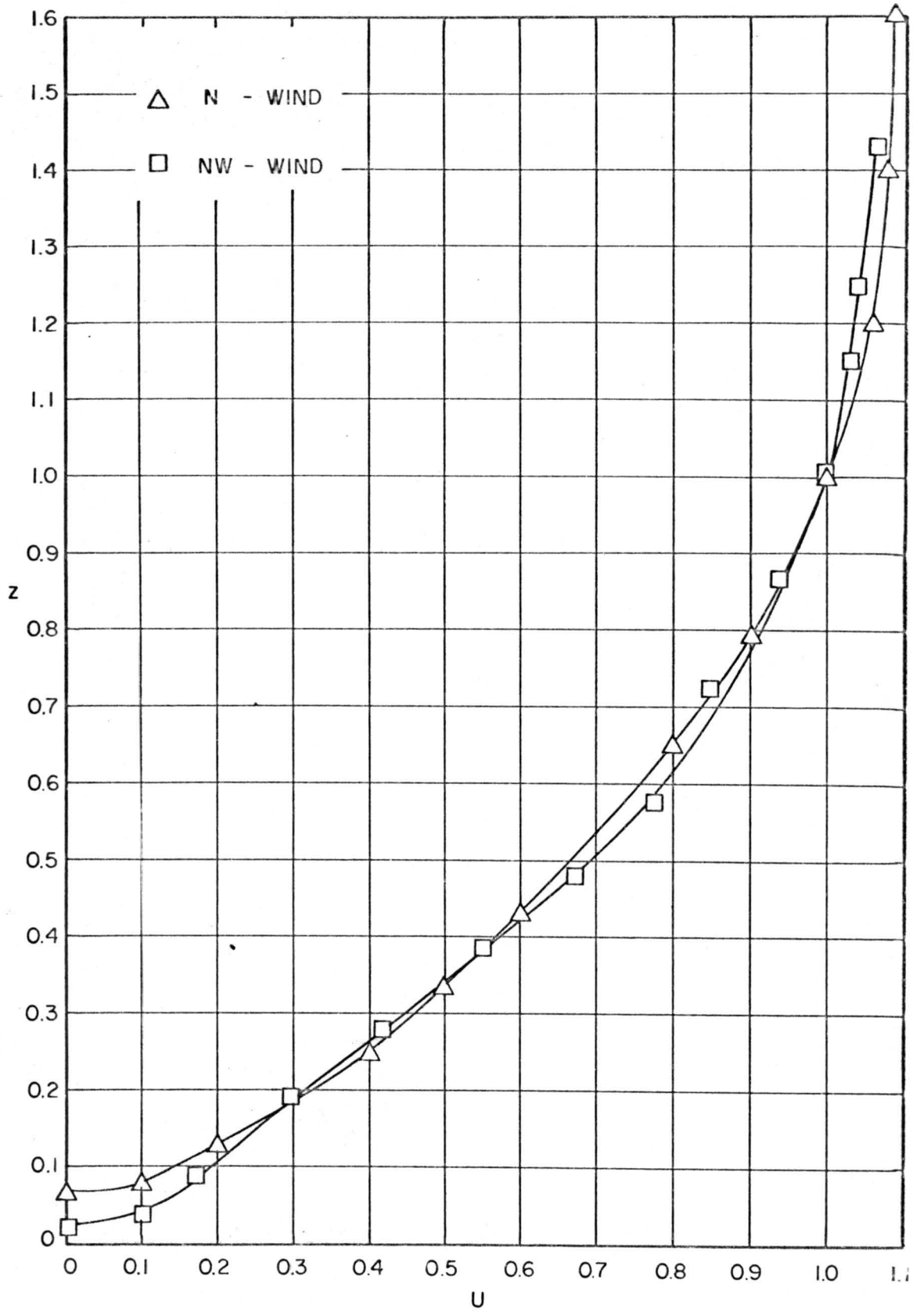

Fig. 4.6 Velocity profiles upstream of the model tower; N and NW wind.

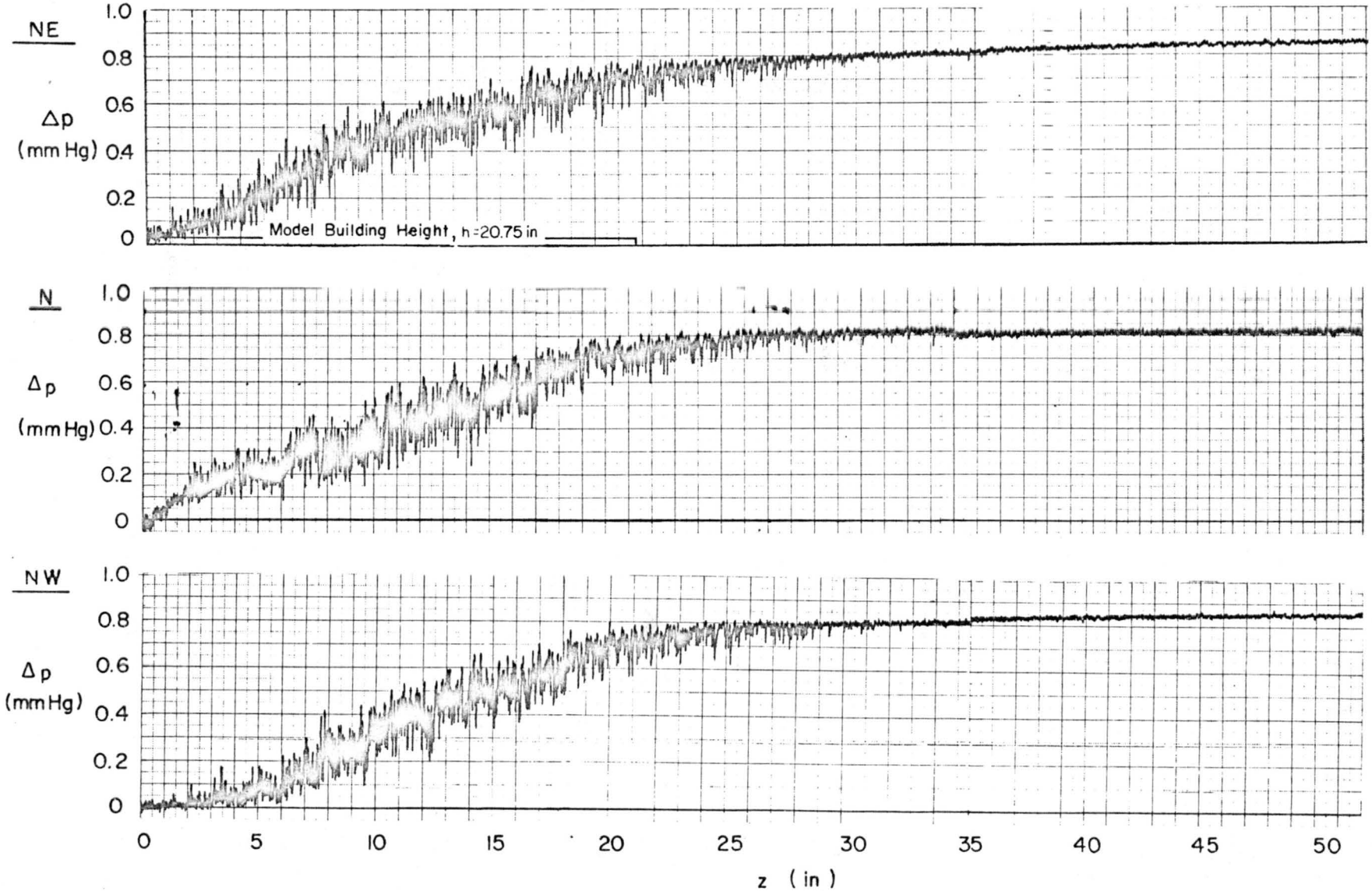

Fig. 4.7 Variation of upstream velocity with height.

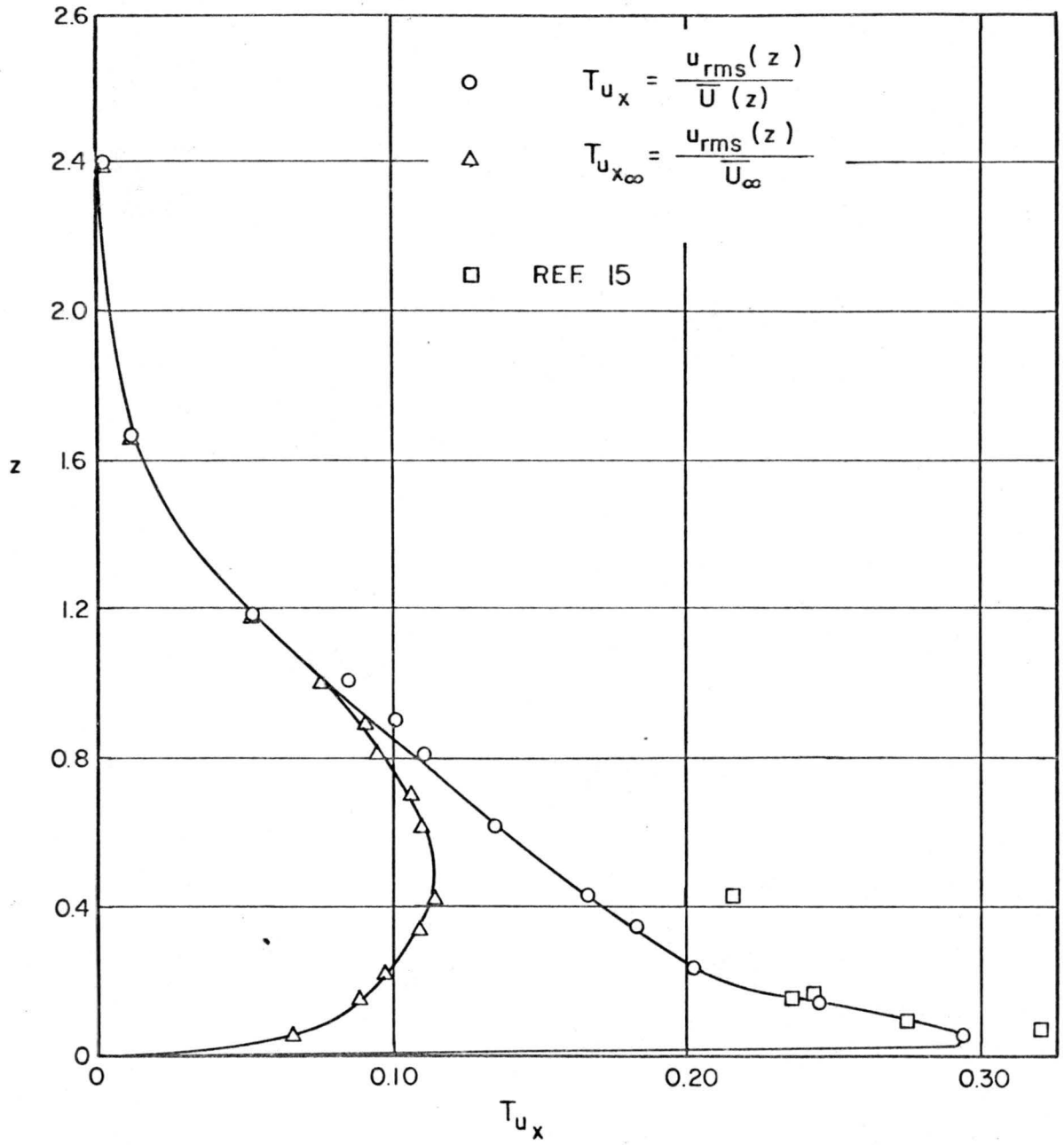

Fig. 4.8 Turbulence intensity variation upstream of model tower; NE wind.

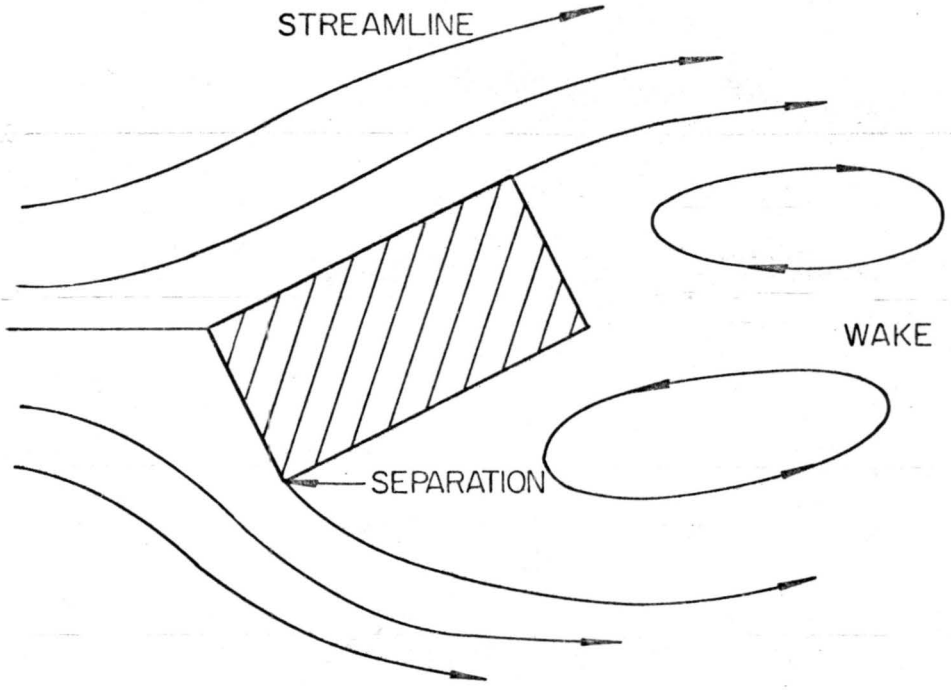

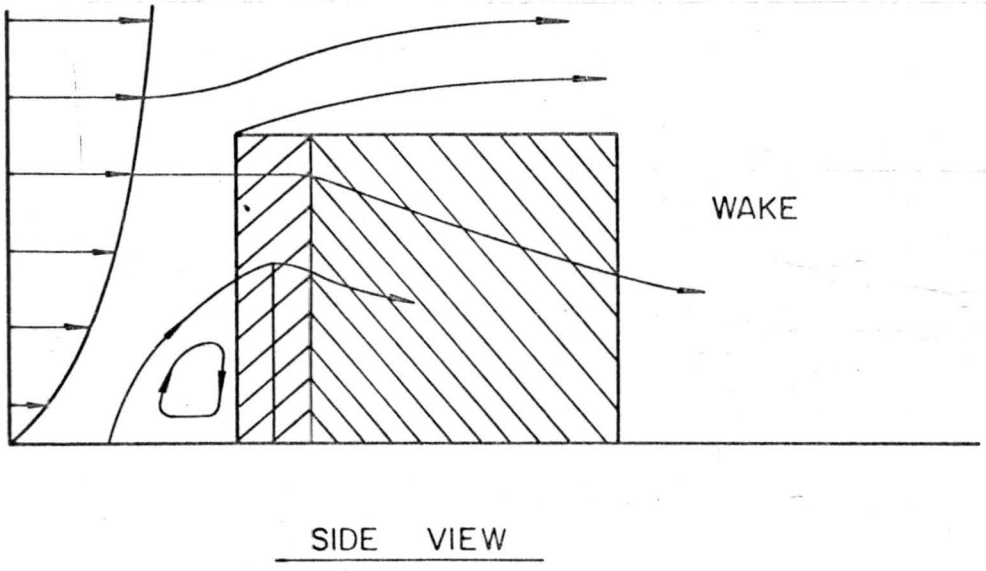

Fig. 4.9 Sketch of flow pattern around a single, tall, sharp edged rectangular structure from Ref. 11.

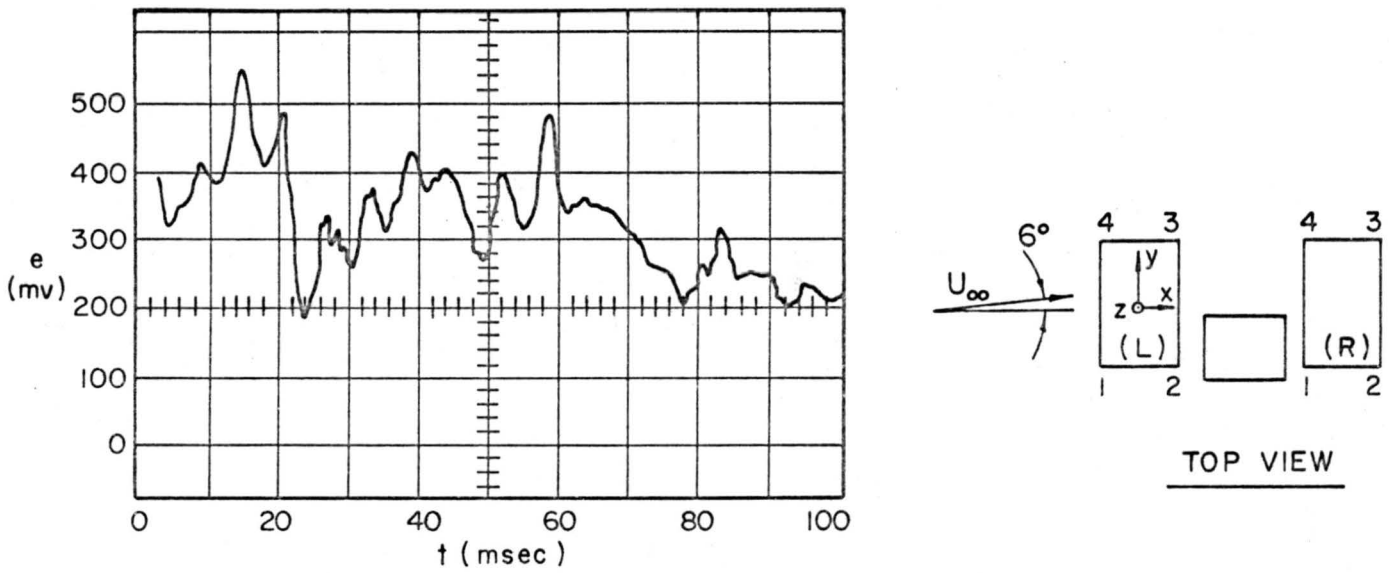

Fig. 4.10 Oscillogram of the fluctuating pressure at x,y,z = 0.07, 0.17, 0.75, (x*, y*, z* = 1.45, 3.5, 15.56 in.) on L tower, NE wind.

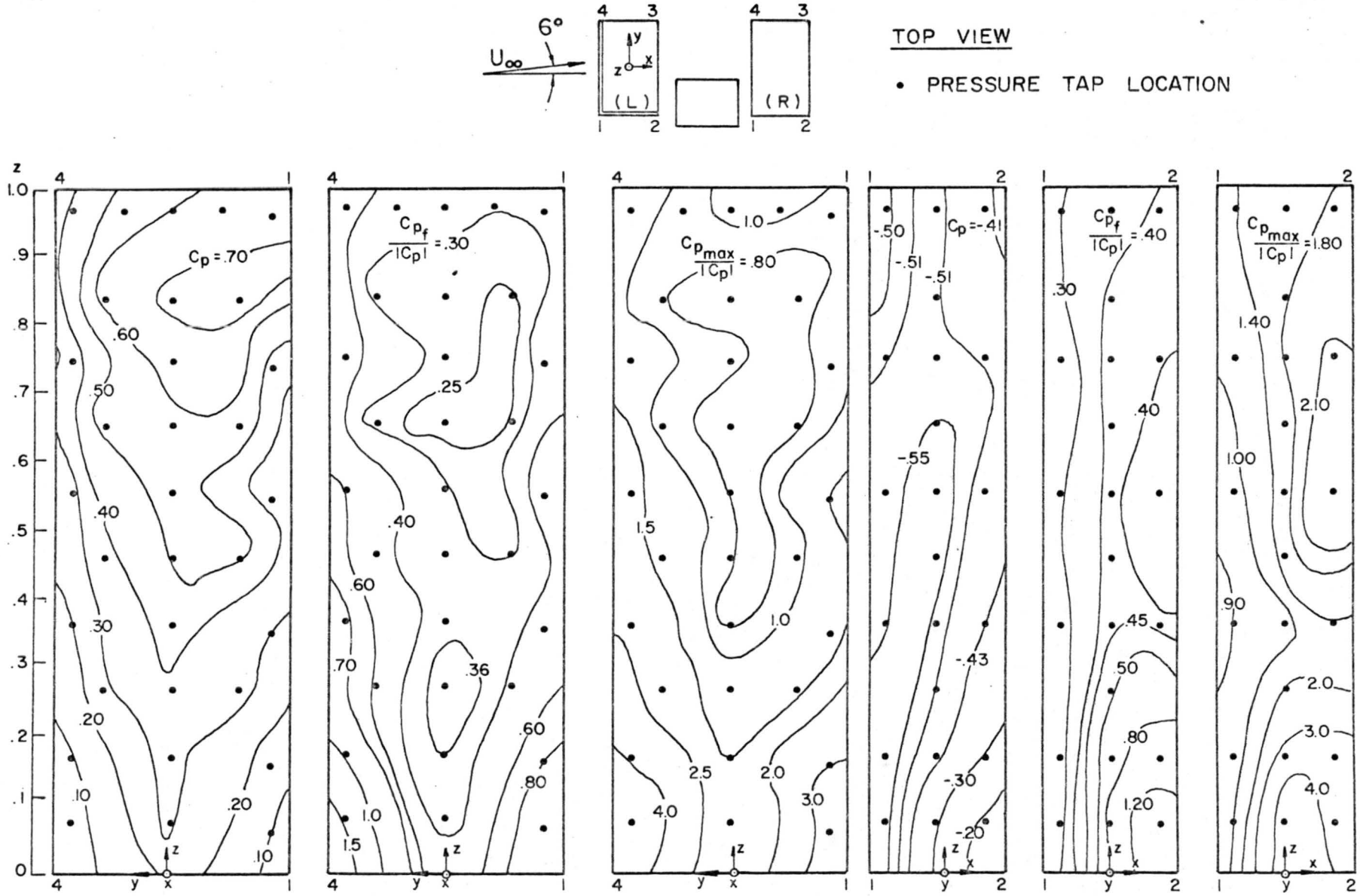

Fig. 4.11a Mean, fluctuating and peak pressure coefficient distribution on faces 4-1 and 1-2 of L tower in NE wind.

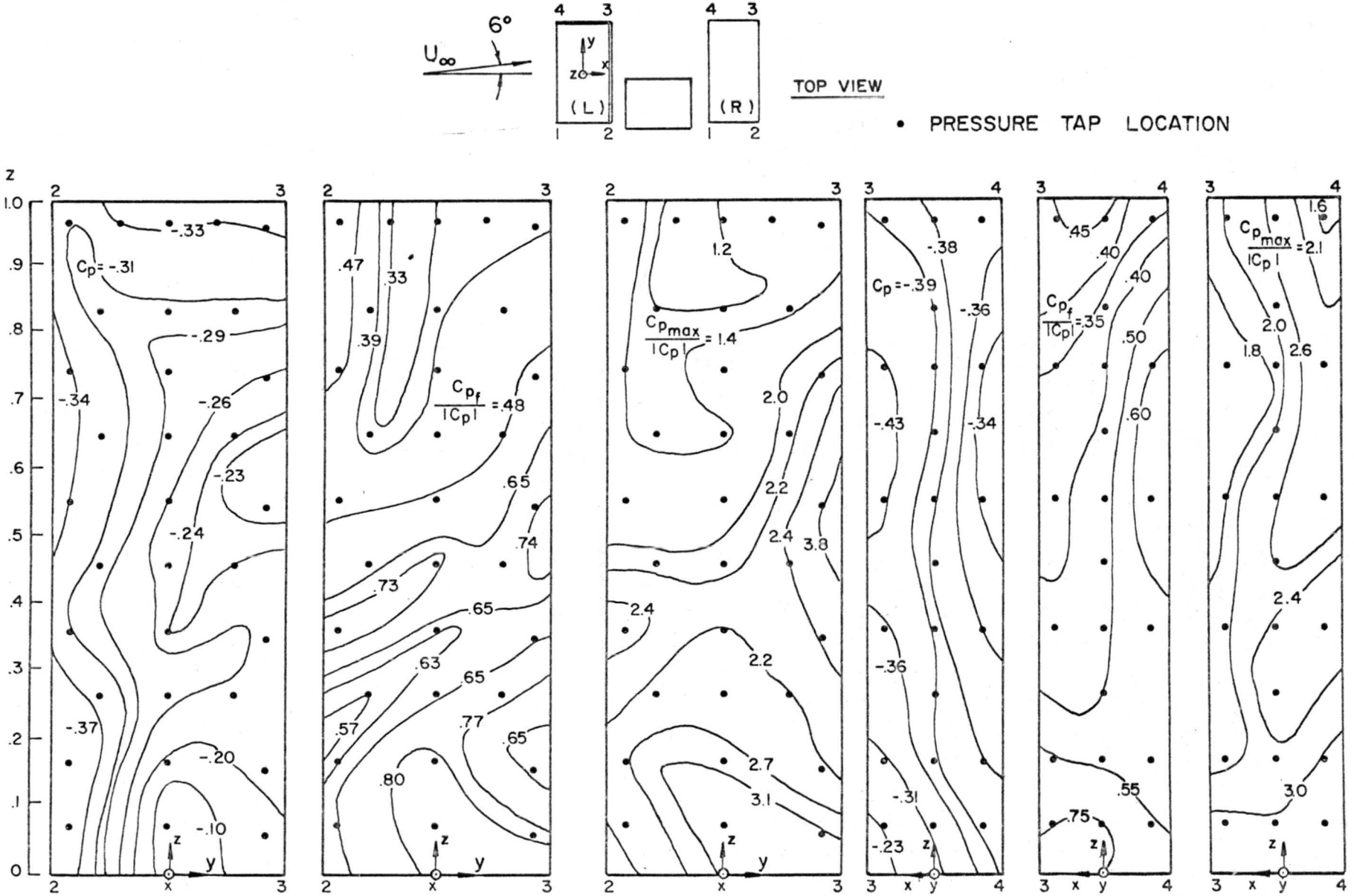

Fig. 4.11b Mean, fluctuating and peak pressure coefficient distribution on faces 2-3 and 3-4 of L tower in NE wind.

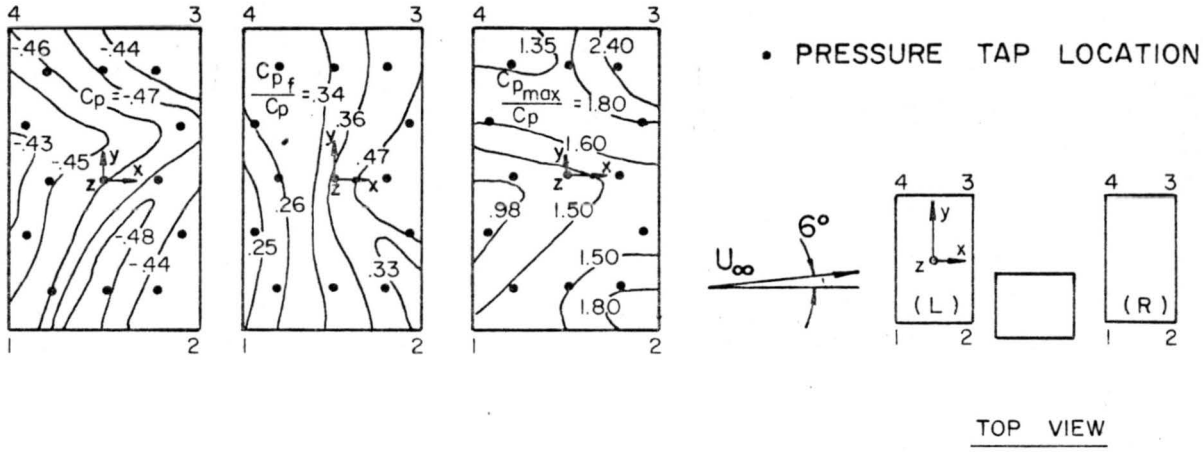

Fig. 4.11c Mean, fluctuating and peak pressure coefficient distribution on roof of L tower in NE wind.

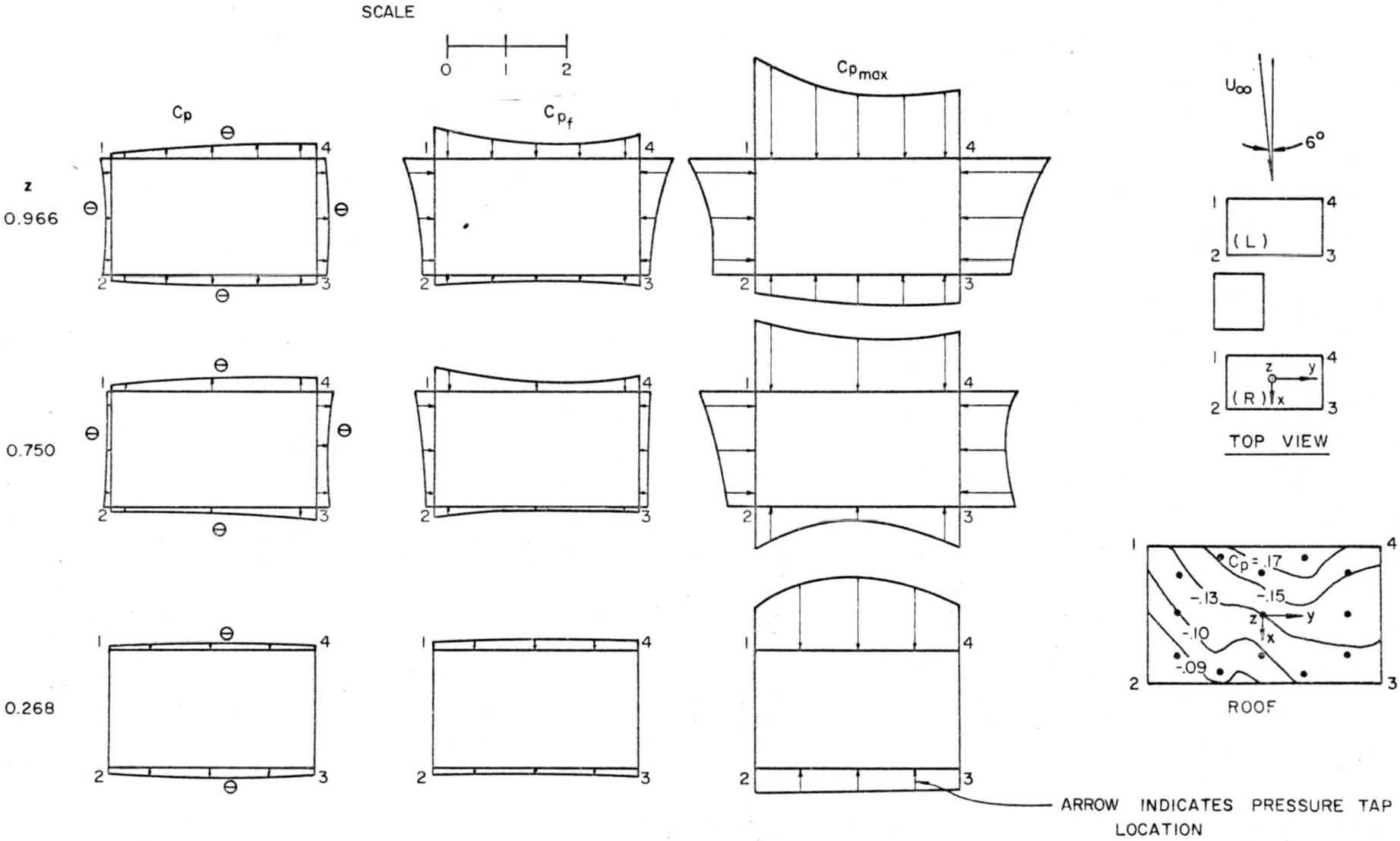

Fig. 4.11d Mean, fluctuating and peak pressure coefficient distribution at z = 0.268, 0.750, 0.966 (z* = 5.56, 15.56, 20.06 in.) and on the roof of R tower in NE wind.

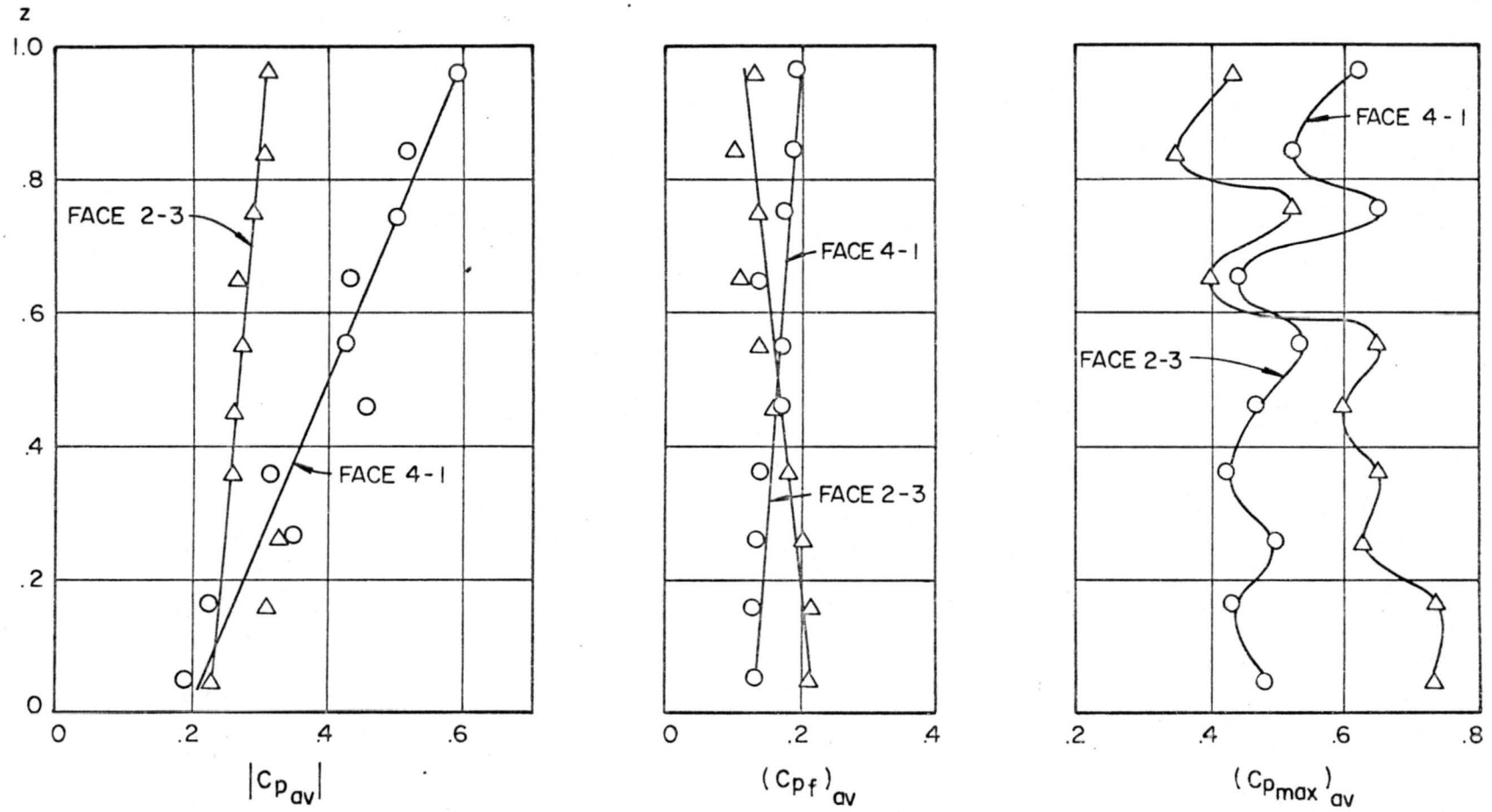

Fig. 4.12 Variation of average c_p, c_{p_f} and $c_{p_{max}}$ as function of height along faces 4-1 and 2-3 of L tower in NE wind.

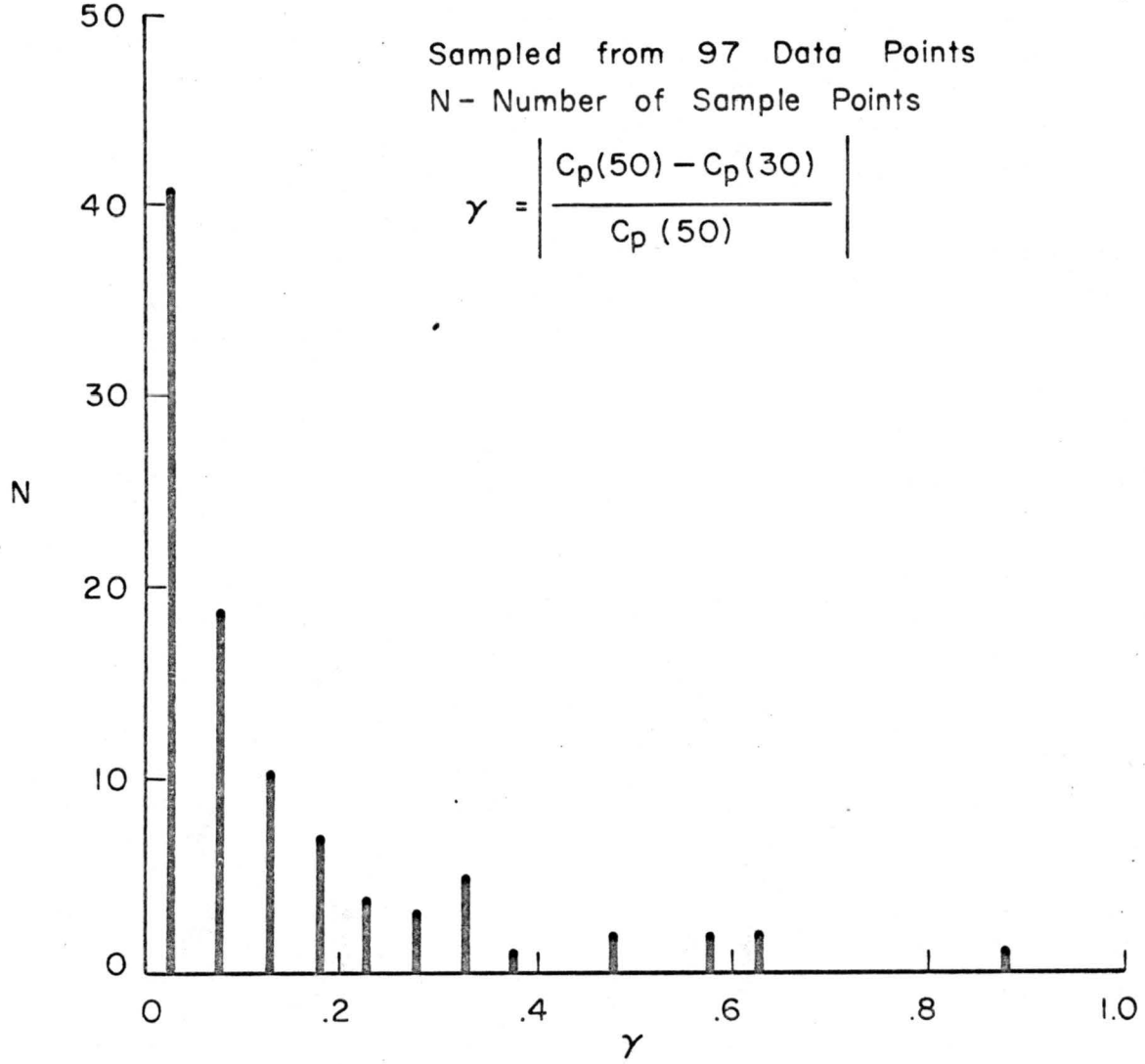

Fig. 4.13 Histogram of normalized pressure coefficient difference; L tower in NE wind.

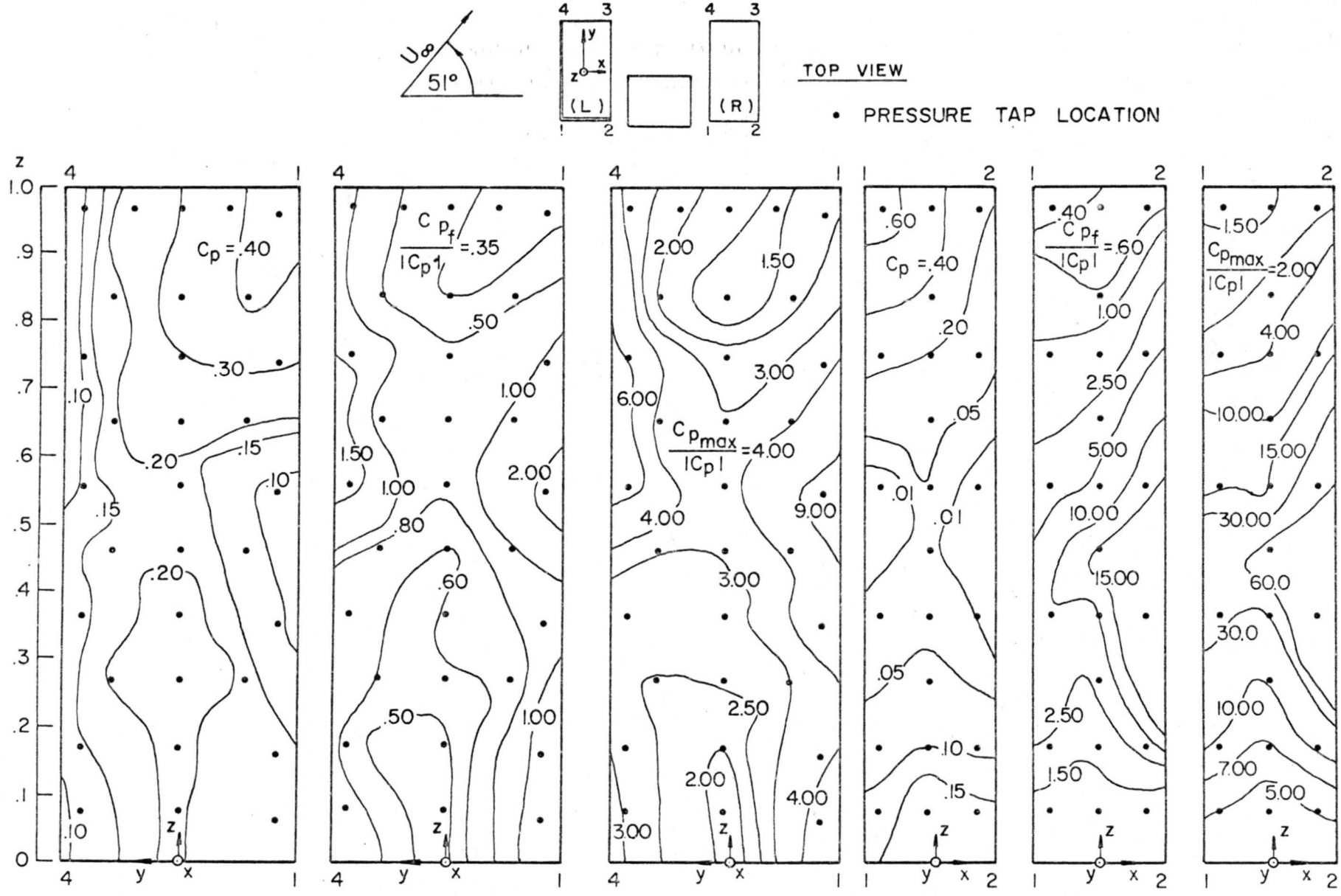

Fig. 4.14a Mean, fluctuating and peak pressure coefficient distribution on faces 4-1 and 1-2 of L tower in N wind.

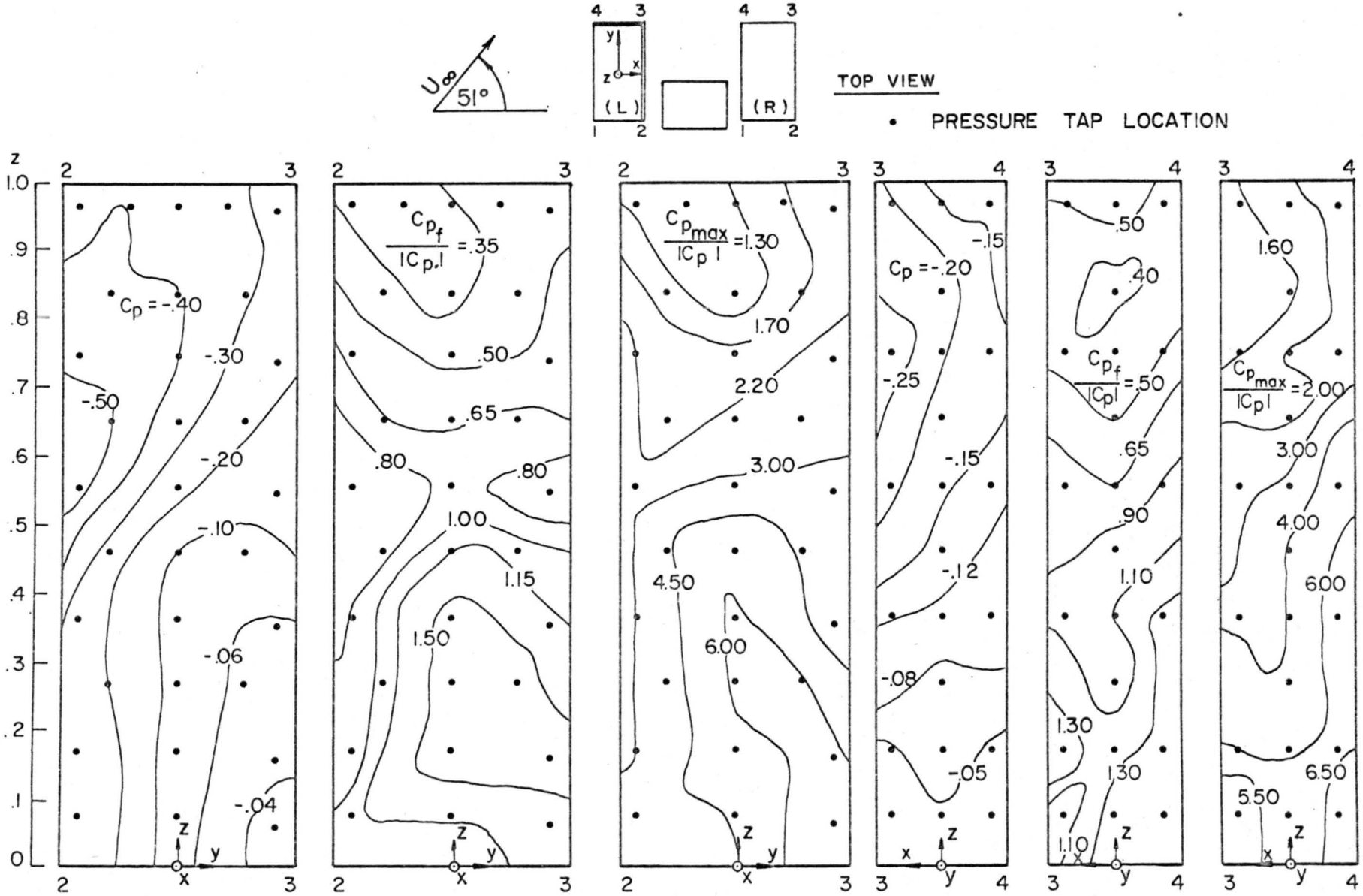

Fig. 4.14b Mean, fluctuating and peak pressure coefficient distribution on faces 2-3 and 3-4 of L tower in N wind.

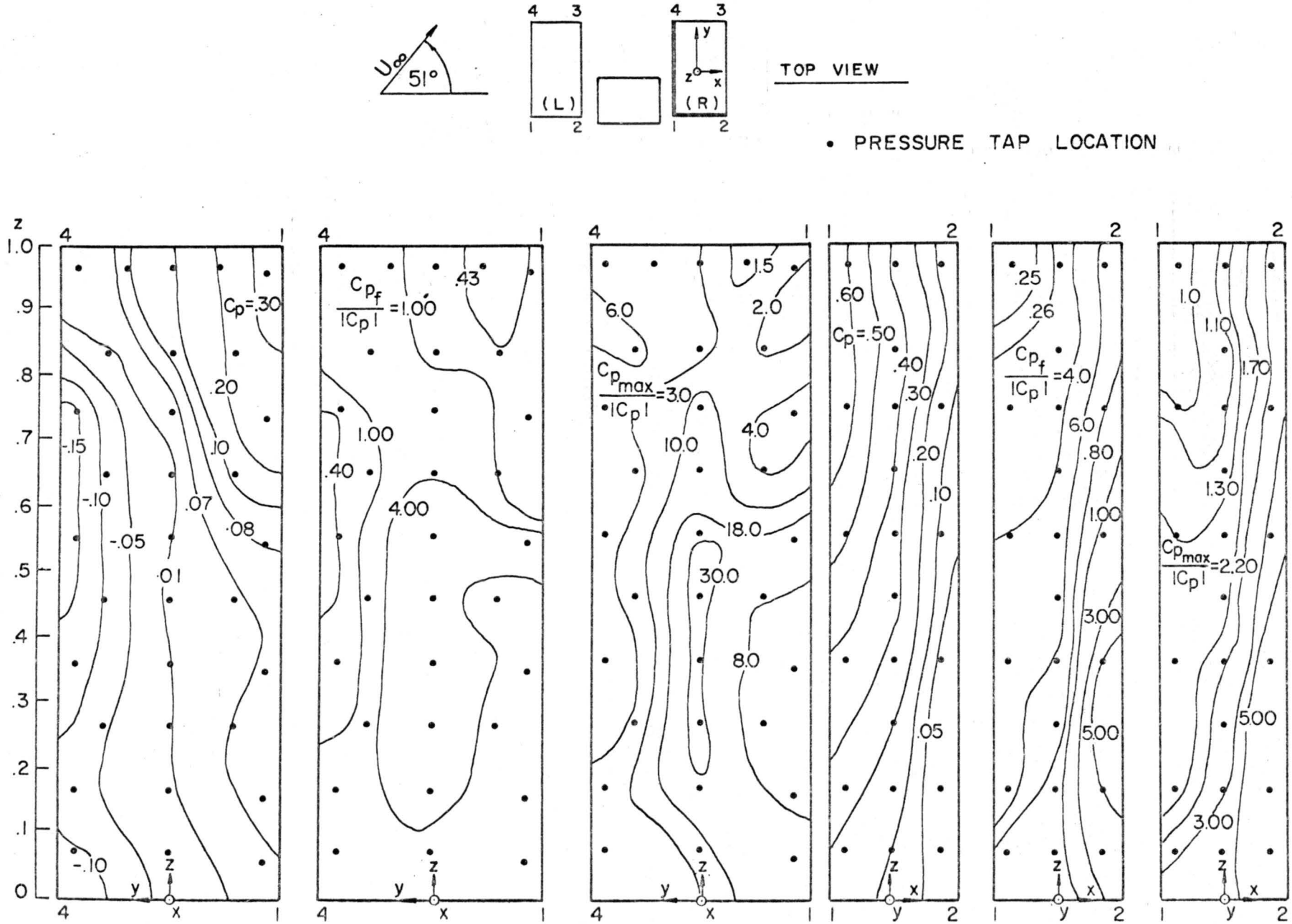

Fig. 4.14c Mean, fluctuating and peak pressure coefficient distribution on faces 4-1 and 1-2 of R tower in N wind.

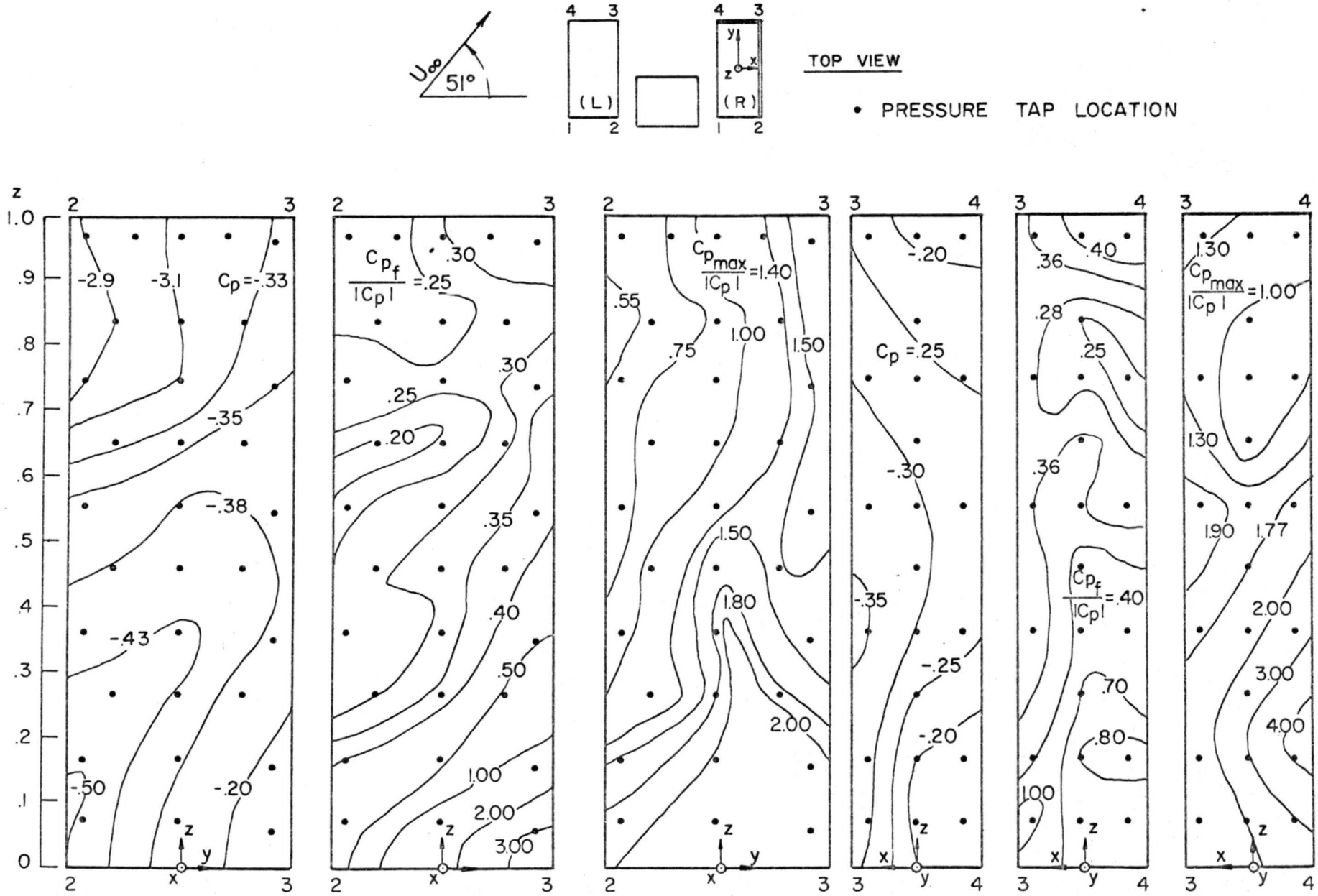

Fig. 4.14d Mean, fluctuating and peak pressure coefficient distribution on faces 2-3 and 3-4 of R tower in N wind.

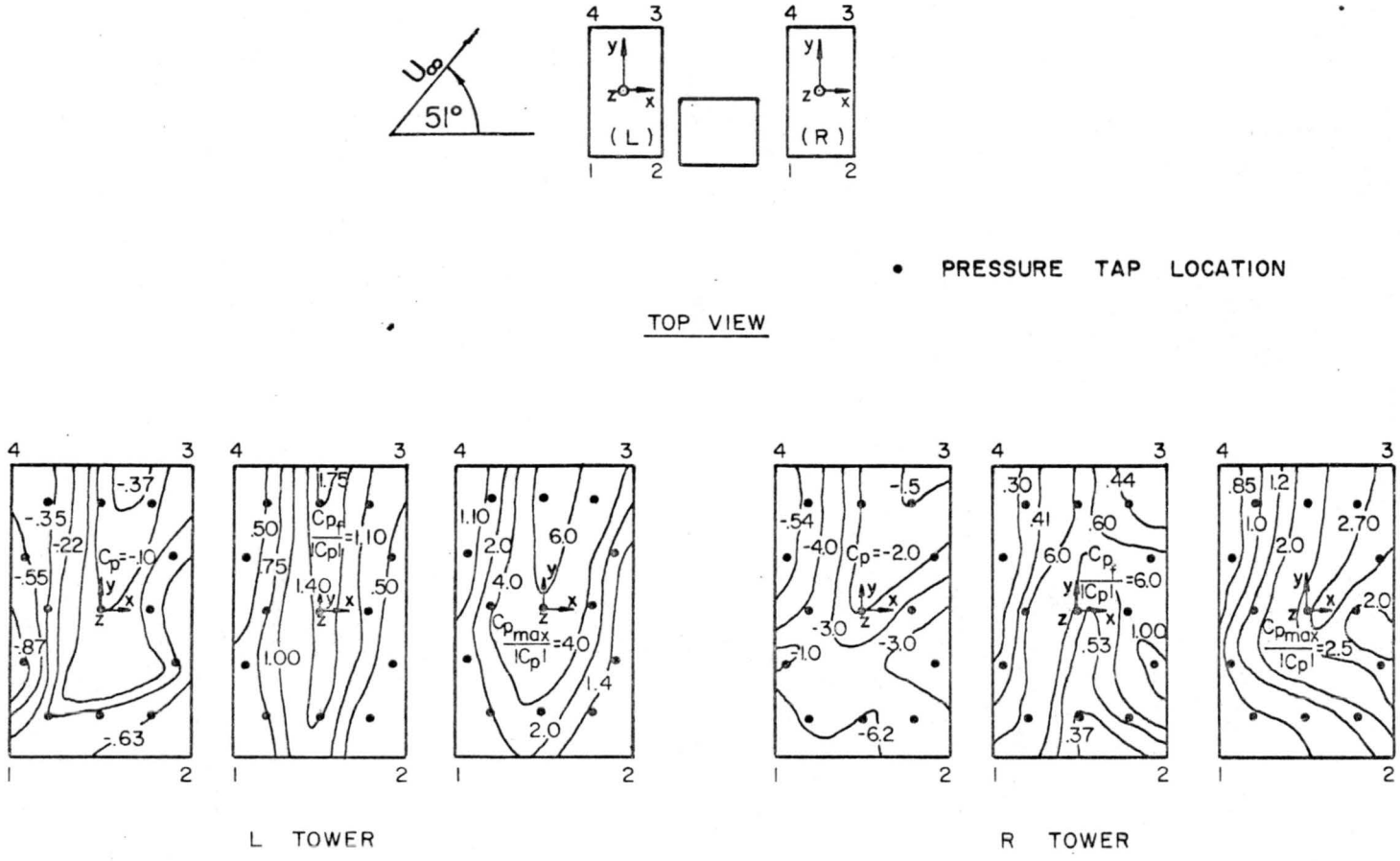

Fig. 4.14e Mean, fluctuating and peak pressure coefficient distribution on roofs of L and R tower in N wind.

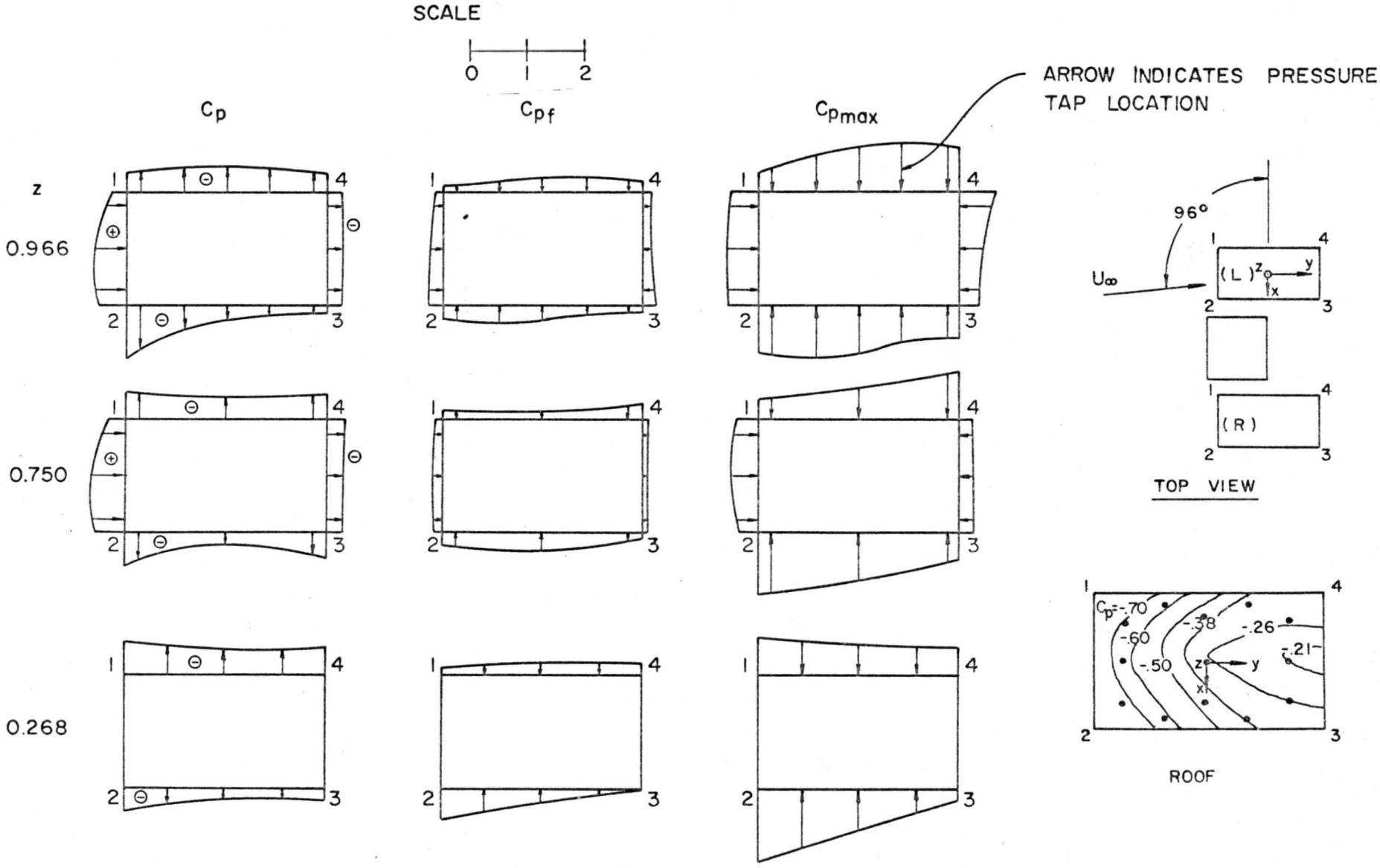

Fig. 4.15a Mean, fluctuating and peak pressure coefficient distribution at z = 0.268, 0.750 and 0.966 (z* = 5.56, 15.56 and 20.06 in) and on the roof of L tower in N wind.

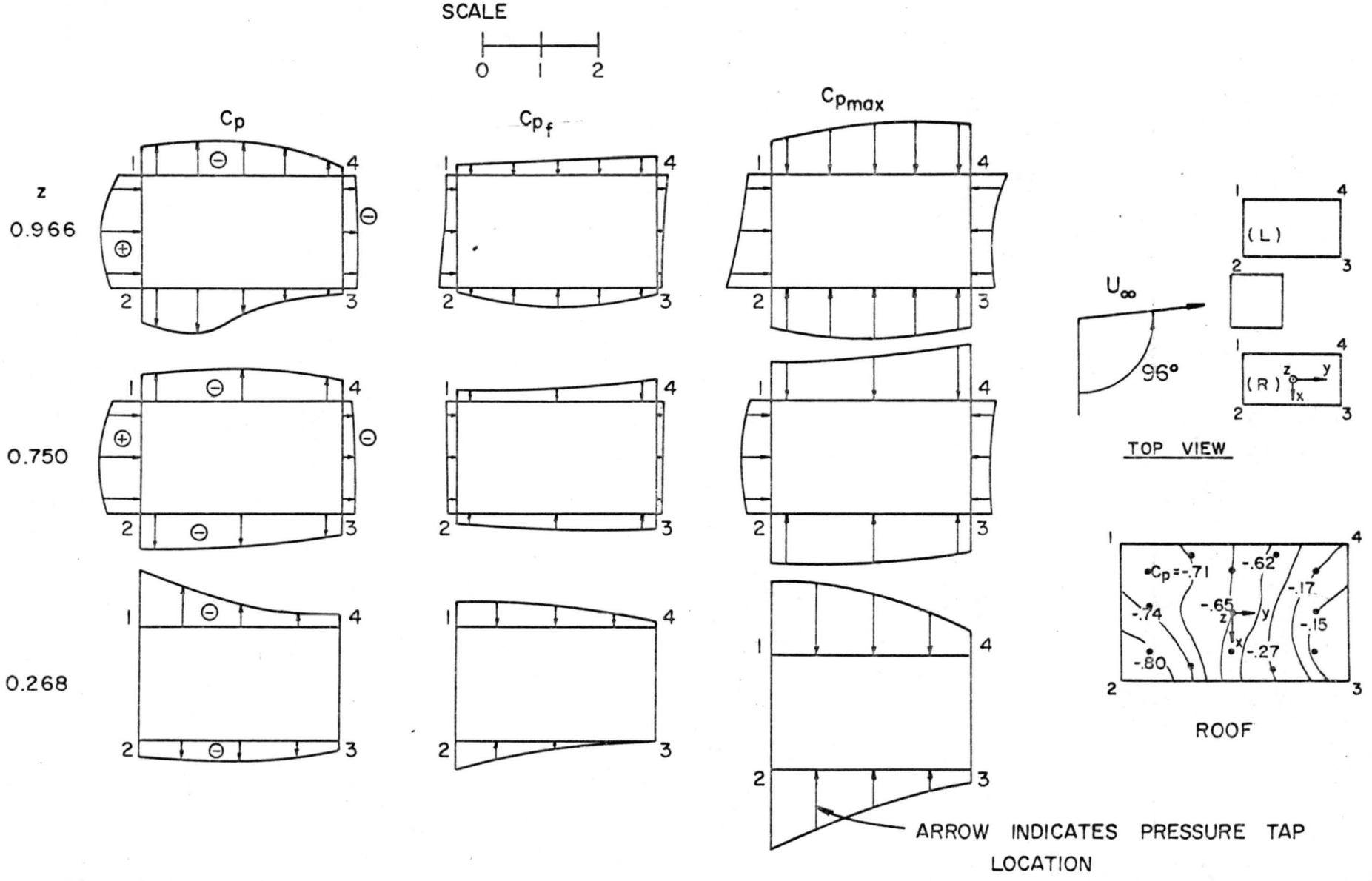

Fig. 4.15b Mean, fluctuating and peak pressure coefficient distribution at z = 0.268, 0.750 and 0.966 (z* = 5.56, 15.56 and 20.06 in.) and on the roof of R tower in NW wind.

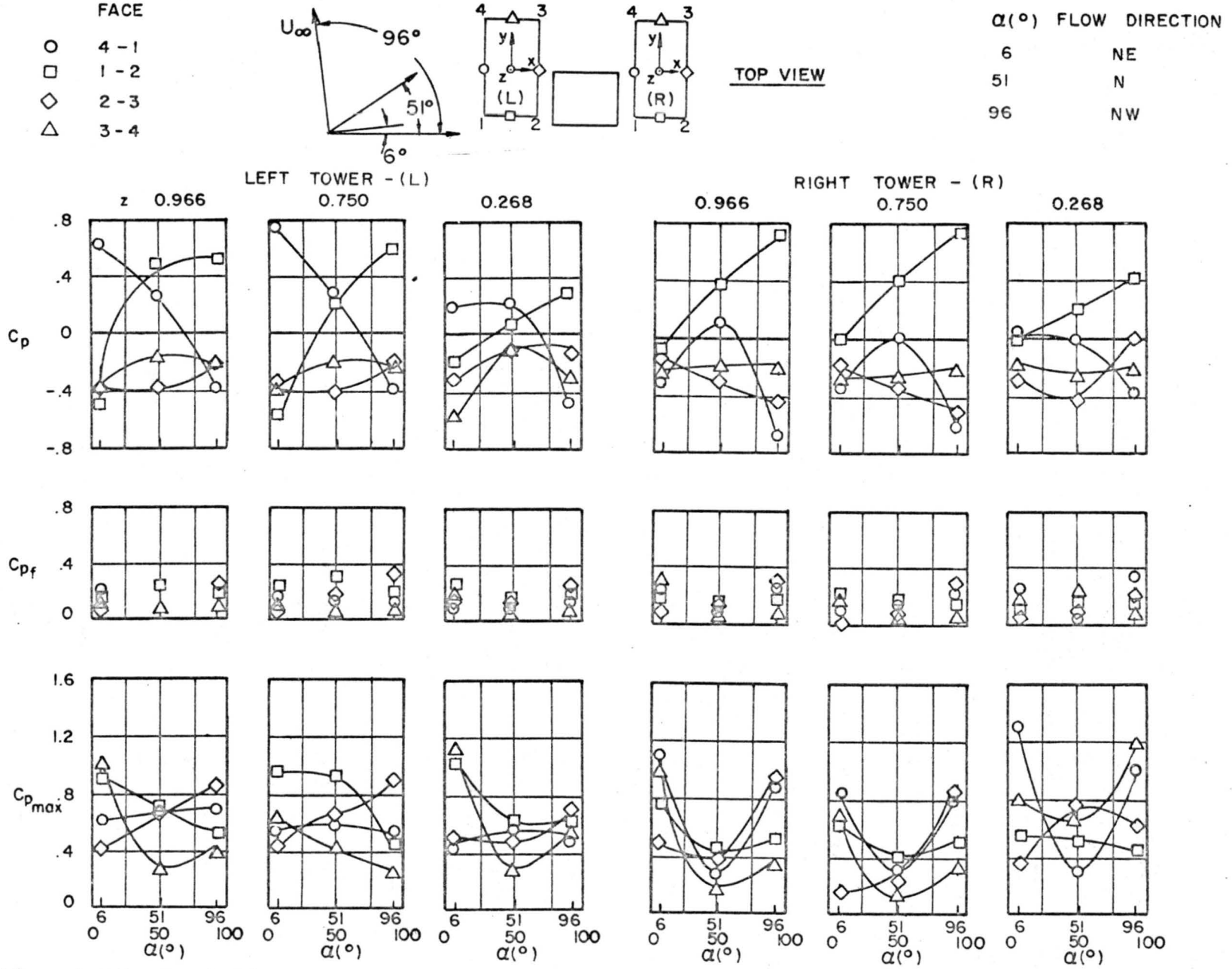

Fig. 4.16 Variation of mean, fluctuating and peak pressure coefficients with flow direction.

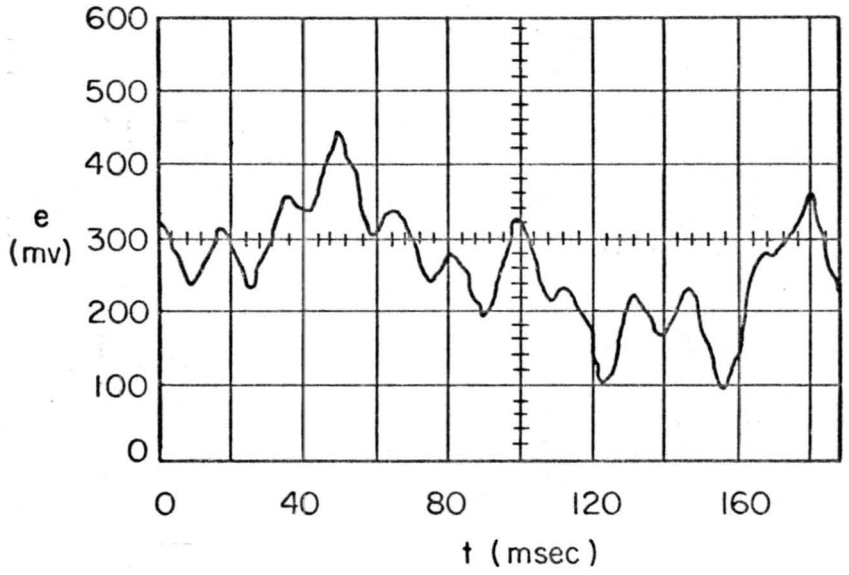

Fig. 4.17 Oscillogram of the fluctuating moment with upstream roughness installed.

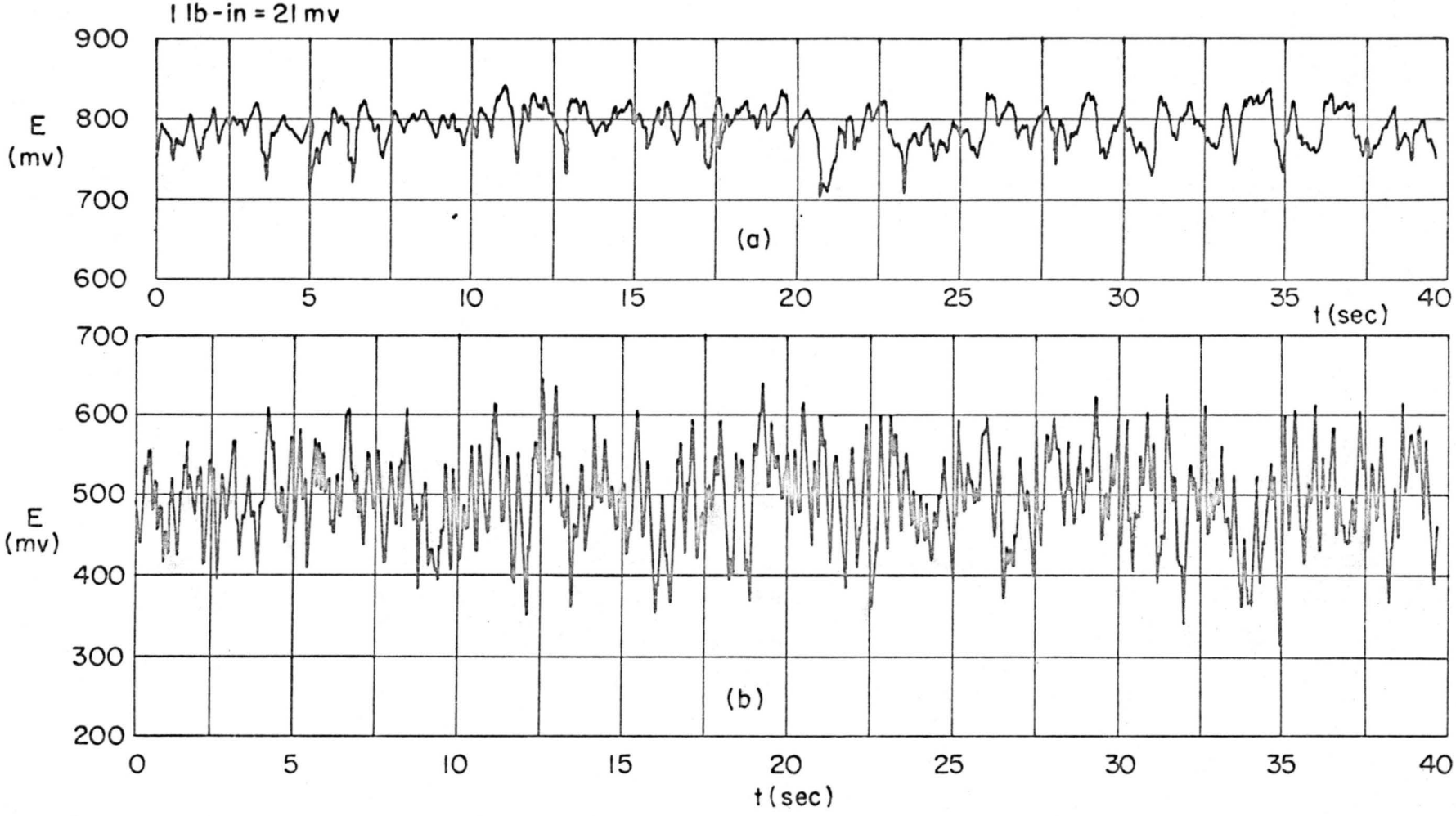

Fig. 4.18 Total overturning moment variation; (a) without upstream roughness; (b) with upstream roughness.

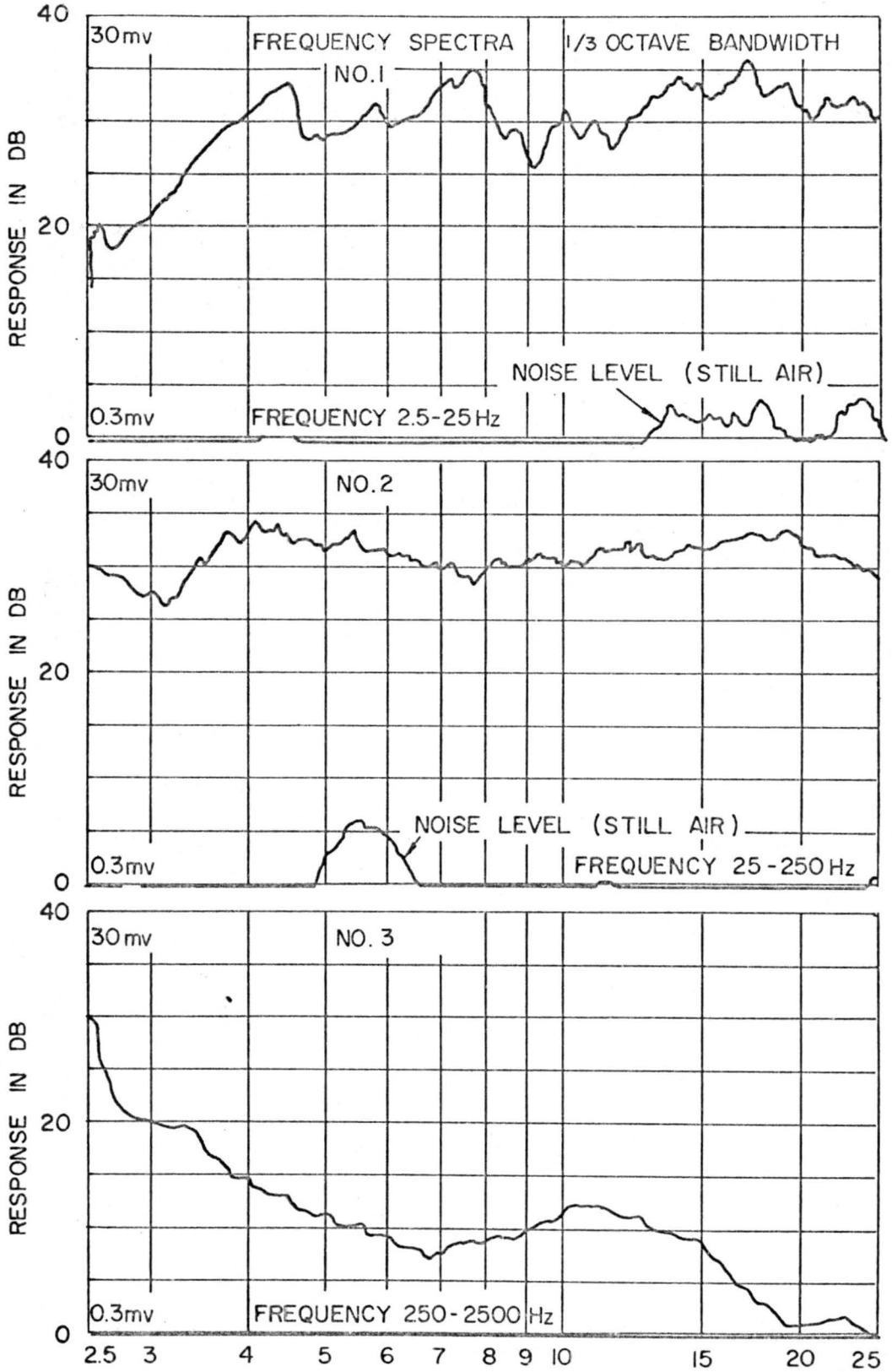

Fig. 4.19 Frequency spectrum of fluctuating pressure at x, y, z = 0.07, 0.17, 0.75 (x*, y*, z* = 1.45, 3.50, 15.56 in.).

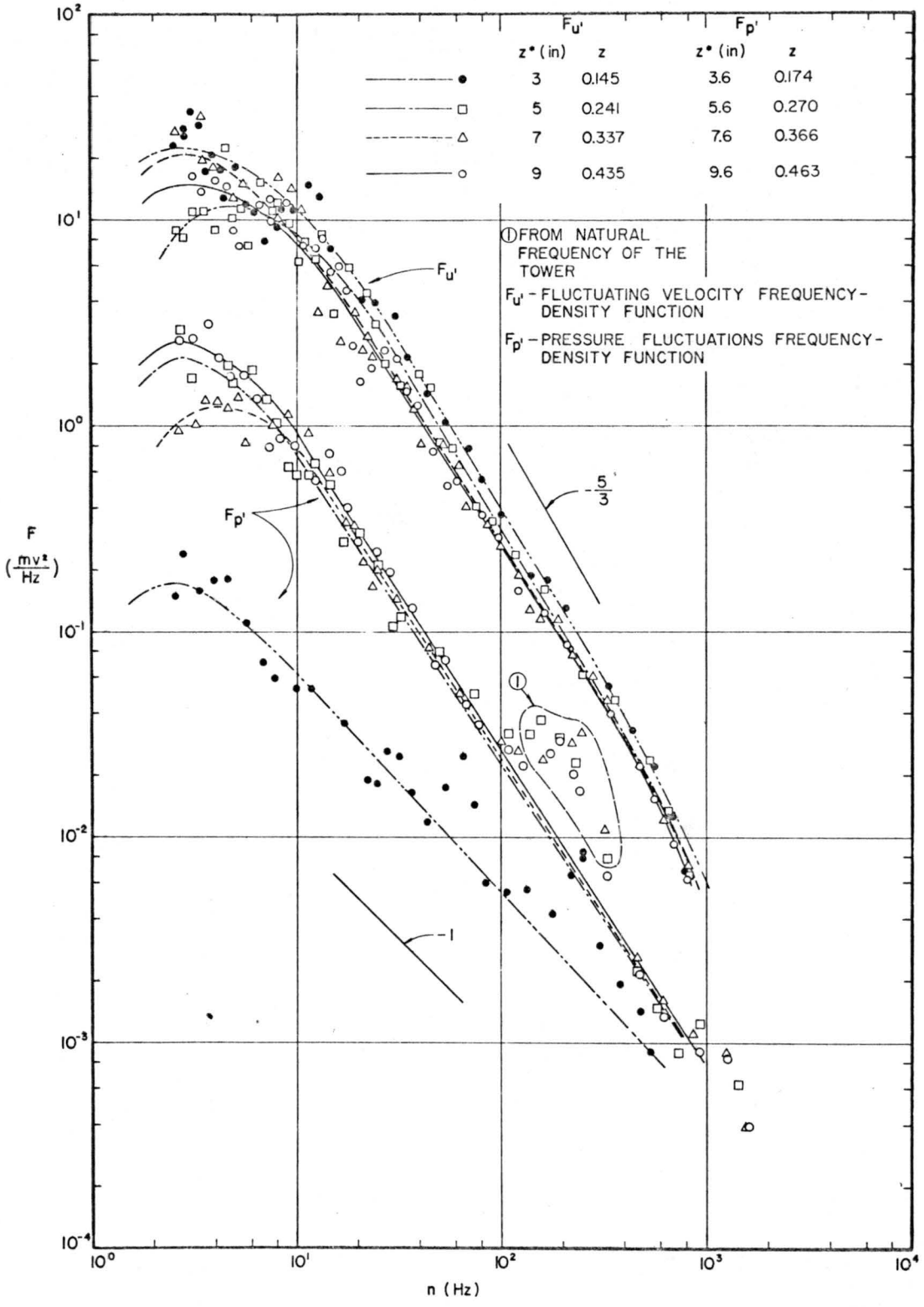

Fig. 4.20 Turbulence-energy and pressure-fluctuations spectra.

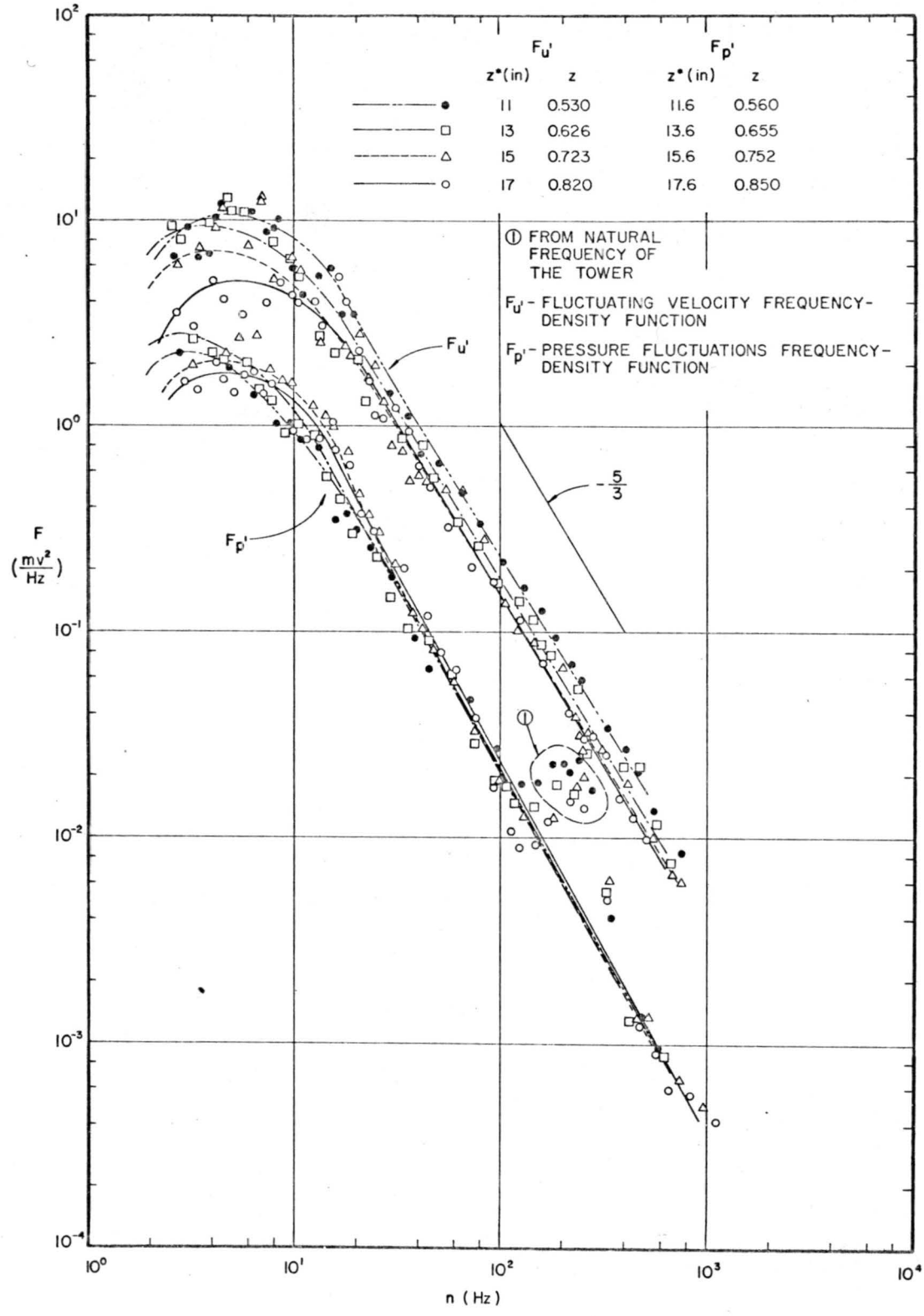

Fig. 4.21 Turbulence-energy and pressure-fluctuations spectra.